DETAILED ANALYSIS OF VOXEL BASED MORPHOMETRY

by

Özlem Özmen Okur

B.S., Electrical and Electronics Engineering, Boğaziçi University, 1998

M.S., Biomedical Engineering, Boğaziçi University Biomedical Engineering Institute, 2004

Submitted to the Institute of Biomedical Engineering

in partial fulfillment of the requirements

for the degree of

Doctor

of

Philosophy

Boğaziçi University

2016

DETAILED ANALYSIS OF VOXEL BASED MORPHOMETRY

APPROVED BY:

Prof. Dr. Cengizhan Öztürk   . . . .

(Thesis Advisor)

Prof. Dr. Tamer Demiralp   . . . .

Prof. Dr. Alp Dinçer   . . . .

Assoc. Prof. Dr. Albert Güveniş   . . . .

Assist. Prof. Dr. Özgür Kocatürk   . . . .

DATE OF APPROVAL: 31.08.2016

ACKNOWLEDGMENTS

To my beloved father Duran Özmen, who suffered so much and lost his life when I was studying for my PhD.

ACADEMIC ETHICS AND INTEGRITY STATEMENT

I, Özlem Özmen Okur, hereby certify that I am aware of the Academic Ethics and Integrity Policy issued by the Council of Higher Education (YÖK) and I fully acknowledge all the consequences due to its violation by plagiarism or any other way.

Name :

Signature:

_____

_____

Date:

_____

ABSTRACT

DETAILED ANALYSIS OF VOXEL BASED MORPHOMETRY

Voxel Based Morphometry, VBM, is one of the most widely used brain morphometry methods which aims to reveal the structural differences between the brain MR images of different populations. It is a whole brain and fully automatic approach in which all the images are registered onto a common template and then segmented into grey matter, white matter and cerebrospinal fluid. After an optional modulation step (regaining the original volume which is shrinked or enlarged during the registration), smoothing takes place in order to make the data more normally distributed and to diminish the inexact nature of the nonlinear registration. Finally, voxel-wise statistical operations are performed between the groups of the images. As revealed in several studies, changes in these steps and changes in their parameters might influence the resulting statistics. Although some short guidelines exist for conducting the processing stages, this thesis tries to explain each main step and gathers the discussions in the literature to make the VBM users aware of some pitfalls and limitations of VBM; and also gives brief descriptions about the other brain morphometry methods to give a view for where VBM stands at. In this thesis, the effect of modulation and masking strategy at the statistical stage were studied and concluded that not using the modulation and using average-based masking for the statistical part increased the detection power of VBM. Additionally, within the scope of this thesis, three clinical applications of VBM are performed and presented: Comparisons of the brain images of mathematicians, SSPE patients, and solvent abusers vs healthy controls.

Keywords: VBM, Brain Morphometry, SPM, Masking, Modulation, MRI, Simulation.

ÖZET

VOKSEL BAZLI MORFOMETRİNİN DETAYLI ANALİZİ

Voksel Tabanlı Morfometri, VTM, farklı insan gruplarının beyin MR imgeleri arasındaki yapısal değişikliği ortaya çıkarmaya çalışan ve en çok kullanılan beyin morfometri metodlarından biridir. VTM'de beyin imgeleri bir bütün olarak ve tamamen otomatik yöntemlerle işlenir. VTM analizi, imgelerin ortak bir şablona kaydedilmesi, bu imgelerin doku gruplarına ayrılması (gri madde, ak madde ve beyin-omurilik sıvısı), seçmeli modülasyon (dokuların, ortak şablona kaydedilmesi sırasında değişen hacimlerinin, özgün hacimlerine döndürülmeleri), yumuşatma (verilerin dağılımının normalleşebilmesi ve imgelerin doğrusal olmayan şekilde kaydedilmesinden kaynaklı hataların azaltılması) ve voksel bazında istatistiki hesaplamalar gibi aşamalardan oluşmaktadır. Birçok çalışmada gösterildiği gibi, bu aşamalarda ya da bu aşamaların parametrelerinde yapılan değişiklikler, VBM analizi sonuçlarını da değiştirebilmektedir. VBM analizinin nasıl yapılacağına dair bazı kısa kılavuzlar olsa da, bu tez, VBM'in ana aşamalarını kısaca açıklayıp, bu aşamalarla ilgili literatürde çıkmış tartışmaları bir araya getirerek, VBM kullanıcılarını, VBM'in yanlış sonuçlara götürebilecek özellikleri konusunda uyarmaya çalışmaktadır. Aynı zamanda, diğer morfometri metodlarına da kısaca değinerek, VBM'in bu alanda nerede durduğuna ilişkin bir fikir verilmeye çalışılmaktadır. Bu tezde, özellikle, modülasyon ve istatistik aşamasında maskeleme stratejisi konusu araştı- rılmıştır ve modülasyonun kullanılmamasının ve istatistiki hesaplamalarda, ortalama imgeye bağlı maskeleme kullanılmasının, VBM'in fark bulma yeteneğini yükselttiği gösterilmiştir. Ayrıca, bu tez kapsamında, VBM ile; matematikçiler, SSPE hastaları ve çözücü kullanıcıları ile normal denekler arasında olmak üzere, üç farklı klinik çalışma yapılmıştır.

Anahtar Sözcükler: VTM, Beyin Morfometrisi, SPM, Maskeleme, Modülasyon, MRI, Simülasyon.

TABLE OF CONTENTS

LIST OF FIGURES

LIST OF TABLES

LIST OF SYMBOLS

β	Parameter vector
c	Contrast vector
c^T	Transpose of c
ϵ	Residuals
$\partial y/\partial x$	Partial derivative of y with respect to x
J	Jacobian matrix
Y	Data matrix

LIST OF ABBREVIATIONS

ADNI	Alzheimer's Disease Neuroimaging Initiative
BA	Brodmann Area
CAT	Computational Anatomy Toolbox
CT	Computed Tomography
CSF	Cerebrospinal Fluid
DARTEL	Diffeomorphic Anatomical Registration Through Exponentiated Lie Algebra
DBM	Deformation Based Morphometry
DICOM	Digital Imaging and Communications in Medicine
EPI	Echo Planar Imaging
FDR	False Discovery Rate
FLAIR	Fluid Attenuation Inversion Recovery
FMRIB	Functional MRI of the Brain
FNIRT	FMRIB's Nonlinear Image Registration Tool
FOV	Field of View
FSIQ	Full-Scale Intelligence Quotient
FSL	FMRIB Software Library
FWHM	Full Width Half Maximum
FWE	Family Wise Error
GLM	General Linear Model
GM	Grey Matter
IgG	Immunoglobulin G
IQ	Intelligence Quotient
LDDMM	Large Deformation Diffeomorphic Metric Mapping
MEACOLP	Morphometry Based on Effective and Accurate Correspondences of Localized Patterns
MNI	Montreal Neurological Institute
MR	Magnetic Resonance

MRI	Magnetic Resonance Imaging
MS	Multiple Sclerosis
NAA	N-acetylaspartate
NDI	Neurologic Disability Index
NEX	Number of Excitations
OASIS	Open Access Series of Imaging Studies
PD	Parkinson's disease
PPMI	Parkinson's Progression Markers Initiative
RBM	Region based morphometry
RFT	Random Field Theory
SBA	Surface Based Analysis
SD	Standard deviation
SPECT	Single-Photon Emission Computed Tomography
SPM	Statistical Parametric Mapping
SPSS	Statistical Package for the Social Sciences
SSPE	Subacute Sclerosing Panencephalitis
SVC	Small Volume Correction
SVD	Sigular Value Decomposition
SVM	Support Vector Machine
TBM	Tensor Based Morphometry
TE	Echo Time
TI	Inversion Time
TIV	Total Intracranial Volume
TGM	Total Grey Matter
TR	Repetition Time
VBCT	Voxel Based Cortical Thickness
VBM	Voxel Based Morphometry
WISC	Wechsler Intelligence Scale for Children
WM	White Matter

1.   Introduction

1.1   General Objectives and Motivation

Brain morphometry concerns with the physical form of the brain by exploring its shape and size. Several morphometric methods investigate the volume, surface or concentration of cortical and subcortical structures and different tissue types in the brain (grey matter, white matter, and cerebrospinal fluid), atrophy or thickening in the grey matter, gyrification and curvature of the cerebral cortex, and many other similar properties. Using these properties, the structural changes in the brain can be explored due to the effects of development and aging, diseases, training and learning, drug administration or exposure to substances, neuronal plasticity, etc. These properties have also potentials for diagnostical purposes like hippocampal volume: As an example of contributions of brain morphometry methods is the usage of hippocampal volumes as a biomarker: Hippocampal volume has been chosen as a biomarker for clinical trials in pre-dementia stage of Alzheimer's disease (EMA/CHMP/SAWP/809208/2011).

MRI is a popular imaging modality in morphometric studies because of its noninvasive nature. Voxel based morphometry, VBM, makes comparisons between different populations by using brain MR images, and it is one of the most widely used methods in morphometry field.

VBM consists of several processing stages including segmentation, registration, modulation, smoothing and statistical inference. There are some dedicated tools for VBM, but VBM can be performed by any tool or combination of the tools. Although there are some general guidelines and/or suggestions for these processing stages, there are not so many strict rules such as the acceptable goodness of the registration and segmentation, the exact kernel width for the smoothing, the acceptable statistical inference methods, etc. It has been shown that the variations in the processing of VBM can alter the results. Therefore, the investigation of these processing parameters and

their effects on VBM are essential issues.

In this thesis, a general information is gathered and a general view in brain morphometry methods is presented, while emphasising on VBM. The effect of the modulation which is generally advised to be used, and also, the effect of an alternative masking strategy in statistics are investigated. Additionally, three different clinical applications using VBM were performed and presented which were about the effects of learning (mathematicians [3]), disease (subacute sclerosing panencephalitis [1]), and exposure to substances (solvent [2]).

1.2   Outline of the Thesis

In the second chapter, VBM processing pipeline is described. Several discussions from the literature on this pipeline are mentioned including the discussions on segmentation, registration, modulation, smoothing, statistical inference methods, masking, usage of multicenter data, minimum number of subjects for a VBM analysis, cross-sectional vs longitudinal studies, and effects of using different processing tools. Additionally, different VBM tools are listed.

In the third chapter, other brain morphometry methods are summarized: deformation based morphometry, cortical surface morphometry, surface-based methods, and feature based methods.

In the fourth chapter, the effects of modulation (although modulation is optional, it's generally used in VBM pipeline) and using an alternative masking strategy (as an alternative to the present masking method in SPM tool) in statistical stage are investigated using both simulated atrophy data and the images of Parkinson's disease patients.

In the fifth chapter, the three different clinical applications of VBM which are performed during the preparation of this thesis are presented. These studies were

titled as "Reduced Gray Matter Volume in the Frontotemporal Cortex of Patients with Early Subacute Sclerosing Panencephalitis", "Smaller Gray Matter Volumes in Frontal and Parietal Cortices of Solvent Abusers Correlate with Cognitive Deficits", and "Increased Gray Matter Density in the Parietal Cortex of Mathematicians: A Voxel-Based Morphometry Study"

Chapter six presents a general summary and conclusion for this thesis.

2.   Voxel Based Morphometry

Brain morphometry is a field in Neuroimaging which concerns with the physical form of the brain in terms of its size and shape: atrophy or thickening in gray matter; volumetric, concentration or shape differences in cortical or subcortical structures; gyrification; cortical curvature; the amount of cerebrospinal fluid, etc. Using these properties, we can observe the changes due to developmental and aging phases, diseases, training and learning.

As a noninvasive imaging modality, MRI is widely used in morphometric studies. Voxel Based Morphometry, VBM, uses structural brain MR images by a whole brain and fully automatic approach to compare the groups of images on a voxel level. It is not only one of the most common morphometric methods but also one of the most common methods in all neuroimaging area.

Although VBM has been first appeared in a few articles in 1990's [4–13], it has been achieved wide applicability after Ashburner and Friston's article in 2000 [14]. Since then, it's been used in thousands of studies[1] including but not limited to neurodegenerative diseases (Parkinson's disease [15], Alzheimer's disease [16], progressive supranuclear palsy [17], multiple sclerosis [18], ...), other neurological diseases (such as subacute sclerosing panencephalitis [1]), psychiatric diseases (anxiety disorders [19], borderline disorder [20], depression [21], ...), investigating the effects of learning and training (mathematicians [3], London taxi drivers [22], bilingual people [23], ...), investigating the effects of aging [24], stress [25], substance consumption [2], and in many more subjects.

VBM presents a statistical parametric map of segmented brain tissue. A VBM analysis consists of several image processing and statistical steps, mainly: Segmenting

---

[1]As of 09.06.2016, when we searched the articles at https://scholar.google.com by the keywords "voxel based morphometry", there were 42300 results. When we search by the keywords "voxel based morphometry, spm" we got 13000, by the keywords "voxel based morphometry, fsl" we got 6220 results.

the brain image into gray matter, white matter and cerebrospinal fluid; normalizing each image to a common stereotactic template; smoothing the segmented images; and finally performing statistical analysis. The resulting map is called as the statistical parametric map which shows the regions that are different between the groups. Section 2.2 describes these stages.

2.1 VBM Tools

The most common tools for the image processing and statistical inference steps of VBM are SPM (http://www.fil.ion.ucl.ac.uk/spm/) which is developed by The Wellcome Trust Centre for Neuroimaging at UCL; and FSL (http://fsl.fmrib.ox.ac.uk/fsl/fslwiki/) which is developed by the Analysis Group, FMRIB, Oxford, UK. Although it is developed mainly for surface based analysis, Freesurfer (http://freesurfer.net) is also used (developed by the Laboratory for Computational Neuroimaging at the Athinoula A. Martinos Center for Biomedical Imaging.

CAT, Computational Anatomy Toolbox for SPM (http://dbm.neuro.uni-jena.de/cat/) is a toolbox created for SPM and by using this tool not only VBM but also surface-based morphometry (SBM), and deformation-based morphometry (DBM) analyses could be achieved.

VBM analyses can also be performed without a dedicated tool; it can be handled by any combination of image processing and statistical tools.

2.2 VBM Pipeline

2.2.1 Normalization and Segmentation

In the segmentation step, brain is segmented into three tissue types: grey matter (GM), white matter (WM), and cerebrospinal fluid (CSF). After or before or in com-

bination with the segmentation step, normalization takes place. Normalization could consist of only a linear or a linear plus nonlinear registration. In this stage, segmented tissues are registered onto a common stereotactic template. Usually, an initial template like MNI 305 [26] is used to roughly register the images, then an average image is created from these images and the original images are reregistered onto this newly created template.

Various normalization and segmentation methods have been utilized in VBM studies. In Ashburner and Friston (2000) [14], normalization was achieved by linear registration with 12 parameters (translation, rotation, scaling and shearing in x, y, and z axes), and then nonlinear registration by a linear combination of smooth spatial basis functions. The aim of this nonlinear registration was to minimize the residual squared differences between the image and the template, while simultaneously maximizing the smoothness of the deformations. The template images were created by the averaging all the images. After the normalization, the images were segmented using a modified mixture model cluster analysis technique.

In optimized VBM (2000) [27], normalization and segmentation were used in an iterative way: After the segmentation, the segmented images are normalized; then, with the parameters yielded from this normalization are used to resegment the original whole brain images.

In Ashburner and Friston (2005) [28] the segmentation and normalization steps are unified. This approach unified tissue classification, bias correction, and image registration within the same generative model.

In 2007, Ashburner and Friston proposed a new registration algorithm, DARTEL (Diffeomorphic Anatomical Registration using Exponentiated Lie algebra) [29]. Starting SPM8, the proposed VBM preprocessing changed to an improved version of unified segmentation plus DARTEL normalization.

With the introduction of SPM12 at the end of 2014, SPM put forward an im-

proved registration method, Shoot, which is similar to DARTEL. DARTEL is still available in SPM. Shoot is based on Large Deformation Diffeomorphic Metric Mapping (LDDMM), but with a different optimisation scheme[30]. Rather than performing a variational optimisation on a series of velocity fields, the algorithm is formulated to use a geodesic shooting procedure, with a Gauss–Newton optimisation strategy.

From the FSL aspect, initially, FSL included only linear registration [31]; the developers of FSL claimed that there was no reason to use nonlinear registration because of poor quality of scanned images at those times and the poor quality of the template (MNI152). However, with the advancements in nonlinear registration methods, data quality, and the correction of EPI distortions, they have also developed a nonlinear registration method, FNIRT.

2.2.2   Modulation

Originally, modulation was not included in VBM processing pipeline; it was first proposed in Good et al's study in 2000 [27]. Although it lacks experimental validity, its aim was quite straightforward: Keeping the original volume of the tissue which was artificially enlarged or shrinked during the normalization. It is achieved by multiplying the voxel values by the Jacobian determinants, which are yielded during the normalization, and which represents the shrinkage/enlargement amount where the Jacobian matrix is as in the following

$$J = \begin{bmatrix} \partial y_1/\partial x_1 & \partial y_1/\partial x_2 & \partial y_1/\partial x_3 \\ \partial y_2/\partial x_1 & \partial y_2/\partial x_2 & \partial y_2/\partial x_3 \\ \partial y_3/\partial x_1 & \partial y_3/\partial x_2 & \partial y_3/\partial x_3 \end{bmatrix} \tag{2.1}$$

where the point (y1, y2, y3) belongs to registered image, and (x1, x2, x3) belongs to the original image.

The modulated VBM is considered as revealing the volumetric differences, whereas the unmodulated version is considered as revealing the differences in concentration.

The "concentration" here should not be confused with the density of the nerves; here, concentration means the proportion of gray or white matter to all tissue types within a region.

2.2.3   Smoothing

Parametric statistical inferences in VBM are performed by assuming that the data is normally distributed. Smoothing makes the data more normally distributed, and usually it's achieved by convolving the images by a Gaussian kernel. Smoothing can also improve the intersubject registration by removing the tiny differences between the subjects. Additionally, smoothing conceals the small false positive regions by averaging the borders with the neighboring voxels (in accordance with the matched-filter theorem), which leads to increased signal-to-noise ratio. However, large kernels may also connect disconnected small regions and create artificially larger areas.

2.2.4   Statistical Analysis

Statistical inferences could be made by various methods, including voxel wise methods, cluster based methods [32], or permutation based methods [33]. SPM uses a voxel wise univariate approach using General Linear Model (GLM) to identify which regions are significantly different. GLM postulates relationships between input and observed data in a model like [34]:

$$Y = X\beta + \epsilon \tag{2.2}$$

where Y is the data (variable), X is the design matrix, β represents the parameter vector, and ϵ represents the residuals. The residuals are considered to have zero mean. The parameters can be estimated by least squares. The fitted data $\hat{Y}$ are defined by

$$\hat{Y} = X\hat{\beta} \tag{2.3}$$

where $\hat{\beta}$ is the estimate of β. The contrast is the linear combination of parameters:

$$c_1\hat{\beta}_1 + c_2\hat{\beta}_2 + ... = c^T\hat{\beta} \qquad (2.4)$$

In VBM, generally, t tests or F tests are used to test the hypotheses. The t-statistics are calculated by:

$$t_{df} = c^T\hat{\beta}/SD(c^T\hat{\beta}) \qquad (2.5)$$

where SD denotes the standard deviation and df is the degree of freedom. For Gaussian errors, t_{df} follows approximately the Student distribution. The null hypothesis assumes that $c^T\hat{\beta}$ equals to zero.

2.2.4.1 Covariates. Any confounding effect should be added to the analysis as a covariate, such as age and sex. In order to eliminate the effect of differences in brain sizes, global normalization should be used. Although, total GM or total WM volumes can be used for the global normalization; generally, total intracranial volume is preferred.

2.2.4.2 Correction for Multiple Comparisons. Uncorrected statistical inferences increase the sensitivity, yet, they increase the false positive rates, too. Although SPM can yield the uncorrected results, and uncorrected results were widely used, and still have been used sometimes, nowadays, the uncorrected results have been highly disfavored. In order to decrease false positive rates, multiple correction is used. Multiple correction is necessary when multiple tests are simultaneously performed like the VBM testing all voxels simultaneously. SPM uses Family Wise Error (FWE) correction by using Random Field Theory (RFT) [35] which assumes that the data follow a certain smooth pattern.

RFT is a less conservative method than the Bonferroni correction, and FDR is less conservative method than FWE. Unlike FWE, FDR has more sensitivity in the

expense of a few more false positives. Permutation tests on the other hand, runs the statistical calculations for all possible models which brings high computational cost but have an advantage of not having an obligation to make any assumptions about the data.

2.2.4.3   Masking.   Masking improves the power of the FWE (Family Wise Error) correction using RFT (random Field Theory), since FWE is more powerful in smaller regions. It is also important for the successful estimation of the smoothness of the residuals, preventing non-brain voxels to skew the distribution of the p-values, and false positives outside of the brain[36]. However, attention is needed to prevent the exclusion of true brain regions by overly restrictive masks.

In SPM, the masks can be explicitly prepared (images of ones and zeros), or automatically computed by defining a constant value for thresholding, or defining a relative ratio to each image's global value. The global value is computed by averaging all voxel values which are above the one eighth of the mean of all voxels.

2.3   Discussions on the VBM Pipeline

2.3.1   Discussions on Registration and Segmentation

Shortly after Ashburner and Fristons's (2000) [14] article, Bookstein (2001) [37] claimed that VBM should not be used until the whole registration steps and characteristics well defined since its results are sensitive to the registration method. Ashburner and Friston opposed to this argument (2001) [38]. They claimed that the method that was proposed by Bookstein (1999) [39] was dependent on the manual landmarking and manual landmarking was also sensitive to the various effects such as changes in the researchers that created the landmarks, and to the data itself.

Although it is supposed that the better the registration, the better the VBM

results and DARTEL was superior to the unified segmentation (prior segmentation + normalization algorithm in SPM), Pereira et al (2010) [40] compared the registration results of different diseases and different anatomical regions by unified segmentation and DARTEL registration, and they have concluded that in some cases unified segmentation is superior to DARTEL, and in some cases just the opposite. Mak et al(2011) [41] have also found the similar results while studying hippocampi of Alzheimer's Disease Patients.

Nordenskjold et al (2013) [42] have shown that SPM and Freesurfer yield different total intracranial volumes which leads to find different associations with cognition and gender. However, they added that for a gold reference they used an interactive segmentation tool which was based on PD weighted MR images, where it was easier to differentiate bone from CSF and they remarked that they observed that SPM categorized bone as CSF at some points.

2.3.2   Discussions on Modulation

Since the aim of the modulation is quite straightforward (keeping the original volume of the tissue which was artificially enlarged or shrinked during the normalization), the experimental validity was not interrogated much. Radua et al (2014) [43] explored this issue. Their images were acquired from 128 healthy subjects. The images (grey matter only) were segmented by FSL. They formed 10 independent pairs of groups, where each pair consists of 32 (16 men/16 women) subjects with similar ages. Then, they simulated large, medium, and small reductions in the cortical thickness at some regions. They analyzed the resulting images by both SPM and VBM, by both voxel-based and cluster-based spatial statistics, and concluded that modulation significantly reduces the sensitivity in both cortical and subcortical abnormalities, and for all sizes. That reduction of sensitivity might be due to the possible multiplicative noise (inter-subject variability on brain shape) that is introduced by the multiplication of not only the data but also the noise by the Jacobian determinant. They have found that although the mean differences between two groups in case of both modulation

and unmodulation were close to each other, the variance of the residuals in modulation was almost 5 times the unmodulated case. They remarked that multiplicative noise is higher in high resolution registration methods (due to larger removals of macroscopic differences). They also noted that the false positive rates were similar in modulated and unmodulated versions.

In 2009 [44], using simulated data (lesions in white matter) we have also found that modulation decreases the sensitivity in white matter.

2.3.3   Discussions on Smoothing

Salmond et al[45] (2002) concluded that provided the data are smoothed with a 12-mm FWHM kernel, nonnormality is sufficiently attenuated to render the tests valid; and in balanced group comparisons, analyses appear to be robust even without smoothing.

Shen et al [46] (2012) demonstrated that a better nonlinear registration method needs smaller kernel size for the smoothing. They also concluded for their simulation data, for a group size of 25, the required kernel size was 8-10mm; for a group size of 50, the required kernel size was 6mm.

2.3.4   Discussions on Statistics and Masking

Scarpazza et al (2015) investigated the suspicion about the false positive rates in VBM [47]. They generated 100 groups for each group sizes of 8, 12, and 16 subjects from the pool of 198 subjects. They found that the false positive rates are always smaller than 5%, by experimenting the following parameters: Smoothing (experimenting by 4mm, 8mm, and 12mm), modulated and unmodulated versions.

Bennet (2009) [48] underlines the rule that in neuroimaging studies uncorrected

results should not be reported since the protection against Type I error is an absolute necessity for moving forward. Their test was on multiple testing using a 50x50 square section of signal in the center of a 100x100 image with added Gaussian random noise. The tests yielded that although the uncorrected results have a power of 0.80, there are number of false positives. Whereas, familywise error rate control decreases the power to 0.16, but no false positive survives. False discovery rate control brings a power of 0.54 with 4.9% false positives.

Bennet (2009) [48] also reminds that small volume correction (SVC) in VBM was misunderstood in some studies. SVC should not be performed on the small region that is determined after the whole brain VBM; that region should be identified in previous independent dataset.

In order to successfully estimate the smoothness of the residuals and also since FWE correction is more successful in smaller areas, we need to use masks. As an improvement to SPM's default threshold masking, Ridgway (2009) [36] proposed another masking tool which is based on an average-based mask. In this tool, not an absolute threshold but rather a threshold which supplies the maximum correlation between the unthresholded average image and the mask that is created by thresholding the average image is used. Both their tests on simulation data and our tests on both real and simulation data [49] have shown that this way of masking improves the sensitivity of VBM.

From the aspect of single case vs group comparisons, single case studies should not be used since they have a very high false positive rates [50]; where these high false positive rate are not seen in case of balanced and equal sized groups' comparisons[47].

Peelle et al. (2012) [51] explored the effects of using different parameters as a covariate for adjusting the global effects. Although, TIV (Total Intracranial Volume) is usually considered as a covariate of no interest in GLM; they reminded that TGM (Total Grey Matter) might be used to find the local variance, mean GM can be used to find the rate of change at a voxel, and LGM (mean GM for a region across subjects)

is highly related to the age-related atrophy.

2.4 Multi-Center Studies

In recent years, there is a growing interest in establishing multi-center, large image data pools to conduct more powerful investigations in neuroanatomy and neurodegenerative diseases like Parkinson's Progression Markers Initiative (PPMI)[2] , Alzheimer's Disease Neuroimaging Initiative (ADNI)[3] , and Open Access Series of Imaging Studies (OASIS)[4] .

A recent study of Takao et al (2014) [52] was on the effects of using multicentered images on VBM. They have concluded that, as long as the ratio of cases to controls is well balanced across the centers, there is often no need to add center as a covariate; on the other hand, in case of ill-balanced ratios, adding centers as a covariate is needed. However, this attenuates the sensitivity of the comparison.

Focke et al (2011) [53] have shown that multicenter scanning can mimic the real physical differences especially in unbalanced group comparisons. Although they have used the same scanner model at two different sites, they have used different head coils, which might be the source of these differences. They have made a remark about the coils in multicenter studies, in which, this issue is usually not taken into consideration. They have also found that SPM outperforms FSL in multicenter data comparisons.

Jovivich et al (2013) [54] have shown that even with different scanner models and different protocols, longitudinal studies might give reasonable results.

---

[2]http://www.ppmi-info.org
[3]http://adni.loni.usc.edu
[4]http://www.oasis-brains.org

2.5   Minimum Number of Subjects for a VBM Analysis

Pell et al (2008) [55] has analyzed the VBM data from hippocampal sclerosis patients (n=30) and control group (n=176), and they found that the detection power is increasing while the number of control subjects is increasing. On the other hand, Friston (2012) [56] claimed that the optimal group size should be between 16-32, in order to avoid unreliable results. He states that in big cohorts, even small changes can become significant; yet in small cohorts, only large effects can become visible. Opposing to that suggestion, Hupe (2015) [57] claims that false positives may arise in small groups due to sampling error, since sampling error is inversely proportional to sampling size.

In a study by Shen (2007) [58], the groups of sizes 50, 35, 25, and 15 were created and the detection power of simulated atrophy was explored. They observed that the simulated atrophy cannot be detected in the group having the size of 15. Tardif et al (2009) [59] observed that, the necessary group sizes may vary according to which part of the brain was observed.

2.6   Cross Sectional vs Longitudinal VBM

Morphometric methods could be longitudinal (using the same subject at different time points) or cross-sectional (at a particular time using different subjects). Some characteristics investigated by VBM are inherently longitudinal, such as growth and aging, responses to some drugs and substances, plasticity, etc. Longitudinal VBM might have more power with respect to cross-sectional VBM in these issues, because sensitivity to small changes will be higher in intra-subject images than the inter-subject images. An example for a longitudinal VBM was performed by Draganski et al (2004) [60] in which the plasticity due to juggling training was investigated.

In longitudinal VBM, there are various ways to register the images: Registering

the images to baseline image, or creating an average template by averaging intersubject or intrasubject images. Registering images onto the baseline image might bring problems such as finding atrophies beyond the physiological possibilities as pointed out at Thompson and Holland (2011) [61]. Registering all images to within subject average can prevent the problems from this asymmetry as described in Ashburner et al (2012) [62].

2.7   Effects of Using different tools in VBM Analyses

Rajagopalan, et al (2014) [63] compared the VBM results of FSL and SPM for Alzheimer's patients (5 men, 13 women) vs control subjects (10 men, 5 women). They have found that the percentage of significantly different voxels greatly differs between the two tools: %22.5 in FSLv4.1.5, and 0.82% in SPM8. Although the segmentation results are very similar in SPM and FSL, the normalization step (DARTEL in SPM and FNIRT in FSL) affects the results. 0.81% of the voxels reached the statistical significance in nonparametric statistical approach, whereas 0.51% voxels reached in parametric approach in SPM. Additionally, SPM and FSL differs in the significant regions, too: In FSL, motor and extramotor regions seem affected, however in SPM, only extramotor regions are found affected.

As mentioned in the section 2.3.1, Nordenskjold et al (2013) [42] have shown that SPM and Freesurfer yield different total intracranial volumes.

Popescu et al (2016) [64] compared SPM, Freesurfer and FSL by using data of MS (Multiple Sclerosis) and Diaz-de-Grenu et al (2014) [65] on Alzheimer's patients. They concluded that these software packages could yield different results.
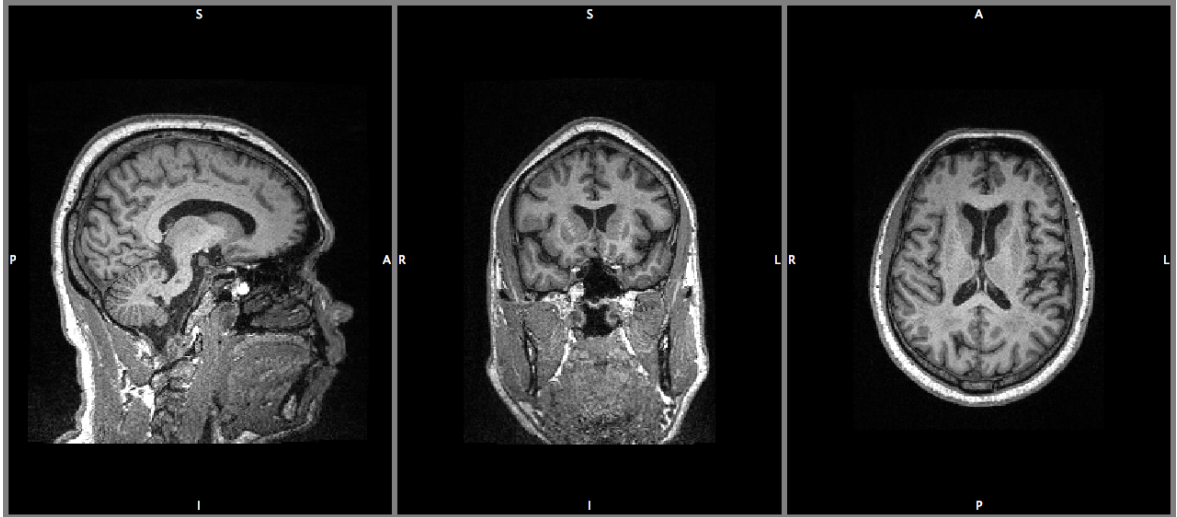
Figure 2.1 The original MR image shown by fslview
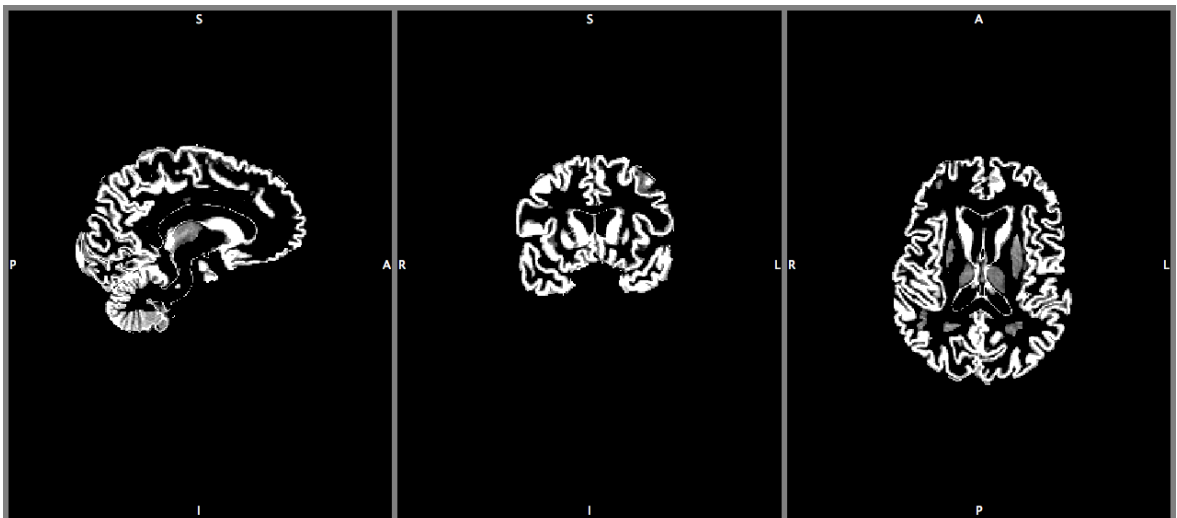
Figure 2.2 Segmented grey matter
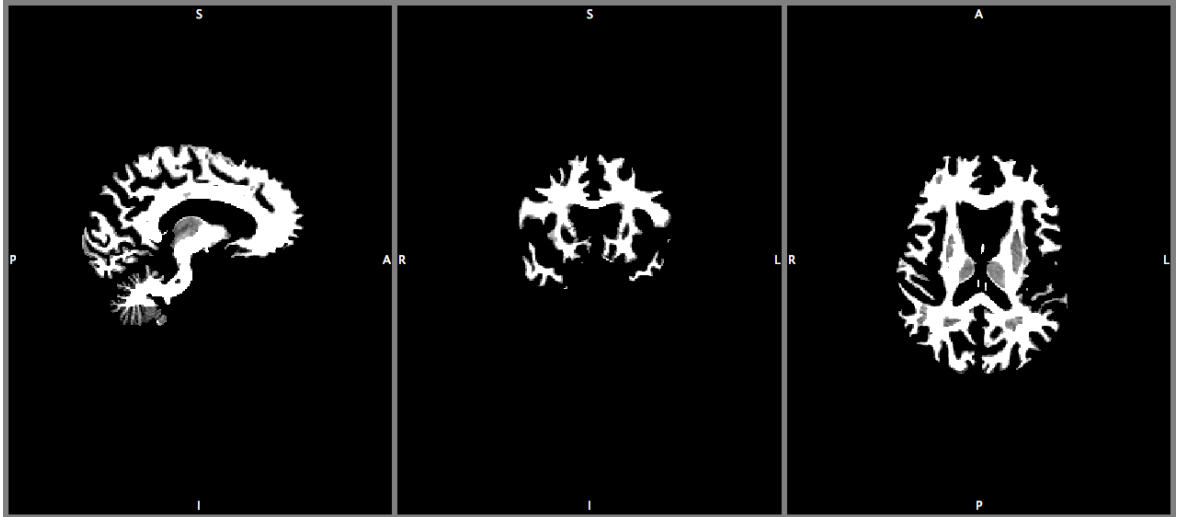
Figure 2.3 Segmented white matter
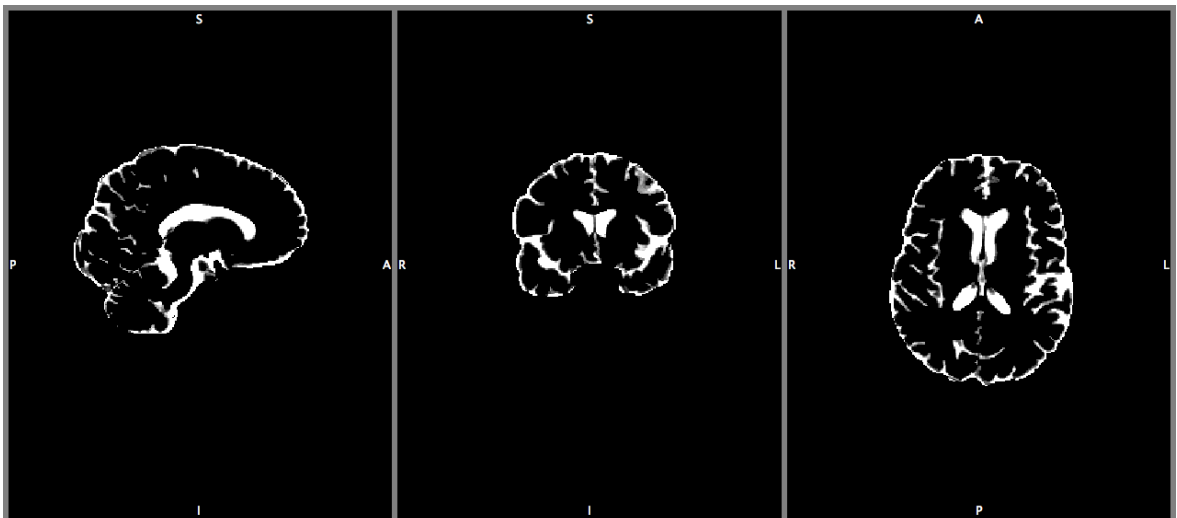
Figure 2.4 Segmented cerebrospinal fluid
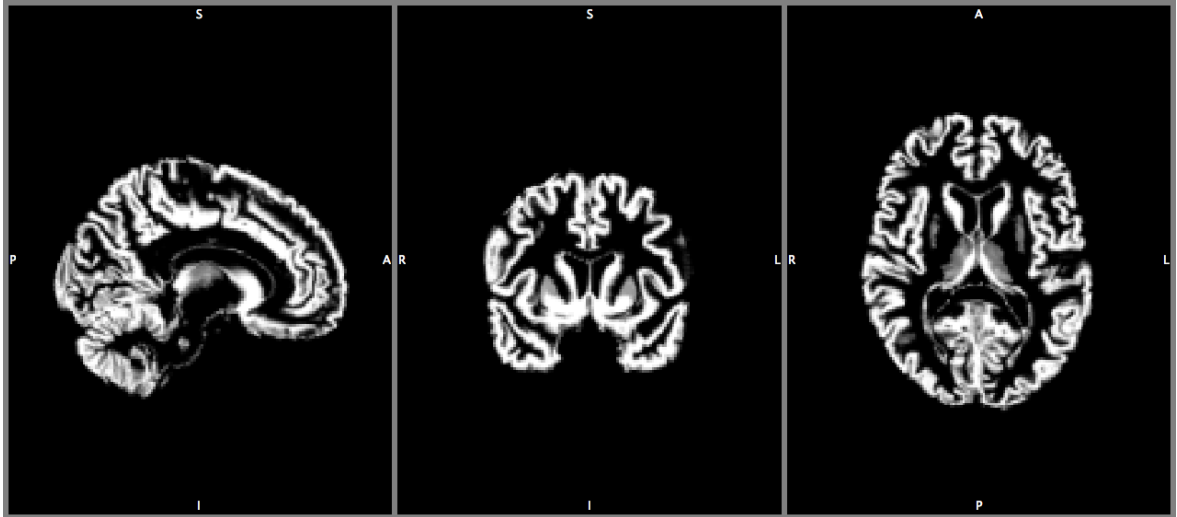
Figure 2.5 Warped grey matter
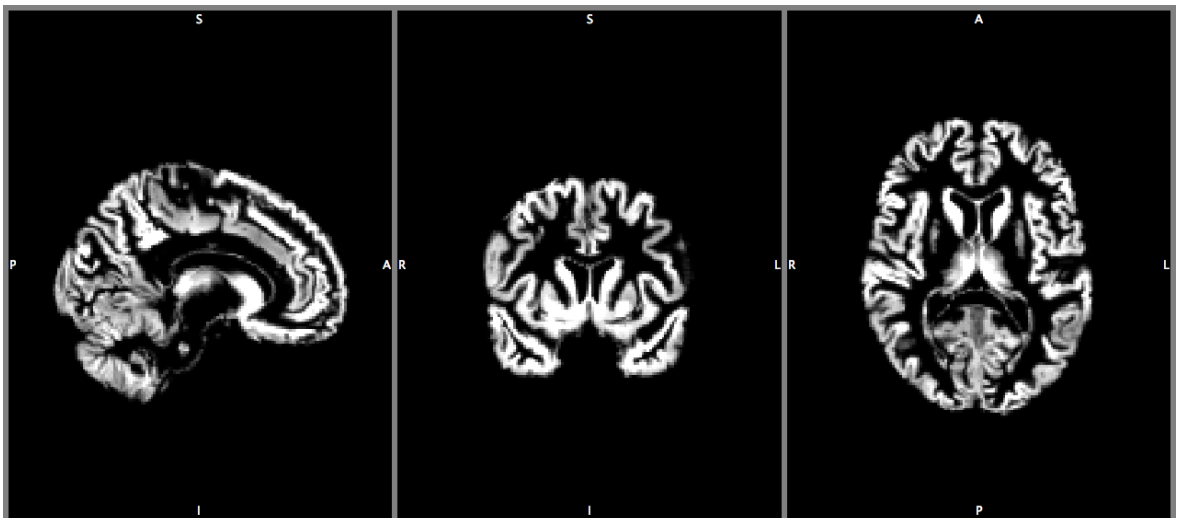
Figure 2.6 Modulated and warped grey matter
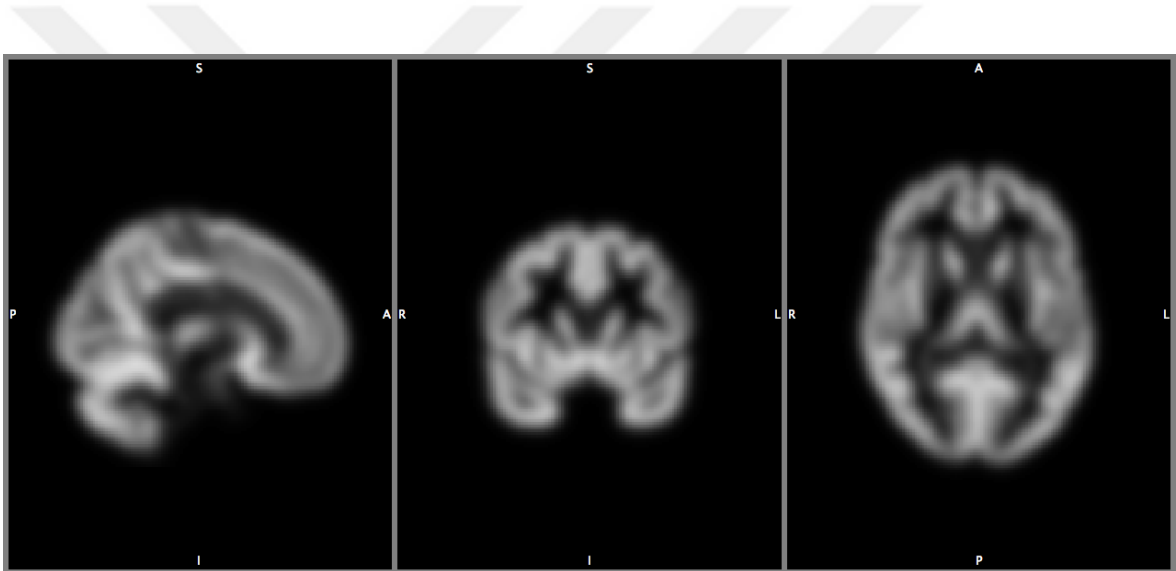
Figure 2.7 Smoothed warped grey matter

SPM{T$_{47}$}
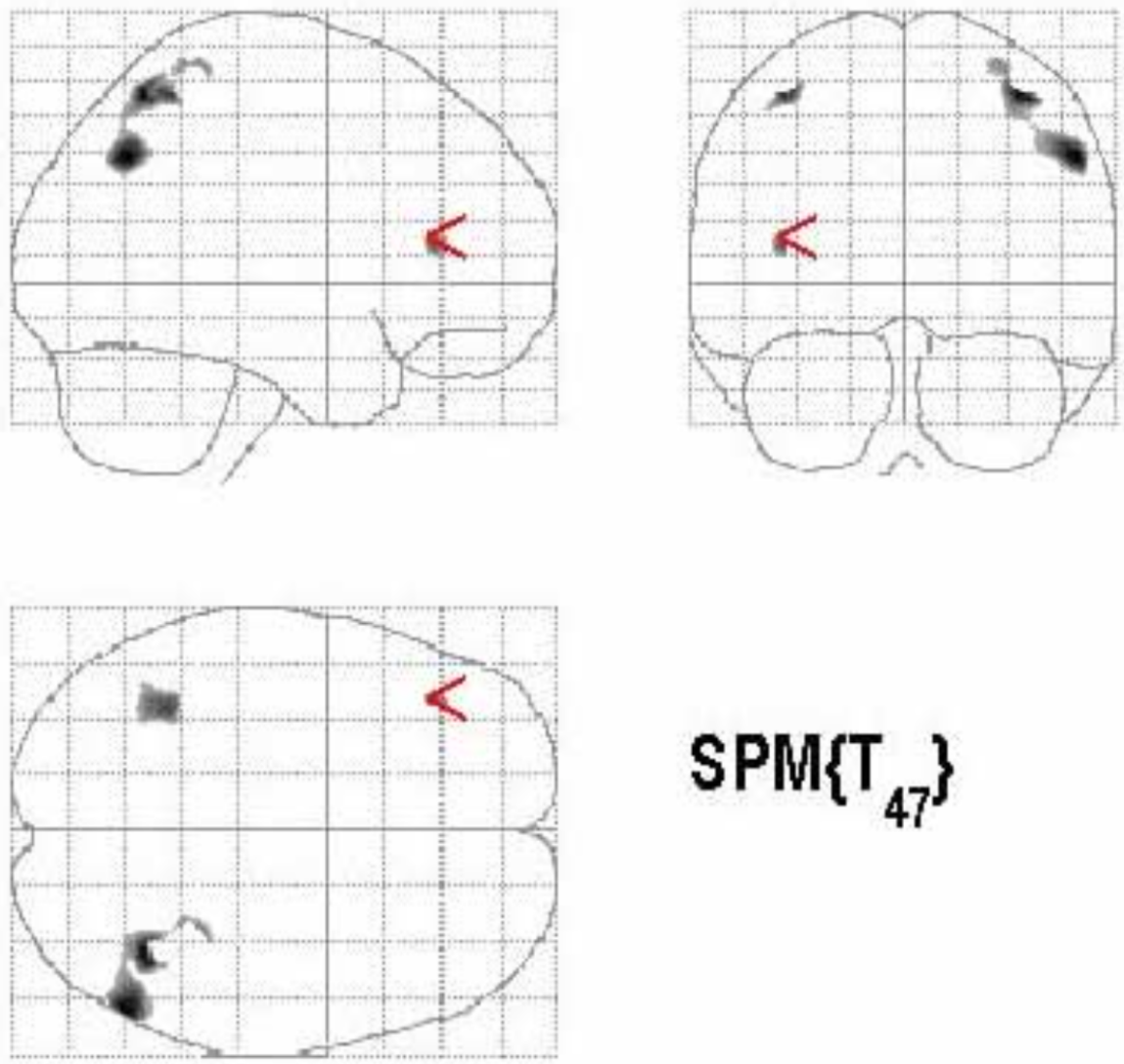
Figure 2.8 Resulting statistical parametric map on the glass brain

3. Other Brain Morphometry Methods

The following sections summarize some of the brain MR morphometry methods other than VBM.

3.1 Deformation Based Morphometry

VBM uses the registered images in its analysis, whereas, Deformation Based Morphometry (DBM) uses not the registered images but the deformation fields that appear during the registration process. In DBM, a single multivariate testing can be used on the parameters which describe the deformation.

As a variant of DBM, Tensor Based Morphometry (TBM) focuses on the differences in the local shapes by using Jacobian determinants (see the equation 2.1) to examine the relative volumes. It establishes a statistical parametric map approach to DBM [66].

3.2 Cortical Thickness Methods

An alternative to volume based morphometry methods is to evaluate the cortical thickness. The initial processing step is similar to VBM: Segmentation of GM, WM, and CSF. The subsequent step is to find the inner and outer surfaces of GM, and then to determine the distance between these two surfaces.

Freesurfer (see section 3.3) is a widely used surface based tool for the cortical thickness measurements. Hutton et al (2008) [67] measured the cortical thickness by their own algorithms (VBCT) which is based primarily on SPM. In their another study (2009) [68], they concluded that VBCT is more sensitive of age-associated decline in grey matter, whereas VBM is sensitive to local surface area and cortical folding.

3.3   Surface Based Methods

Surface Based Analysis (SBA) is based on the cortical surface measurements. There are various tools for SBA including Freesurfer (http://surfer.nmr.mgh.harvard.edu), Brain Voyager (http://brainvoyager.com), and Brain Visa (http://brainvisa.info). The first step of the SBA is the extraction of cortex from the MRI data [69]. The inner surface of the cortex is the *white surface*, which is the surface between GM and WM. The outer surface of cortex is the *pial surface* which resides between GM and CSF or dura mater. The surfaces can be reconstructed by the construction of meshes of triangles on the surfaces, in which the corners of the triangles are called as vertex. Then, these surfaces can be inflated after marking the gyri and sulci areas.

With these surfaces in hand, various morphometric measurements can be done including surface area measurements, gyrification and curvature analysis, cortical thickness (the distance between the white and pial surfaces).
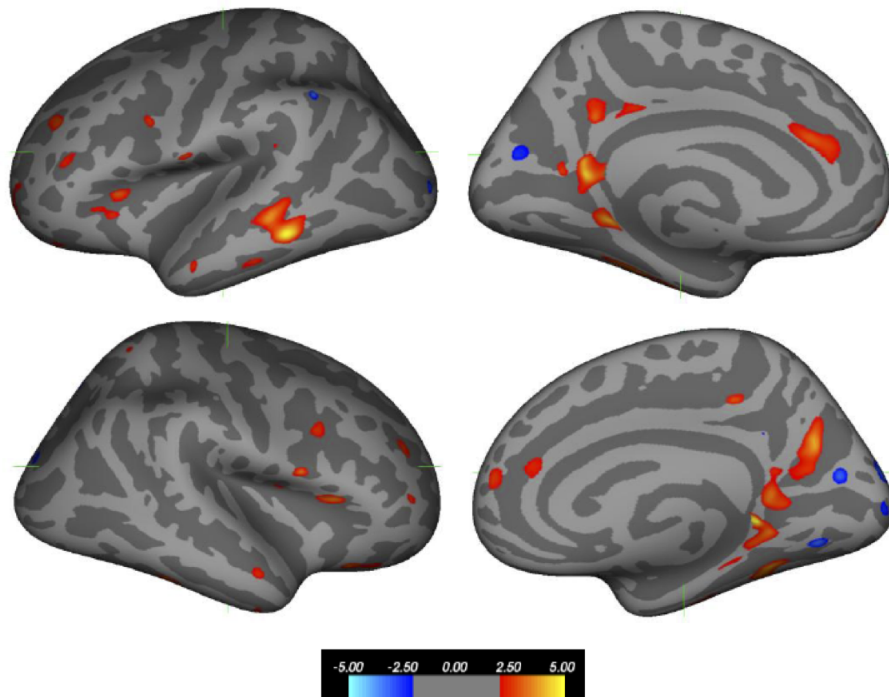
Figure 3.1 An inflated surface with results of a cortical thickness comparison by Freesurfer

3.4 Feature Based Methods

There are some new and promising morphometric methods based on pattern or feature discovering. One of them is the Feature Based Morphometry, as proposed in Toews et al (2010) [70]. It's described as a data-driven technique based on discovering patterns for group wise morphologic comparisons. A similar algorithm was developed by Wang et al (2012) [71] under the name of MEACOLP (Morphometry Based on Effective and Accurate Correspondences of Localized Patterns).

A further improvement on feature based morphometry was developed by Chen et al (2014) [72] using local feature based SVM (support vector machine) approach.

In K-SVD -a dictionary learning algorithm-, images are represented as a linear combination of small images. Pattern Based Morphometry, which was based on K-SVD, was proposed by Gaonkar et al (2011) [73].

It is claimed that these methods do not depend on general linear model but on the characterization on the individual level, therefore have the superior potential for the clinical translation and also they are inherently multivariate approaches which might increase the sensitivity [74].

4. Effects of Unmodulation and Thresholding by Average Based Masking on VBM

4.1 Introduction

Voxel-based morphometry (VBM) [14] is one of the most popular analysis tools in neuroimaging. VBM is an unbiased and fully automated voxel-based statistical approach that aims to reveal the structural differences between groups of whole-brain MR images. Parkinson's disease (PD) has been widely investigated using VBM in numerous studies [15, 75–93]. These studies have examined patients in early, mild, moderate, and severe stages of PD [15, 75, 78, 79, 84, 87] with or without the symptoms of dementia [83], freezing [77], tremor-dominancy and predominantly postural instability gait difficulty [81], excessive daytime sleepiness [85], subjective memory complaints [86], depression [90] and several other symptoms (Table 4.1).

In VBM, the images go through an image-processing pipeline before the statistical analysis. As a first step, the images are segmented into tissue types (GM, WM, and CSF) and normalized (registered) onto a common template. An optional modulation can be applied to the segmented images by multiplying the voxels by the Jacobian determinants in an attempt to regain the original volumes [27]. Although modulation is generally recommended and widely used in all VBM studies, a recent study by Radua et al. emphasized that modulation lacks experimental validity and decreases the power of detection in mesoscopic differences [43]. After the modulation or bare segmentation and normalization step, the images are smoothed.

In VBM, the final statistical operations are performed at the voxel level. To arrive at a successful estimation of the smoothness of the residuals, and because FWE using random field theory is more successful in smaller regions, masking is applied to determine the voxels to be included in the statistical analysis [36]. As a masking strategy, absolute thresholding is the most widely recommended and used method.

Ridgway et al stated that this approach might miss some true positive regions and suggested using average-based mask after careful observation of the images.

In early-stage, nondemented PD patients, previous VBM reports (those that used corrected results only) were unable to identify any affected regions [15, 78, 79, 84, 87], whereas some of these studies reported correlations between GM atrophy and phonemic verbal fluency (at precuneus, cerebellum and caudate) [75] and olfactory function (at pyriform cortex) [89]. As we see in the supplemental Table 4.1, most of the PD-VBM studies used modulated images (26 of 32 studies used modulation; unmodulated studies: [88, 91]; studies that were not specified if modulated or not: [77, 80, 92, 93]), and also, most of the PD-VBM studies did not note their masking strategies; whereas the studies that mentioned it primarily used absolute thresholding and none of them used averaged based masking. Therefore, in order to investigate the effects of unmodulation and averaged-based masking on VBM, in this study, we performed a series of VBM analyses to search for the structural brain differences in early-stage, nondemented PD patients using an average-based mask in the statistical analysis step instead of absolute thresholding and without modulating the data after the normalization. To validate these choices, we also created an atrophy simulation data set.

Table 4.1: Previous PD-VBM studies. AT: Absolute thresholding, NM: Not Mentioned, SVC: Small Volume Correction

Article	Subjects	Tool	Tissue	Modu-lation	Smooth-ing	Global calculations and nuisance variables	Masking	Statistical threshold
Ellfolk, 2014	28 Younger (mean age<65) Early stage (mean disease duration<3 years) nondemented, 27 Healthy	SPM8	GM	Yes	10mm	Age, TIV. (Multiple regression with semantic, phonemic, and alternating fluency)	AT=0,1	Uncorrected (p<0.005) FWE (p<0.05) at cluster level
Gerrits, 2014	97 PD: 8 MCI, 4 Demented, 6 Unknown, 46 Healthy	SPM8	GM	Yes	10mm	Total GM volume(Age, sex, education, total GM volume in regression analysis)	AT=0.2	Uncorrected (p<0.001) with cluster size>50
Herman, 2014	30 Freezing PD, 76 Nonfreezing PD (2nd analysis: 22 Freezing PD matched with 22 Nonfreezing PD)	SPM5	GM	NM	NM	With or without age and disease duration	NM	Uncorrected (p<0.005)FWE (p<0.05) at cluster level
Lee, 2014	49 Early stage nondemented right-handed, 53 Healthy	SPM8	GM	Yes	8mm	TIV, age, sex (Multiple regression with disease stage, disease duration, motor impairment)	AT=0,2	FWE (p<0.05)

Article	Subjects	Tool	Tissue	Modu-lation	Smooth-ing	Global calculations and nuisance variables	Masking	Statistical threshold
Lopes Gama, 2014	11 PD with hallucinations (6 of them cognitive dysfunction), 28 PD without hallucinations, 10 Healthy	SPM8	GM	Yes	12mm	NM	AT=0,05	Uncorrected (p<0.001) than SVC with FWE p<0.05
Menke, 2014	20 Early stage nondemented right handed, 20 Healthy	FSL	GM	Yes	3mm	NM	NM	FWE (p<0.05)
Agosta, 2013	17 Early stage, 46 Mild stage, 14 Moderate stage, 12 Severe stage, 42 Healthy	SPM8	GM	Yes	8mm	TIV (regression with UPDRS III and MMSE)	NM	FWE (p<0.05)
Lin, 2013	10 PD, 13 Healthy	SPM8 (with and with-out DAR-TEL)	GM	NM	8mm	NM	NM	Uncorrected (p<0.05) with cluster size>50

Article	Subjects	Tool	Tissue	Modu-lation	Smooth-ing	Global calculations and nuisance variables	Masking	Statistical threshold
Rosenberg-Katz, 2013	30 tremor-dominant PD, 29 predominately postural instability gait difficulty PD	SPM5	GM	Yes	8mm	Age and disease duration	AT=0.2	FDR (p<0.05)
Braga-Pereira, 2012	20 Nondemented PD, 20 Healthy	SPM8	GM WM	Yes	12mm	age and sex	AT=0.1	FWE (p<0.05)
Compta, 2012	15 PD demented, 18 PD nondemented, 12 Healthy	SPM5	GM	Yes	8mm	TIV, age, (UPDRS III in all PD groupmultiple regression with CSF as independent and GM volumes as dependent)	GM	Healthy>DEMENTED and NONDE-MENTED>PD:FWE (p<0.05) Healthy > NON-DEMENTED:Uncorrected (p<0.005)
Ibarretxe-Bilbao, 2012	16 Early PD, 15 Healthy	SPM8	GM	Yes	12mm	TIV (in longitudinal VBM: scan interval in months)	NM	FWE (p<0.05)

Article	Subjects	Tool	Tissue	Modulation	Smoothing	Global calculations and nuisance variables	Masking	Statistical threshold
Kato, 2012	9 PD with excessive daytime sleepiness, 13 PD without excessive daytime sleepiness, 22 Healthy	SPM5	GM	Yes	12mm	TIV, age, sex	NM	Patient vs Healthy:FDR (p<0.05) Between patient groups:Uncorrected (p<0.001), k>50, z>3.0
Yong Hong, 2012	15 PD without subjective memory complaints, 20 PD with subjective memory complaints, 25 Healthy	SPM8	GM	Yes	6mm	Age and GM volume	NM	Uncorrected (p<0.001), cluster size>100mm3
Biundo, 2011	33 PD with impulse control disorders, 24 PD without impulse control disorders,Â 22 Healthy	SPM8	GM	Yes	8mm	TIV, age, number of years of education, sex, group(regression analysis: GM and TMTB-A scores)	NM	Cluster-level FWE (p<0.05), cluster size>100for the areas not surviving but anatomically expected:Uncorrected (p<0.01)
Ceresa, 2011	36 Dyskinetic PD, 36 Nondyskinetic PD, 32 Healthy	SPM8	GM	Yes	8mm	TIV, age(Correlation analysis using age at onset and therapy duration)		FWE (p<0.05) For correlation analysis: Uncorrected (p<0.001), cluster size>10

Article	Subjects	Tool	Tissue	Modu-lation	Smooth-ing	Global calculations and nuisance variables	Masking	Statistical threshold
Focke, 2011	21 PD, 22 Healthy	SPM8	GM WM	Yes	8mm	TIV	AT=0.05	Uncorrected (p<0.001) with cluster size>50
Meppelink, 2011	11 Visual Hallucinations PD, 13 without VH PD, 14 Healthy	SPM5	GM	Yes	10mm	Total GM volume	NM	Uncorrected (p<0.001) with cluster level pFWE<0.05
Kostic, 2010	16 PD with depression, 24 PD without depression, 26 Healthy	SPM5	GM WM	Yes	8mm	TIV, age, sex	Masking by the results of other contrasts	FWE (p<0.05) and uncorrected (p<0.001), cluster size>20
Lee, 2010	20 PD demented, 18 Healthy	SPM8	GM	Yes	6mm	NM	NM	Uncorrected (p<0.001) with cluster size >50
Martin, 2009	26 Early stage, 14 Healthy	SPM5	GM WM	Yes	12mm	TIV, age, sex, group, education	NM	FDR (p<0.05), cluster size>50
Pereira, 2009	36 PD, 20 Healthy	SPM5	GM	No	12mm	(Visiospatial and visioperceptual test scores in multiple regression analysis)	NM	FDR (p<0.05)

Article	Subjects	Tool	Tissue	Modulation	Smoothing	Global calculations and nuisance variables	Masking	Statistical threshold
Sanchez-Castaneda, 2009	16 PD demented, 16 Healthy	SPM5	GM	Yes	8mm	Education in years, UPDRS-III score, disease duration in predefined ROIs	NM	FWE (p<0.05) in predefined ROI's extracted by Pick Atlas of SPM
Wattendorf, 2009	15 Early stage PD, 12 Moderately Advanced PD, 17 Healthy	SPM5	GM	Yes	8mm	Total GM volume (In PD group: H-Y score, disease durationMultiple regression by olfactory performance)	NM	Uncorrected (p<0.001), cluster size>800 voxels
Feldmann, 2008	23 Depressed PD, 27 Nondepressed PD, 16 Healthy	SPM2	GM	Yes	8mm	Age, sex (MADRS scores in multiple regression analysis)	NM	FDR (p<0.05)
Ibarretxe-Bilbao, 2008	9 Demented, 16 PD with Visual Hallucinations, 19 PD without Visual Hallucinations, 56 Healthy	SPM2	GM	NM	6mm	(Correlation analysis using memory and GM volume)	NM	FDR (p<0.05) on hippocampal volume
Beyer, 2007	8 Nondemented with MCI, 12 Nondemented without MCI, 16 DEMENTED, 20 Healthy	SPM2	GM	No	12mm	Age, sex, disease duration	NM	Uncorrected (p<0.001) than SVC with FWE p<0.05, cluster size>200mm3

Article	Subjects	Tool	Tissue	Modu-lation	Smooth-ing	Global calculations and nuisance variables	Masking	Statistical threshold
Ramirez-Ruiz, 2007	18 PD with Visual Hallucinations, 20 PD without Visual Hallucinations, 21 Healthy	SPM2	GM	Yes	12mm	TIV, MMSE, Hamilton, Hoehn-Yahr scores	NM	Uncorrected (p<0.001) with cluster level pFWE<0.05
Nagano-Saito, 2005	39 Nondemented (19 Advanced Nondemented), 9 Demented, 31 Healthy	NM	GM	NM	8mm	In some comparisons: disease duration(Multiple regression: intellectual tests)	NM	Uncorrected (p<0.001) with cluster level pFWE<0.05
Summer-field, 2005	16 Demented, 13 Nondemented, 13 control	SPM99	GM	Yes	NM	NM	NM	Uncorrected (p<0.001), cluster size>10 voxelsÂ in predefined ROI's extracted by Pick Atlas of SPM
Burton, 2004	31Â PD, 26 Demented, 36 Healthy	SPM99		NM	NM	TIV or mean GM	NM	Uncorrected (p<0.001)
Brenneis, 2003	12 PD, 12 Control	SPM99	GM WM CSF	NM	10mm	NM	NM	P < 0.05 corrected for multiple comparisonIn putamen: SVC

4.2 Materials and Methods

4.2.1 Data

We performed VBM analyses on PD vs control images (4.2.1.1), and also on images with simulated atrophy vs control images (4.2.1.2).

4.2.1.1 Original PD Images. The images were taken from the Parkinson's Progression Markers Initiative (PPMI) database located in the Laboratory of Neuro Imaging (LONI) database at the University of Southern California in Los Angeles, CA. Although the images were taken with different scanners at different centres, all the patients in our study were scanned using the same MR scanner model (Siemens Tim Trio 3T, Germany) with exactly the same sequence parameters (MPRAGE GRAPPA, T1 weighting, voxel size 1x1x1 mm, TE 2.98 ms, TR 2300 ms, TI 900 ms, flip angle 9o). After excluding subjects which differ in their imaging parameters, and who were very young (<50 years), very old (>80 years), left-handed, or demented. After excluding subjects which differ in their imaging parameters, and who were very young (<50 years), very old (>80 years), left-handed, or demented, as well as subjects with cognitive impairments (Montreal Cognitive Assessment, MoCA < 25), and the image sets with minor Gibbs effect artefacts; we were left with 21 early-stage PD patients (from the original patient pool) and 20 healthy subjects. The subjects' demographic information is presented in Table 4.2.

4.2.1.2 Simulation Data. Artificially modified PD-MR images were produced to simulate GM atrophy in cubic regions that were centered at the left hand motor area [94] and had an edge length of 18 mm. Since, morphological reductions are used by several studies to simulate atrophy or lesion (e.g. Acosta et al [95]), in this study, cortical thinning was achieved by eroding GM voxels at the GM-CSF border and then smoothing the voxels around the border, as seen in Figure 4.2.1.2. The mean volume of an atrophied region was 270 ± 140 mm3.

Table 4.2
Demographic information of the PD patients and healthy groups.

	PD (n=21)	Control (n=20)	P-value
Male/female	11/10	15/5	0.1
Age (years)	62.4 ± 6.1	64.5 ± 5.1	0.2
Disease duration (years)	3.1 ± 1.3	NA	NA
Age at onset (years)	59.4 ± 6.5	NA	NA
MoCA score	28.1 ± 1.4	27.9 ± 1.1476	0.5
Hoehn-Yahr score	1.6 ± 0.6	NA	NA
TIV (ml)	1476 ± 147	1394 ± 131	0.07
Center scanning the images			
Center 1	2	2	
Center 2	3	5	
Center 3	4	3	
Center 4	2	1	
Center 5	4	3	
Center 6	1	2	
Center 7	3	2	
Center 8	2	2	
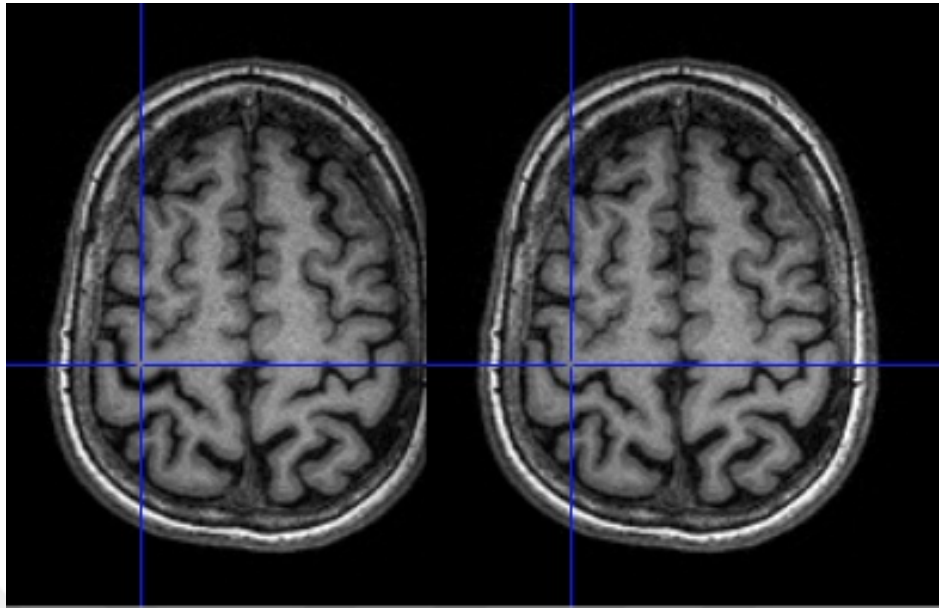
Figure 4.1 Simulation of atrophy centered at the left hand motor area of the precentral gyrus

4.2.2 Image Processing and Analysis Tools

The VBM8 toolbox (http://dbm.neurfo.uni-jena.de/vbm/download/) of SPM8 (Statistical Parametric Mapping, http://www.fil.ion.ucl.ac.uk/spm/software/spm8/) running on MATLAB R2014a (www.mathworks.com) software was employed for the VBM pre-processing and statistics.

For a VBM analysis with SPM8, we followed the recommendations of Ashburner [96]: The images were first segmented using a unified segmentation procedure [28], and the DARTEL algorithm was used to normalize the images [29]. Then the images were smoothed with a 10-mm kernel size after the modulation of segmented and normalized images. At the statistical stage, images were corrected by TIV, using sex and age as nuisance variables and masking to exclude non-GM voxels to increase the power of the corrections for multiple comparisons. Absolute thresholding was denoted as the primary method of masking, and 0.2 was selected as a preferred threshold for the GM masking. Additionally, although our images were scanned in the same scanner model and with exactly the same scanning parameters, we included the centre as a covariate in the general linear model of the SPM (eight centres in total). In addition to this

Table 4.3

VBM results with the simulation region at the left hand motor area of the precentral gyrus ($P<0.05$, after correction for multiple comparisons, using FWE.

	Modulation	Masking strategy	Max T	Cluster size
1	Yes	Absolute threshold: 0.2	6.53	101
2	Yes	Average based mask	6.53	117
3	No	Absolute threshold: 0.2	6.12	48
4	No	Average based mask	6.12	214

standard procedure, we also performed the analyses without modulation and using an average-based mask instead of absolute or relative thresholding. Average-based mask was created using the tool of Ridgway et al [36]. In their tools, they used the average of all subjects which is thresholded by not an absolute threshold but rather by a threshold which supplies the maximum correlation with the unthresholded average image. Finally, we used FWE correction with $p<0.05$ in all the results.

4.3 Results and Discussion

4.3.1 Simulation

VBM analyses of the PD-MR images with simulated atrophy vs. the control images was repeated four times under the following conditions: A) the traditionally accepted procedure: modulation + absolute thresholding with a threshold of 0.2; B) modulation + average-based masking; C) no modulation + absolute thresholding; and D) no modulation + average-based masking. As shown in Table 4.3, the largest cluster size was achieved with the "no modulation" + "average-based mask" combination with a cluster size of 214, whereas in the generally followed practice (modulation + absolute thresholding), the cluster size was 101.

4.3.2 VBM: PD vs. Control

The VBM analysis without modulation and with average-based masking of the MR images from the PD patients vs. the control group revealed atrophies in the superior temporal (49 voxels with maximum T=5.20 using FWE) and middle temporal gyri (20 voxels with maximum T=5.18 using FWE), which were not detected using modulation or absolute thresholding (Figure 4.3.2). We can also mention the identification of atrophy in the postcentral gyrus with the caveat that the cluster size of this atrophy was less than 10 voxels. With similar cohorts, similar smoothing kernels (in the supplemented table, we see that 25 of the 29 studies used the kernel sizes between 8-12mm, where 3 studies did not mention the size of the smoothing kernel at all); with similar scanner field strength (3T scanners in the majority of the studies); these regions were not detected in previous VBM studies; however, they were previously detected by other studies employing other methods besides VBM in similar cohorts, or by VBM in PD patients in whom the disease had progressed as explained in the following paragraphs:
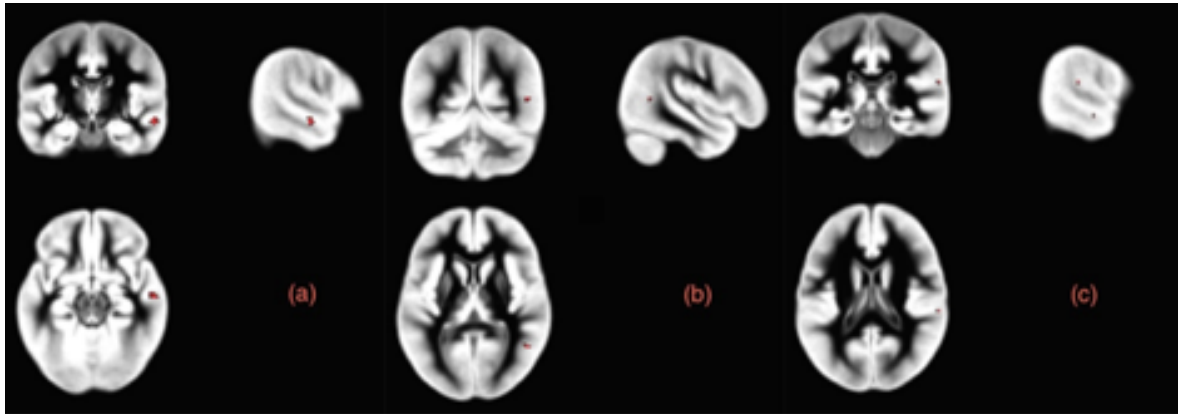
Figure 4.2 Atrophied regions according to the VBM results of PD patients vs. healthy controls. (a) Superior temporal, (b) middle temporal and (c) postcentral gyri in the unmodulated images found by smoothing with a 10-mm kernel size, using TIV in the global calculations and sex, age, and centre info as covariates, and using FWE correction with p<0.05

Superior temporal gyrus: Using cortical thickness analyses, Ibarretxe-Bilbao [97] (early, nondemented PD patients) and Braga-Pereira [82] (mixed PD group) reported atrophy of the superior temporal gyrus. Using VBM, Kato [85] (FDR; covariates:

TIV, age, sex; smoothing: 12 mm; modulated images) reported GM atrophy in the same region in PD patients who suffer from excessive daytime sleepiness. Middle temporal gyrus: Using VBM, Agosta [15] (FWE, covariate: TIV; smoothing: 8 mm; modulated images) reported atrophy in the right middle temporal gyrus in moderate and severe PD patients. They found atrophy in early-stage patients too, however not by VBM but ROI analysis. Using cortical thickness analysis, Pellicano [98] (nondemented, but mixed disease duration and Hoehn-Yahr stages) detected atrophy in the same region. Postcentral gyrus: Using VBM, Rosenberg-Katz [81] (FDR, covariates: age and disease duration; smoothing: 8 mm; modulated images) also reported that the postcentral gyrus is atrophied in tremor-dominant PD relative to postural instability and gait difficulty PD. In addition, Braga-Pereira [82] (FWE, covariates: age and sex; smoothing: 12 mm; modulated images) reported atrophy in the same gyrus in nondemented patients with mixed disease duration and Hoehn-Yahr stages (11.8 $\pm$ 4.9 years, 2.8 $\pm$ 0.9, respectively).

The tendency to use modulation is much more common than the use of unmodulated analysis in VBM studies. The aim of the modulation is to regain the original volume which changes during the normalization, and it is achieved by multiplying each voxel by the Jacobian determinants of the transformation, where Jacobian determinants indicate the degree of shrinkage or enlargement. Maybe because of this straightforward aim, its experimental validity has not been investigated much, as claimed in Radua et al [43]. Their findings indicated that modulation might decrease the sensitivity of detecting mesoscopic differences (such as cortical atrophy), which is contrary to the current VBM processing practices. They demonstrated that modulation reduces the statistical significance of a t-test, possibly because of the multiplicative noise as a result of the modulation; since noise is also multiplied by Jacobian determinants during the modulation. Furthermore, this effect is more severe with the higher resolution registration methods (SPM's current registration is based on DARTEL, which is a high resolution registration method; whereas the registration method used by Good et al [27] -the article that optimized VBM in which modulation is a main part was proposed- was a low-resolution normalization) Radua et al have also shown that there is not any significant difference regarding false positive rates between modulated and unmodu-

lated analyses. From the aspect of a masking strategy, there are several reasons to include certain voxels in the statistical calculations, mostly related to increasing the power of multiple corrections. Ridgway et al [36] have shown that SPM's generally accepted method of threshold masking (thresholding by a constant value or by a relative fraction of each image's global value), bears a critical risk of excluding those regions most vulnerable to atrophy; therefore, this method carries the risk of false negatives; especially when we count the neurodegenerative diseases into account, because in these images the grey matter densities can fall behind the thresholds. In accordance with their findings, we have shown that average-based masking with modulation increases the voxel sizes of clusters in VBM results. Considering the clinical results of this small data set from various scanners, it should be noted that larger data sets are needed in order to achieve meaningful clinical results.

4.4 Conclusion

In the MR images of early and nondemented PD patients, using unmodulated data and average-based masking in the statistical analysis step of VBM, we found atrophied regions in the superior and middle temporal gyri (and a minor cluster in the postcentral gyrus) that could have been easily missed by the generally followed practice of VBM with modulation and absolute thresholding. These atrophied regions have been found in previous studies using methods other than VBM in similar cohorts, or via VBM only in groups in more progressed cases of PD. The results of the atrophy simulation data set also supported our choice of parameters.

5. Clinical Applications of VBM

We have performed VBM analyses for three different clinical data sets as described in the following sections.

5.1 Reduced Gray Matter Volume in the Frontotemporal Cortex of Patients with Early Subacute Sclerosing Panencephalitis [1]

BACKGROUND AND PURPOSE: Subacute sclerosing panencephalitis (SSPE) is a persistent infection of the central nervous system by the measles virus. Patients in the initial stages of SSPE show behavioral symptoms and usually normal cranial MR imaging findings. We aimed to investigate the gray matter volume changes in patients with early SSPE.

MATERIALS AND METHODS: Seventeen patients with SSPE with normal cranial MR imaging findings and 30 sex- and age-matched control subjects were included in the study. Clinical parameters of the patients were quantified by using a neurologic disability index (NDI) as defined previously. We obtained T1-weighted magnetization-prepared rapid acquisition gradient echo images from the patients and control subjects, and we applied an optimized method of voxel-based morphometry. We performed a cross-sectional analysis to search the gray matter volume differences between the patients and control subjects. The correlation between the gray matter distribution and the duration of symptoms, immunoglobulin G index, and NDI scores was tested.

RESULTS: We found that the cortical gray matter volume of patients was reduced in the frontotemporal regions including the bilateral cingulate cortex and amygdala. There was no correlation between the gray matter distribution of patients and the duration of symptoms or the NDI scores.

CONCLUSIONS: The current study demonstrated gray matter volume reduction in the frontotemporal cortex of patients with SSPE without any apparent lesions on conventional MR imaging. Because the cingulate cortex and amygdala are involved in emotion processing, gray matter loss in these regions may contribute to the development of early behavioral symptoms of SSPE.

5.1.1 Introduction

Subacute sclerosing panencephalitis (SSPE) is a slow virus infection of the central nervous system, which is caused by the measles virus [99]. It is a rare infectious disease in developed countries. An incidence of 1 case per million patients with measles infection a year was reported in developed countries [99]. However, it is still prevalent in underdeveloped and developing countries [100]. The characteristic clinical presentation of SSPE usually starts with nonspecific cognitive decline and behavioral changes, such as memory impairments, decreased scholastic performance, reduction of social interactions, and emotional instability [99]. Following the behavioral changes, involuntary movements, such as myoclonic jerks and choreoathetosis, develop. Myoclonic jerks initially affect the head and then involve the trunk and limbs with progression of disease. Spasticity, visual disturbances, and language difficulties usually accompany the involuntary movements. In late stages of the disease, mental deterioration evolves, spasticity progresses into opisthotonus, and terminal patients pass into a vegetative state.

T2-weighted hyperintense signal-intensity changes in the cerebral cortex, periventricular white matter, basal ganglia, and brain stem and atrophic dilation of cerebral sulci are the cranial MR imaging findings of SSPE that frequently develop in the late stages of the disease [101–105]. Conventional cranial imaging performed in the initial stages of SSPE usually does not reveal any pathology. However, recent MRspectroscopy studies have demonstrated that the metabolic alterations caused by neuronal loss and gliosis were present even in normal-appearing cerebral tissue in the initial stages of SSPE [106, 107]. Voxel-based morphometry is an automated statistical image-analysis

method that is used to search gray matter volume differences between various subject groups [14]. Voxel-based morphometry can detect minor morphologic changes that could not be detected by visual case analyses.

The purpose of the current study was to investigate the gray matter volume changes in the initial stages of SSPE. We studied patients with a diagnosis of SSPE whose conventional cranial MR imaging findings appeared normal. We hypothesized that neuronal degeneration/loss starting in the early stages of SSPE would cause cerebral gray matter loss that could be detected by using voxel-based morphometry. We performed a cross-sectional voxel-based morphometry study to search the gray matter volume differences between the patients with SSPE and age- and sex-matched control subjects. We also studied the correlations between the gray matter distribution and the clinical variables.

5.1.2 Materials and Methods

<u>5.1.2.1 Patients.</u> We studied 22 patients with a diagnosis of SSPE. Because cerebral parenchymal lesions would cause segmentation errors during image analysis, we excluded 5 patients whose conventional cranial MR images revealed cortical or white matter lesions. Thus, 17 patients (11 girls and 6 boys) were included into the study. The mean age of the patients was 9.5 ± 2.2 years (range, $7 - 14$ years). Table 5.1 summarizes the demographic data and the clinical findings of these patients. The diagnosis of SSPE was based on the presence of clinical symptoms, typical electroencephalography findings (bilateral periodic high-amplitude slow wave bursts), and high antimeasles antibody titers in serum (>1:180) and CSF (>1:4). The mean age of initial measles infection was 28 months (ranging between 8 and 45 months).

We used the clinical staging of patients as defined by Jabbour et al. [108]. Briefly, stage 1 indicated behavioral changes; stage 2, the presence of myoclonus, incoordination, choreoathetosis, and motor convulsions; stage 3, opisthotonus, decerebrate rigidity, and coma; and stage 4, diminished rigidity, less frequent myoclonus, and loss

Table 5.1
Demographic data and the clinical findings of patients

Patient No.	Age	Sex	Duration of Symptoms (weeks)	Stage	NDI Score	IgG Index	Symptoms
1	10	M	8	1	10	37	ALP, DSP
2	12	F	3	1	15	37	DSP, DSI, EI
3	7	F	16	2	20	99	Moderate depression, DSI, INS
4	14	F	8	1	10	73	ALP, DSP
5	9	F	5	1	10	113	DSI, EI
6	7	F	24	2	25	108	ALP, DSP, DSI, INS
7	8	F	12	2	15	433	DSP, INS
8	13	F	8	1	15	17	IPE, EI, DSP
9	10	M	6	1	10	13	ALP, DSI
10	9	F	6	1	15	105	EI, IPE
11	10	F	4	1	15	31	ALP, DSP, DSI, EI
12	7	M	5	1	15	709	DSI, IPE
13	13	F	18	2	25	22	ALP, DSP, DSI, INS
14	7	M	8	1	20	161	DSP, EI, IPE
15	9	M	12	2	25	47	DSP, INS
16	9	F	4	1	15	1370	ALP, DSP, DSI, IPE
17	9	M	5	1	10	126	DSP, IPE

Note:—ALP indicates altered personality/behavior; DSP, decreased scholastic performance; DSI, decreased social interactions; EI, emotional instability; IPE, inappropriate emotions; INS, involuntary spasms; NDI, neurologic disability index; IgG, immunoglobulin G.

of cerebral cortical function. Clinical parameters were also quantified by using a neurologic disability index (NDI) as defined previously for patients with SSPE by Dyken et al [109], in which motor, sensory, and mental states were evaluated; higher scores indicated poorer neurologic status. Neurologic examinations, clinical staging, and NDI scoring were performed by an experienced pediatric neurologist (B.T.). All patients were treated with oral isoprinosine (dosage, 100 mg/kg/day).

The patients were compared with a control group composed of 30 healthy subjects (20 girls and 10 boys). The mean age of the control subjects was 9.3 ± 2.4 years (range, $7 - 14$ years). None of the control subjects had a history of any neurologic or psychiatric disorder. The exclusion criteria for the patient and control groups also included any contraindication for MR imaging, a history of previous head trauma leading to hospitalization, and a previous history of febrile or nonfebrile convulsion. Written informed consent was obtained from the parents of the patients and control subjects. The study was approved by the local human subject committee.

5.1.2.2 Image Acquisition. Cranial MR imaging studies were performed on a 1.5T superconducting whole-body MR imaging system (Symphony Maestro; Siemens

Medical Systems, Erlangen, Germany) with a standard quadrature head coil. Conventional cranial MR imaging was performed to search for any pathologic finding that would lead to the exclusion of patients from the study. MR images were evaluated by an experienced neuroradiologist who was blinded to whether images were from a patient or control subject. The conventional cranial MR imaging protocol included axial fluid-attenuated inversion recovery (FLAIR) (TR = 9800 ms, TE = 110 ms, TI = 2100 ms, NEX = 2), axial T1-weighted spin-echo (TR = 500 ms, TE = 18 ms, NEX = 3), and coronal T2-weighted fast spin-echo (TR = 9200 ms, TE = 110 ms, NEX = 3) sequences. For voxel-based morphometry, high-resolution anatomic images of the whole brain were acquired from the patients and control subjects with T1-weighted magnetization-prepared rapid acquisition gradient echo sequences (TR = 11.08 ms, TE = 4 ms, TI = 300 ms, relaxation delay time = 500 ms, flip angle = 15Â°, FOVx256x192 mm, matrix size = 256 x 192), yielding 128 sagittal sections with a defined voxel size of 1x1x1.3 mm.

5.1.2.3 Voxel-Based Morphometry Protocol and Data Preprocessing.

We applied an optimized method of voxel-based morphometry by using SPM2 (http://www.fil.ion.ucl.ac.uk/spm/software/spm2; Wellcome Department of Cognitive Neurology, London, UK) running under Matlab (MathWorks, Natick, Mass) [14, 27]. Preprocessing of the data involved spatial normalization of all images into a standardized anatomic space, segmentation into gray and white matter, modulation, and spatial smoothing with a Gaussian kernel. T1-weighted MR images were normalized to the standard T1 template of the Montreal Neurologic Institute (MNI). The normalized images were smoothed and averaged to obtain a study-specific T1 template. All of the original structural MR images in native space were then normalized to this study-specific template. The normalized images were segmented into CSF, gray matter, and white matter compartments by using the SPM2 priors. Afterward, CSF, gray matter, and white matter images were smoothened with an 8-mm full width at half maximum (FWHM) kernel and averaged to obtain study-specific CSF, gray matter, and white matter priors for later segmentation of native images. The original T1-weighted images were segmented with the study-specific T1 template and gray matter, white

matter, and CSF priors. This segmentation step involves an affine transformation of each scan to the template with a subsequent back-projection into native space. We also performed a correction for volume changes (modulation) by modulating each voxel by the Jacobian determinants derived from the spatial normalization. Anautomated brain-extraction procedure that incorporated a segmentation step was used to remove nonbrain tissue. The extracted gray and white matter images were then normalized to the specific gray and white matter templates. The normalization parameters were then applied to the original structural images in native space to reduce any contribution from nonbrain voxels and to afford optimal spatial normalization of gray matter. These normalized images were segmented into gray and white matter. Finally, the normalized and segmented images were smoothed with an 8-mm FWHM isotropic Gaussian kernel.
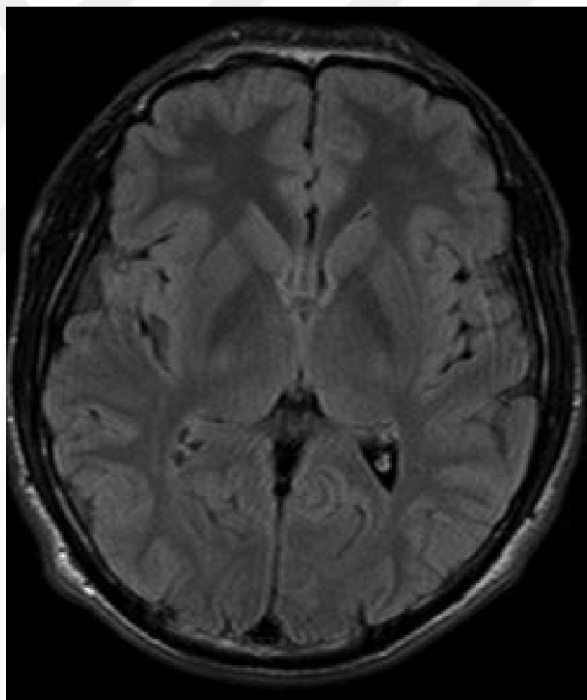
Figure 5.1 Axial FLAIR (TR = 9800 ms, TE = 110 ms, NEX = 2) image of a patient with stage 2 disease reveals normal findings.

5.1.2.4   Statistical Analysis.   The normalized modulated smoothed gray matter data were analyzed by using SPM2, within the framework of the general linear model on a voxel-wise comparison. Regional differences in gray matter volume between the patients and control subjects were assessed by using analysis of variance. Because the patients and control subjects did not show a significant difference in age and sex

distribution, we did not enter these variables as covariates. The total intracranial volumes of the subjects were calculated and used as a covariate in the comparison analysis. The findings were considered significant at a voxel level of P<.05, corrected for multiple comparison familywise error (FWE), with an extended threshold looking for clusters with at least 20 contiguous voxels. The relationship between the clinical variables (duration of disease, immunoglobulin G [IgG] index, NDI scores) and cortical gray matter volume was investigated by regression analysis (P<.05, FWE-corrected). For localizing purposes, the MNI coordinates were converted to Talairach coordinates by using a dedicated script (mni2tal.m; available at: http://www.mrc-cbu.cam.ac.uk/ Imaging/Common/mnispace.shtml).

An automated software was used to retrieve the brain labels for the Talairach coordinates (http://www.talairach.org/client.html).

5.1.3 Results

The differences between the mean age and sex distribution of patients and control subjects were not significant (P > .05). Five of the patients were in stage 2 of the disease, and the remaining 12 patients had stage 1 SSPE. The mean clinical stage of the patients was 1.29. The mean duration of symptoms was 8.9 ± 5.7 weeks (range, 3 − 24 weeks) (Table 5.1). Behavioral and personality changes were present in the clinical history of all patients (100%). The parents or teachers of 11 patients had noticed a recent decline in school performances of the patients. In addition to the behavioral changes, 5 patients also had involuntary movements in the head and limbs (myoclonic jerks). The neurologic evaluation of the patients revealed a mean NDI score of 15.8 $\pm$ 5.3 (range, 10 − 25). The findings of FLAIR and T2-weighted MR images of all patients and the control subjects were normal (Fig 5.1.2.3). Voxel-based comparison analysis revealed that the patients had significantly reduced cortical gray matter volume in the frontotemporal cortical regions compared with those in the control subjects (Table 5.2). The regions with gray matter loss in patients included the anterior cingulate cortex (Talairach coordinates: x = -7, y = -15, z = 41 [Brodmann area, (BA 24)];

Table 5.2

Cortical regions with decreased gray matter volume in patients compared with control subjects

Anatomic Regions (BA)	Talairach Coordinates: Patients vs Control Subjects			Max. Z Values
	X	Y	Z	
Left amygdala	−32	−1	−12	5.49
Left uncus (BA 38)	−27	3	−33	5.24
Left cingulate gyrus (BA 31)	−10	−23	38	5.15
Left cingulate gyrus (BA 24)	−7	−15	41	5.32
Left superior temporal gyrus (BA 38)	−30	4	−11	5.24
Left middle temporal gyrus (BA 37)	−46	−59	−1	3.51
Right cingulate gyrus (BA 24)	6	0	35	5.68
Right inferior frontal gyrus (BA 44)	52	3	13	5.16
Right superior temporal gyrus (BA 38)	33	3	−9	5.10
Right fusiform gyrus (BA 20)	52	−35	−19	4.98
Right amygdala	30	−3	−10	5.13

Note:—Max indicates maximum; BA, Brodmann area.

x = 6, y = 0, z = 35 [BA 24]) and the bilateral amygdala (x = –32, y = 1, z = -12; x = 30, y = -3, z = -10) (Fig 5.1.3). The correlation analysis revealed that there was no significant association between the NDI scores and gray matter distribution of the patients. Moreover, there was no relationship between the IgG index or clinical stage and gray matter volumes of patients.

5.1.4   Comment

The uniformity of clinical progression in patients with SSPE suggests acommonpattern of neuropathologic progress in the central nervous system. Previous autopsy reports revealed that inflammatory infiltrations in cortical gray matter are the prominent pathologic finding in the early periods of SSPE [99, 110]. In later stages of the disease, the neuropathologic findings spread into adjacent subcortical white matter. Early involvement of cortical gray matter would explain the nonspecific subtle behav-
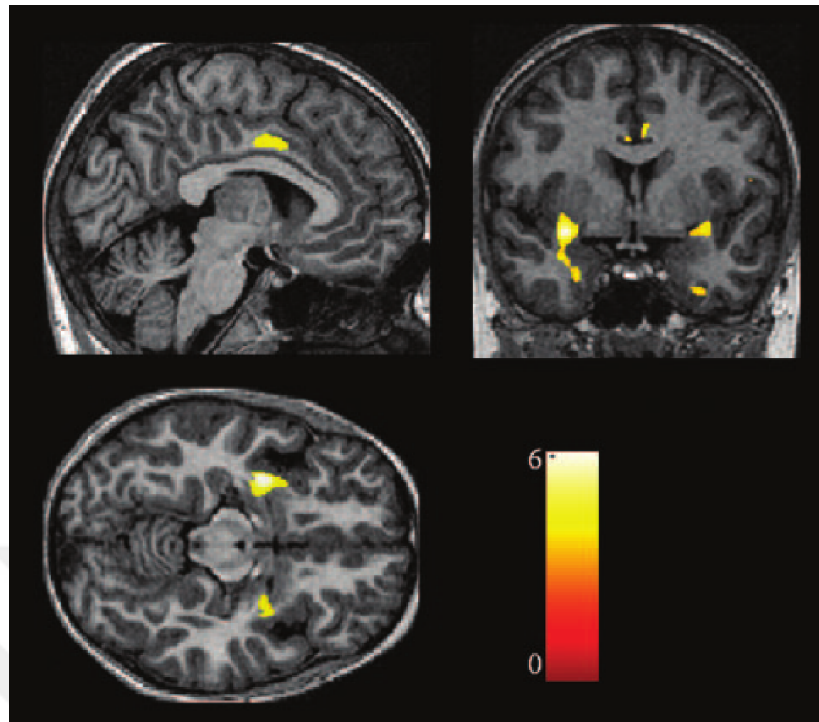
Figure 5.2 Statistical parametric maps demonstrating the structural difference in gray matter volumes. Significant gray matter volume decrease (P < .05, corrected) is overlaid in color on the normalized T1-weighted images of a healthy control subject. Only clusters of voxels consisting of at least 20 voxels are displayed. The color scale shows the range of Z values. It shows the reduced gray matter volumes in bilateral medial temporal regions, including the amygdala, cingulate gyri, and right inferior frontal gyrus.

ioral symptoms that are frequently seen in the initial stages of SSPE. However, contrary to the early cortical involvement shown by the neuropathologic studies, conventional MR imaging examinations performed in patients with early disease usually reveal normal findings. Thus, cortical involvement in early SSPE could not be demonstrated in previous neuroimaging studies. The results of the current study revealed the reduced gray matter volume in the bilateral frontotemporal cortex, including the amygdala and cingulate cortex, of the patients with stage 1 and 2 SSPE. Decreased frontotemporal cortical gray matter volume is consistent with the results of previous neuropathologic studies emphasizing the cortical involvement in the early periods of SSPE. The results of previous neuroimaging studies revealed that findings of cranial imaging performed in the initial stages of SSPE usually appear normal and that parenchymal lesions develop as the disease progresses [99, 105]. In the current study, we demonstrated the gray matter volume reduction in the patients with normal-appearing MR imaging findings in early stages of the disease. When we consider the results of the current and

previous studies together, it suggests that a subtle loss of frontotemporal gray matter may precede the appearance of morphologic T2-weighted lesions in early SSPE. Kanemura et al investigated the frontal lobe volume in a patient with early SSPE. They measured the whole parenchymal volume of frontal lobes including the white and gray matters volumes. They found a decreased frontal lobe volume compared with that in healthy control subjects, which seems to be a finding consistent with the results of the current study. In another article, Kanemura and Aihara [111] reported the decreased apparent dif- fusion coefficient in the normal-appearing frontal lobe of a patient with SSPE. They also found a correlation between the frontal diffusion changes and clinical parameters. They speculated about the possibility of an association between frontal neuropathologic changes and some of the clinical findings of SSPE.

Neurodegenerative diseases leading to progressive neuronal loss cause reduced cortical gray matter attenuation and volume in the related regions of brain [112]. SSPE is caused by persistent infection of neurons and oligodendrocytes by the measles virus. Neuronal degeneration, neuronal loss, demyelination, and gliosis are the main neuropathologic findings of SSPE. The decreased gray matter volume in the frontotemporal cortex of our patients might be the consequence of neuronal degeneration/loss in those regions of brain.

The cingulate gyrus and amygdala are components of the limbic cortex, which is involved in the processing of emotions [113, 114]. A complex neural network, including the prefrontal and anterior cingulate gyrus, hippocampus, insular cortex, and amygdala, is involved in the processing of various aspects of emotions. The pathologies affecting the anterior cingulate gyrus and amygdala cause emotional and behavioral symptoms. The amygdala is also involved in the regulation of emo-ions. Thus, any pathology affecting the amygdala may cause dysregulation of emotional processing leading to over- or underexpression of emotions. The initial symptoms of patients with SSPE include emotional instability, inappropriate emotions, inappropriate expression of emotions, and other behavioral changes. Cortical involvement in the cingulate gyrus and amygdala may explain the emotional and behavioral symptoms of early SSPE.

Cognitive decline, which is usually recognized as a recent decrease in scholastic performance of the patient, is another common symptom of early SSPE. The anterior cingulate cortex together with the orbitofrontal cortex takes part in the processing of decision making. The amygdala is also involved in reward-based learning and decision making [115]. Recent studies have shown that the amygdala is a critical structure in a neural system necessary for implementing advantageous decisions. Thus, the gray matter volume reduction in the anterior cingulate cortex and the amygdalamaycontribute to the appearance of cognitive decline during the initial stages of SSPE. However, we did not find a significant correlation between the NDI scores of patients and their cortical gray matter distribution. The NDI scoring is a gross evaluation of the motor and sensory functions as well as the mental states of patients with SSPE. The lack of a correlation between the NDI scores and gray matter volume might be because we studied only patients in the initial stages of the disease, and their NDI scores were distributed in a narrow range.

The correlation analysis in the current study did not reveal any association between the duration of symptoms and gray matter distribution in patients. This finding suggests that the gray matter loss in the frontotemporal regions might have developed at very early periods of the disease. The relatively narrow range of duration of symptoms among patients might be another explanation of this finding. Furthermore, we did not find any correlation between the IgG index and the gray matter distribution. This finding indicates that there is no association between the degree of neuroimmunologic reaction and gray matter loss in early SSPE.

Several quantitative imaging studies with a region-of-interest design such as quantitative diffusion MR imaging and proton MR spectroscopy [106, 107, 116] have been conducted to investigate the in vivo neuropathologic findings in patients with early SSPE. Because conventional imaging findings usually appear normal in early SSPE, quantitative imaging studies investigating patients with early SSPE require a prior hypothesis of localization. The frontotemporal weighting of cortical gray matter loss demonstrated by the current study may guide future studies investigating early imaging findings of SSPE.

A few limitations of the current study should be mentioned. First, because of the ethical issues, we did not perform a longitudinal study. A longitudinal study would give valuable information about the evolution of gray matter loss during the clinical progression of the disease. The second limitation may be that we could not measure the severity of the patients' emotional symptoms. Thus, we could not investigate the correlation between volumetric changes in gray matter and severity of behavioral symptoms. Although the comparison analysis revealed a gray matter reduction in the emotion-related regions of the brain, a correlation analysis would be helpful to investigate the association of the severity of emotional symptoms and gray matter distribution. In conclusion, the results of the current study demonstrated the decreased gray matter volume in the frontotemporal cortex of patients in the early stages of SSPE. The gray matter volume reduction in the cingulate gyrus and amygdala, which are related to decision making and emotion processing, maycontribute to the development of behavioralsymptomsof early SSPE.

5.2 Smaller Gray Matter Volumes in Frontal and Parietal Cortices of Solvent Abusers Correlate with Cognitive Deficits [2]

BACKGROUND AND PURPOSE: Abuse of toluene-containing organic solvents by inhalation is a prevalent practice among adolescents. Long-term abuse of toluene causes cognitive deficits. The mechanism of cognitive deficits induced by long-term toluene abuse has not yet been defined. In the current study, we assessed the effects of chronic toluene abuse on cortical gray matter volume and the association between cognitive impairment and cortical gray matter volume distribution in chronic toluene abusers.

MATERIALS AND METHODS: Fifteen toluene abusers and 20 healthy control subjects matched in sex, age, education level, and handedness were investigated by structural MR imaging. The cognitive states of the subjects were assessed by using

the third edition of the Wechsler Intelligence Scale for Children (WISC-III). The voxel-based comparison and correlation analyses of MR images were performed by using SPM5 software.

RESULTS: The voxel-based morphometric analysis revealed that toluene abusers had significantly lower gray matter volumes in the bilateral frontotemporal and right parietal cortices. In addition, the lower gray matter volumes in the frontal and parietal regions correlated with the duration of toluene abuse. There was a positive correlation between the WISC performance scale scores and gray matter volumes in the frontal and parietal cortices of the abusers.

CONCLUSIONS: The results of the current study demonstrate that chronic toluene abusers have smaller gray matter volumes than nonabusers in various regions of the brain. Moreover, the cognitive deficits are associated with the lower gray matter volumes in the frontal and parietal cortices of chronic toluene abusers.

5.2.1 Introduction

The first reports of solvent abuse were published in the 1950s in the United States [117]. Today, abuse of organic solvents has become an important health and social problem in the developed as well as the developing countries [118–120]. Solvent abuse is particularly prevalent among adolescents [120, 121]. School-based surveys conducted in the United States and Australia revealed the rates of experimental solvent use up to 26% during adolescence [118]. The common methods of solvent abuse among adolescents are *sniffing* (direct inhalation of solvent from a container), *huffing* (inhalation of solvent by holding a soaked rag over the nose and mouth), and *bagging* (inhalation of solvent from a plastic bag). It is known that long-term solvent use has significant toxic effects on the human central nervous system [118, 120, 122–125]. Despite its high prevalence and serious health and social consequences, today relatively little is known about the mechanism of solvent-induced central nervous system toxicity [118, 121].

Toluene, also known as methylbenzene, is a lipid-soluble aromatic hydrocarbon that is commonly used as a solvent in industry. It is also a common component of many household products such as paint thinners, spray paints, ink, and glue. After inhalation, toluene is easily absorbed by the lungs. Because of its high lipid solubility, it readily diffuses and accumulates in tissues with a high lipid composition, such as the central nervous system. Toluene is thought to be the cause of central nervous system toxicity in solvent abusers [122, 126]. Several previous studies have shown that regular long-term abuse of toluene causes severe and irreversible cognitive impairment [120, 125, 127, 128]. Hormes et al [123] reported that among chronic toluene abusers, the cognitive deficits are inattention, apathy, memory dysfunctions, and visuospatial impairment. Rosenberg et al [129] compared the cognitive abilities of chronic toluene abusers with those of alcohol abusers and cocaine users. They found significant deficits in working memory and executive function in the toluene abusers.

Nevertheless, the exact pathologic mechanism of cognitive impairments caused by chronic toluene exposure has not yet been defined. Because of prevalent comorbid drug use among solvent abusers, the findings reported in the limited numbers of autopsy cases are controversial and inconclusive [119, 120, 127]. Several neuroimaging studies have been conducted to investigate the neurotoxic effects of toluene abuse. MR imaging studies reveal that chronic toluene abuse causes T2-weighted hyperintense white matter lesions starting in the periventricular region during the early years of abuse, and these lesions later spread to subcortical U fibers [118, 120, 129–134]. Dilation of cortical sulci, thinning of the corpus callosum, and thalamic T2- weighted hypointensity were the other MR imaging findings in chronic solvent abusers. The presence of white matter lesions on cranial MR imaging was significantly associated with the greater cognitive impairment among the chronic toluene abusers [130, 135, 136]. Thus, the results of previous neuroimaging studies point to white matter as the target tissue for the development of cognitive impairment in chronic toluene abusers [129]. Consistent with this hypothesis, Filley et al [127] found a significant correlation between the severity of white matter changes onMRimaging and the severity of cognitive impairment. Furthermore, Aydin et al [130] reported an association between the type of white matter lesions on MR imaging (restricted or diffuse) and both duration of toluene abuse

and neurologic deficits. Finally, Filley et al [122] hypothesized that toluene-induced cognitive dysfunction may be directly attributed to cerebral white matter involvement. However, the results of other studies indicate the possibility that the cortex is involved in the development of toluene-induced cognitive impairments [137, 138].

The autopsy findings of a chronic toluene abuser showed severe neuronal loss in the second, third, and sixth layers of the cerebral cortex, in addition to widespread demyelination and giant axonopathy in the white matter [137]. This autopsy revealed that long-term toluene exposuremayaffect the cerebral cortex as well as white matter. Supporting the findings reported by Escobar and Aruffo [137], some animal studies have shown that toluene inhalation causes Purkinje cell loss in the cerebellum and neuronal loss in the hippocampus of rats [139]. Moreover, Von Euler et al [138] showed that chronic toluene exposure causes impairment in spatialmemoryand reduced cortical area in the parietal cortex of rats. Taken together, the results of these studies indicate that cortical involvement may contribute to the development of toluene-induced cognitive impairments.

In the current study, we assessed the effects of chronic toluene abuse on cortical gray matter volume. We also assessed the association between cognitive functions and cortical gray matter volume distribution in chronic toluene abusers. We did not have an a priori hypothesis about the localization of cortical gray matter volume changes, and we used a voxel- based whole-brain statistical analysis method to assess the cortical gray matter volume differences.

5.2.2 Materials and Methods

5.2.2.1 Subjects. We studied adolescents between 12 and 19 years of age who regularly abused toluene-containing solvents by inhalation for a period of at least 6 months. Toluene abusers were recruited among adolescents who were admitted to a rehabilitation program for solvent abusers. Thecommonsolvent abused by all the participants was paint thinner. The patients who abused other substances, such as

marijuana, amphetamines, and cocaine, were excluded from the study. The exclusion criteria for the toluene abusers and control subjects also included any contraindications for MR imaging, a history of any disorders known to cause cognitive deficits other than toluene-induced cognitive dysfunctions, neurodegenerative or demyelinating diseases, history of seizures, central nervous system infection, cerebrovascular disease, diabetes mellitus, steroid treatment for any reason, head trauma causing loss of consciousness or requiring hospitalization, a history of a previous psychotic or manic episode, a history of previous treatment with an antipsychotic agent, and a parental history of any psychotic disorder.

Sixteen male chronic toluene abusers meeting the defined criteria were included in the study (mean age, 15.5 years). The information about age of onset for toluene abuse and total duration of toluene abuse was gathered from the abusers and their parents by using a structured structured interview. Calculation of the absolute daily dosage of inhaled toluene was impossible because of the easy vaporization of thinners and issues related to the methods of abuse that made such calculations impossible, such as variability in the frequency of huffing, the amount of thinner inhaled during each huffing episode, and different physical properties of the rags used. Therefore, we used the amount of thinner bought weekly (as cans per week) to represent the amount of weekly toluene consumption [130]. Data on the prevalence and amount of weekly alcohol consumption and tobacco smoking among the abusers and control subjects were also collected. Because the subjects did not have regular income, the frequency of alcohol intake was irregular in both groups. Therefore, the amount of weekly alcohol consumption was calculated by considering the number of consumed drinks during their last drinking week (12-g alcohol per drink). Twenty sex-, age-, and education-level matched and right-handed (headedness-matched with the abusers) healthy control subjects were recruited from the community (mean age, 15.6 years). The control subjects had no history of substance or drug abuse. All the toluene abusers and control subjects were right-handed (based on the Edinburg Handedness Inventory). Written informed consent was obtained from subjects who were <18 years of age during the study. If the subject was <18 years of age, written informed consent was obtained from his or her parent. The study was approved by the local Human Subjects Committee.

Table 5.3

Demographic and clinical characteristics of the toluene abusers and control subjects

	Abusers (n = 15)	Control Subjects (n = 20)	P Value
Age (yr)	15.53 ± 1.30	15.60 ± 1.09	.44 (ns)
Education (yr)	6.53 ± 2.55	7.75 ± 1.20	.07 (ns)
Prevalence of alcohol consumption (%)	7/15 (46%)	7/20 (35%)	.48 (ns)
Prevalence of tobacco smoking (%)	9/15 (60%)	11/20 (55%)	.76 (ns)
Amount of weekly alcohol intake (g/week)	16.00 ± 22.06	10.80 ± 16.47	.31 (ns)
Amount of smoking (cigarettes/day)	8.53 ± 4.47	6.50 ± 2.76	.21 (ns)
Age at onset of abuse (yr)	12.76 ± 1.83	–	
Duration of abuse (months)	31.86 ± 18.74	–	
Weekly inhalant use (cans/week)	12.60 ± 0.77	–	
WISC-III results			
Performance scale scores	60.80 ± 12.88	99.75 ± 4.22	<.001
Verbal scale scores	67.13 ± 12.44	100.05 ± 3.85	.008
FSIQ scores	63.06 ± 15.97	100.40 ± 4.00	.005

Note:—FSIQ indicates full-scale intelligence quotient; WISC-III, *Wechsler Intelligence Scale for Children;* ns, not significant; –, no data.

5.2.2.2 Cognitive Assessment.   General cognitive functions and intellectual abilities of all subjects were assessed by using the third edition of the Wechsler Intelligence Scale for Children (WISC-III). The WISC-III battery consists of 6 verbal and 5 performance scale subtests. Verbal and performance scores and a full-scale intelligence quotient (FSIQ) of all subjects were calculated. WISC-III tests and MR imaging studies of the toluene abusers were performed at least 3 weeks after their last solvent use to avoid the acute effects of toluene.

5.2.2.3 Image Acquisition.   Cranial MR imaging studies were performed on a 1.5T superconducting whole-body MR imaging system (Symphony Maestro; Siemens Medical Systems, Erlangen, Germany) with a standard quadrature head coil. High-resolution anatomic images of the whole brain were acquired from the solvent abusers and control subjects with a T1-weighted magnetization-prepared rapid acquisition of gradient echo sequence (TR = 11.08 ms, TE = 4 ms, TI = 300 ms, relaxation delay time = 500 ms, FA = 15Â°, FOV = 256x192mm, matrix size = 256x192) yielding 128 sagittal sections with a defined voxel size of 1x1x1.3 mm. We also obtained axial fast spin-echo T2-weighted images (TR = 9200 ms, TE = 110 ms, number of acquisitions = 3) from all of the subjects to search for any pathologic findings defined in the study exclusion criteria.

5.2.2.4 Voxel-Based Morphometry Preprocessing. Data analysis was performed by using the SPM5 software package (Wellcome Department of Cognitive Neurology, London, UK) running under Matlab 2007a (MathWorks, Natick, Mass). We used the VBM5 toolbox (http://dbm.neuro.uni-jena.de) for image preprocessing, which included normalization, segmentation, and modulation steps [14, 140]. The VBM5 toolbox uses anewtissue-segmentation method implemented in SPM5. The details of the unified segmentation method performed in VBM5.1 toolbox have been described elsewhere [140]. The segmented images were modulated with the Jacobian determinants of the deformation parameters obtained by normalization to the Montreal Neurologic Institute standard space to analyze volume differences. Finally, the modulated gray matter images were smoothed with a 10-mm full width at half maximum gaussian kernel and statistically analyzed. The total intracranial volume was included as a covariate during statistical analysis.

5.2.2.5 Statistical Analysis. We investigated the regionally specific gray matter volume differences between the toluene abusers and control subjects by using voxel-by-voxel analysis of the covariance test. The total intracranial volumes of the subjects were entered as a covariate. Because the abusers and control groups did not show significant differences in age and sex distribution, tobacco use, and education levels, we did not enter these variables as covariates. Because the difference between the mean amounts of weekly alcohol consumption of the abusers and control subjects was not significant, we did not consider alcohol consumption as a covariate in the voxel-based morphometry analysis. The findings were considered significant at a voxel level of P < .05, family-wise error (FWE) corrected, with an extended threshold looking for clusters with at least 10 contiguous voxels. The relationship between the duration of toluene abuse and cortical gray matter volume distribution was evaluated with regression analysis (P<.05, FWE corrected). The association was also assessed between the scores obtained from the performance, verbal subtests, and FSIQ on one hand and the cortical gray matter volume changes on the other.

The differences in demographic findings between the toluene abusers and con-

trol subjects were investigated by using Mann-Whitney U test, as integrated in the Statistical Package for the Social Sciences, Version 15.0 for Microsoft Windows (SPSS, Chicago, Ill). The differences in the prevalence of alcohol consumption and tobacco smoking were tested by using the χ^2 test. The correlations of the scores obtained from the WISC tests with duration of abuse and with weekly solvent consumption were assessed by using linear regression analysis.

5.2.3 Results

The demographic findings of the toluene abusers and control subjects are given in Table 5.3. The differences in age or education levels between the toluene abusers and control subjects were not significant (P > .05). The prevalence of alcohol use and the amount of weekly alcohol consumption between the abusers and control subjects were not significant (P > .05).

There was no significant difference in the prevalence of tobacco smoking and the amount of daily tobacco consumption between the toluene abusers and control subjects (P > .05). The scores obtained from the performance and verbal subtests of the WISC-III and the FSIQ scores of the toluene abusers were significantly below the scores obtained from the control subjects (P<.01; Table 5.3). The performance scale scores were slightly lower than the verbal scale scores in the toluene abusers (P = .46). The WISC-III scores of the toluene abusers correlated negatively with the duration of toluene abuse (P< .05). There was no correlation between the WISC-III scores of the abusers and the amount of weekly solvent consumption (P>.05).

The voxel-based image analysis revealed lower cortical gray matter volumes in the abusers than in the control subjects in the following brain regions: bilateral medial frontal gyrus (Brodmann areas [BAs] 9 and 10); right orbitofrontal (BA 11), right superior frontal gyrus (BA 8), right angular gyrus (BA 39), right superior parietal lobule(BA7), right parahippocampal gyrus (BA 36), and left middle temporal gyrus (BA 22) (Fig 5.2.3 and Table 5.4). The duration of toluene abuse correlated negatively

with the cortical gray matter volumes of the toluene abusers in the right superior frontal gyrus(BA6), right inferior temporal gyrus (BA 20), right superior temporal gyrus (BA 22), right occipital lobe (BA 19), left middle frontal gyrus (BA 9), left inferior temporal gyrus (BA 37), and left precentral gyrus (BA 6) (Fig 5.2.3 and Table 5.5). The reduced gray matter volumes in the left middle frontal gyrus (BA 9) and the right superior parietal lobule (BA 7) of the abusers correlated with lower WISC-III performance scale scores (Fig 5.2.3 and Table 5.6). The voxel-based regression analysis showed that in none of the brain regions examined did the gray matter volume correlate significantly with weekly solvent consumption.
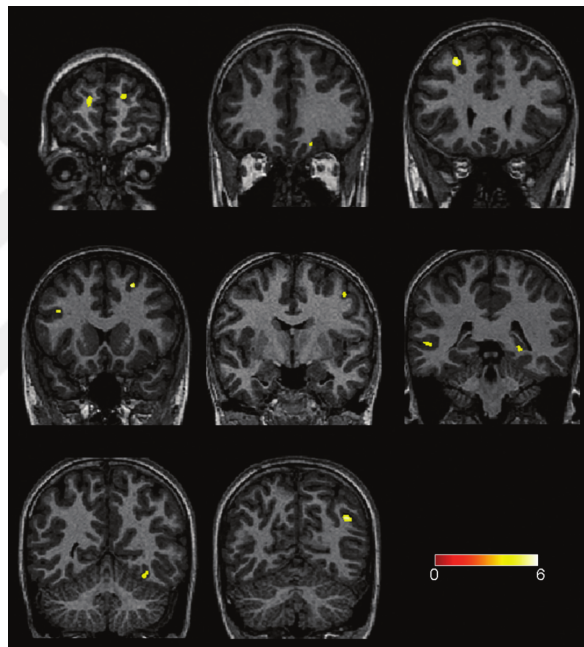
Figure 5.3 Significant gray matter volume decreases in the toluene abusers compared with the control subjects (P < 0.05, FWE-corrected). T values of cluster with a significant decrease are overlaid on the normalized T1-weighted images of a control subject

5.2.4 Discussion

In this study, we investigated the adverse affects of chronic toluene exposure on cognitive functions and gray matter morphology. We found that chronic toluene abusers had significantly lower WISC-III IQ scores than healthy control subjects. The performance scale of WISC-III consists of tests measuring visuospatial skills and information-processing speed such as picture completion, block design, and digit-symbol coding.

Table 5.4
The regions with the smaller cortical gray matter volume in toluene abusers compared with control subjects

Anatomic Regions	BA	Talairach Coordinates			Max. T value	Cluster Size
		X	Y	Z		
Right medial frontal gyrus	10	15	59	17	4.98	34
Right superior frontal gyrus	8	23	19	47	5.26	38
Right orbitofrontal gyrus	11	16	34	−19	4.75	16
Right middle frontal gyrus	8	24	−19	47	5.43	36
Right precentral gyrus	6	47	−7	47	5.18	32
Right superior parietal lobule	7	17	−47	59	5.67	57
Right angular gyrus	39	44	−62	31	5.21	43
Right parahippocampal gyrus	36	25	−40	−4	4.99	27
Left medial frontal gyrus	10	−10	58	14	5.23	42
Left middle frontal gyrus	8	−24	23	46	4.55	68
Left middle frontal gyrus.	9	−42	19	27	5.36	26
Left middle temporal gyrus	22	−53	−38	1	5.08	37

Note:—BA indicates Brodmann area; Max., maximum.

Table 5.5
Cortical regions that showed a negative correlation between the gray matter volume and duration of abuse among the toluene abusers

Anatomic Regions	BA	Talairach Coordinates			Max. T Value	Cluster Size
		X	Y	Z		
Right superior frontal gyrus	6	10	33	53	5.78	27
Left middle frontal gyrus	9	−40	18	28	7.63	56
Left precentral gyrus	6	−55	−4	35	5.45	18
Right inferior temporal gyrus	20	57	−30	−16	5.82	27
Right superior temporal gyrus	22	50	−50	9	5.38	25
Left inferior temporal gyrus	37	−55	−56	−5	5.29	22
Right occipital lobe, cuneus	19	10	−81	25	5.98	31

Table 5.6
Cortical regions in which the cortical gray matter volumes were positively correlated with the Wechsler performance scale scores of the toluene abusers

Anatomic Regions	BA	Talairach Coordinates			Max. T Value	Cluster Size
		X	Y	Z		
Left middle frontal gyrus	9	−41	20	26	7.45	29
Right superior parietal lobule	7	26	−47	61	7.08	21
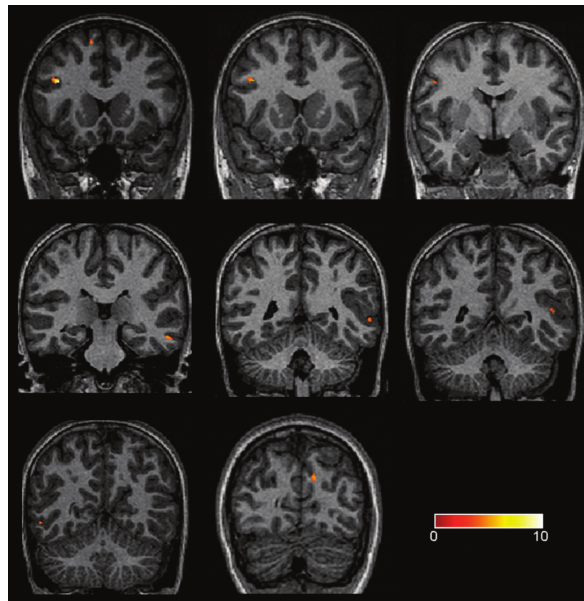
Figure 5.4 Significant negative correlations between the gray matter volume and duration of toluene abuse (P<.05, FWE-corrected). T values of cluster with a significant correlation are overlaid on the normalized T1-weighted images of a control subject.

However, the verbal scale subtests of the WISC-III assess language skills, such as comprehension, vocabulary, and similarities between objects or concepts. In the current study, both the verbal and performance scale scores of the toluene abusers were slightly lower than those of the control subjects. Nevertheless, the performance scale scores were significantly lower than the verbal scale scores in the toluene abusers. Thus, the results of the current study show that the visuospatial abilities of toluene abusers were more severely impaired than their language skills. The previous neuropsychological studies in chronic toluene abusers reported a pattern of neurocognitive disturbance consisting of impaired attention, information- processing speed, executive function, learning and memory, visuospatial dysfunction, and relatively preserved language skills [118, 122, 125, 127–129].

Yamanouchi et al [128] assessed the cognitive functions of the toluene abusers by using the Wechsler Adult Intelligence Scale (WAIS). With results similar to ours, they found significantly reduced WAIS performance scale scores among abusers, which were associated with the severity of pontine atrophy. In contrast to the results of the current study, they found a relative sparing of language skills. In our study, the negative correlation of the performance scale and FSIQ scores with the duration of
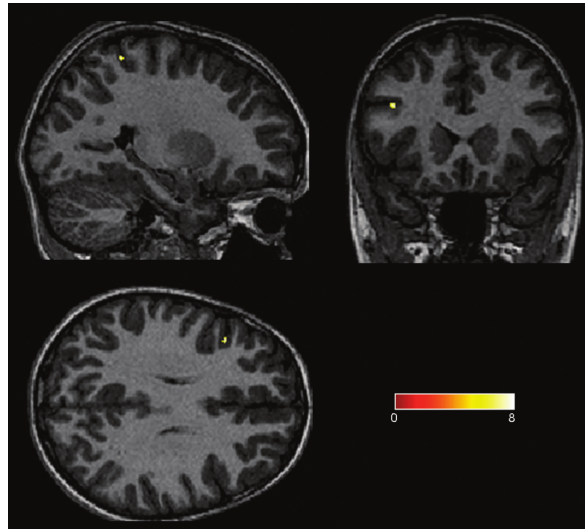
Figure 5.5 Significant positive correlations between the gray matter volume and WISC performance scale scores of the toluene abusers (P < .05, FWE-corrected). T values of cluster with a significant correlation are overlaid on the normalized T1-weighted images of a control subject.

abuse indicates that the cognitive deficits of the toluene abusers are related to the long-term toluene exposure.

In the literature, a handful of studies have investigated the effects of long-term toluene exposure on the cerebral cortex. Kucuk et al [141] studied cerebral perfusion abnormalities in toluene abusers by using technetium Tc99m hexamethylpropyleneamine oxime single-photon emission CT (SPECT). They found hypo- and hyperperfused regions in the frontal, temporal, and parietal cortices. In another SPECT study, Okada et al [142] used iodine 123I inosine monophosphate to measure the cerebral perfusion in the chronic toluene abusers and found significantly decreased cerebral blood flow in the prefrontal cortex. Furthermore, the hypoperfusion in the prefrontal cortex was related to behavioral disturbances observed in the abusers. In an animal study, Von Euler et al [138] investigated the effects of long-term toluene exposure on the behavior and brain sizes of rats. They found that toluene exposure led to the impairment of visuospatial skills and selective decrease in the parietal cortex size of the rats.

In our study, the voxel-based comparison revealed significantly lower gray matter volumes at multiple locations within the cerebral cortex of the toluene abusers compared with the control subjects. The correlation of lower gray matter volumes in the

frontal, temporal, and occipital lobes with the duration of toluene abuse demonstrates the association of the gray matter loss with long-term toluene exposure. Previous animal studies showed that chronic toluene changes in the N-methyl D-aspartate receptor subunits in the medial prefrontal cortex of rats suggest an increase in neuronal excitability [118]. These findings highlight the potential for excitotoxic neuronal damage with chronic toluene exposure [118].

Cerebral cortical gray matter is composed of neurons and glia in a laminar arrangement. Neurodegenerative disorders leading to neuronal loss cause cortical gray matter volume reduction, which can be detected by morphometric MR imaging analysis [143, 144]. In the current study, the smaller gray matter volumes in the toluene abusers may be associated with neuronal loss in the related regions of the brain. Consistent with this hypothesis, animal studies have shown that long-term toluene inhalation causes neuronal loss in the hippocampal region of rats [139]. Furthermore, the autopsy findings of a chronic toluene abuser revealed decreased neuronal attenuation in the cerebral cortex [137]. In that study, the investigators found severely damaged second, third, and sixth neuronal layers of the parietal cortex. Reactive gliosis and vacuolation of myelin sheaths accompanied the neuronal loss. Aydin et al [131] conducted a proton MR spectroscopy study to investigate neurochemical changes in the thalamus and white matter of toluene abusers. N-acetylaspartate (NAA) levels were reduced in the cerebral white matter, which indicated an impairment of the neuroaxonal integrity. However, as acknowledged by the authors, neurochemical changes in the cerebral cortex were not assessed, and the source of the reduced NAA level in white matter could not be specified. Neuronal loss, together with axonal and myelin damage, may have been related to the reduction of the NAA level in white matter.

In the current study,wealso report a significant correlation of the WISC-III performance scale scores with the lower gray matter volumes in the dorsolateral prefrontal cortex (BA 9) and superior parietal lobule (BA 7) of toluene abusers. According to the parietofrontal integration theory of intelligence, BA 7 and BA 9 are the key regions that form the core of general intelligence [145, 146]. The superior parietal lobule (BA 7) is the somatosensory association region that is involved in visuospatial processing. Pre-

vious functional studies have shown that processing of 3D object imagination, mental rotation of objects, and perspective-taking are related to the function of the superior parietal lobule [147–149]. Previous studies have also shown an association between visuospatial intelligence and increased gray matter volume in the superior parietal lobule [150]. The performance scale of WISC-III is based mainly on visuospatial skills, such as object assembly and block design. In the present study, the smaller gray matter volumes in the superior parietal lobule of the toluene abusers may be associated with the impairment of the visuospatial skills and lower WISC-III performance scale scores.

The dorsolateral prefrontal cortex (BA 9) is involved in the processing of working memory. Previous functional studies have shown that tasks that stimulate working memory cause strong activation of the dorsolateral prefrontal cortex [151, 152]. Together with BA 11 and 10 regions, the dorsolateral prefrontal cortex is also involved in planning, reasoning, decision-making, and executive functioning. Working memory is one of the core structures of general intelligence [145, 153]. Any factor that causes impairment in working memory leads to a decrease in all components of intelligence. Previous studies have shown that the gray matter volume inBA9 correlates with both verbal and spatial intelligence [145]. Thus, the gray matter loss in the dorsolateral prefrontal cortex may be related to the lower WISC-III scores in the toluene abusers.

A few limitations of the current study should be mentioned. First, the current study had a cross-sectional design. Because most of the abusers did not consent to a second MR imaging scan, we could not perform a longitudinal study. A longitudinal study for a long period of time would give valuable information about the evolution of gray matter volume and cognitive functions. Second, we recruited healthy control subjects who were matched with the abusers in age, sex, and education level. However, the solvent abusers may have had other psychosocial premorbid factors that may have affected the results. Finally, this study did not investigate the effects of toluene abuse on white matter. Future studies that use advanced and quantitative white matter imaging methods, such as diffusion tensor imaging and magnetization transfer imaging, mayhelp to clarify the relationship between cognitive dysfunctions and white matter changes in toluene abusers.

In conclusion, the results of the current study show that chronic toluene abusers have smaller gray matter volumes than nonabusers in various regions of the brain. Moreover, the cognitive deficits are associated with the lower gray matter volumes in the frontal and parietal cortices of chronic toluene abusers.

5.3 Increased Gray Matter Density in the Parietal Cortex of Mathematicians: A Voxel-Based Morphometry Study [3]

BACKGROUND AND PURPOSE: The training to acquire or practicing to perform a skill, which may lead to structural changes in the brain, is called experience-dependent structural plasticity. The main purpose of this cross-sectional study was to investigate the presence of experience-dependent structural plasticity in mathematicians' brains, which may develop after long-term practice of mathematic thinking.

MATERIALS AND METHODS: Twenty-six volunteer mathematicians, who have been working as academicians, were enrolled in the study. We applied an optimized method of voxel-based morphometry in the mathematicians and the age- and sex-matched control subjects. We assessed the gray and white matter density differences in mathematicians and the control subjects. Moreover, the correlation between the cortical density and the time spent as an academician was investigated.

RESULTS: We found that cortical gray matter density in the left inferior frontal and bilateral inferior parietal lobules of the mathematicians were significantly increased compared with the control subjects. Furthermore, increase in gray matter density in the right inferior parietal lobule of the mathematicians was strongly correlated with the time spent as an academician (r = 0.84; P < .01). Left-inferior frontal and bilateral parietal regions are involved in arithmetic processing. Inferior parietal regions are also involved in high-level mathematic thinking, which requires visuospatial imagery, such as mental creation and manipulation of 3D objects.

CONCLUSION: The voxel-based morphometric analysis of mathematicians' brains revealed increased gray matter density in the cortical regions related to mathematic thinking. The correlation between cortical density increase and the time spent as an academician suggests experience-dependent structural plasticity in mathematicians' brains.

5.3.1 Introduction

Genetic, epigenetic, and environmental factors interact to produce the fine structure of the human brain [22, 60, 154, 155]. Genetically determined cortical architecture may need to undergo functional and structural changes to meet the increasing demands of a complex environment. The training to acquire or practicing to perform a skill may lead to structural changes in the brain, which is called experience-dependent structural plasticity. A previous MR imaging study revealed that memorizing a huge amount of spatial information increased the cortical gray matter density in the right hippocampus of the human brain, which represents the spatial navigation center [22]. Thus, the human brain can make regional structural reorganizations associated with experience and learning [23, 60, 156–158].

Music is one of the most fascinating products of the human brain. Because becoming a professional musician requires a long, intense, and highly specific training during the early periods of brain maturation, the musician's brain has been used as a model to study the development of experience-dependent structural plasticity [159, 160]. During their professional training period, musicians learn to convert musical symbols to complex motor actions, memorize long and complex musical artworks, and acquire the capability of perfect tone discrimination. The performances of these very complex tasks cause experience-dependent adaptive changes in the task-related regions of their brain [159–166]. The morphometric MR studies conducted in the musicians revealed the presence of increased gray matter density in the motor and auditory cortex and the cerebellum compared with nonmusicians [165]. It has been proposed that longterm and intense practice by pianists to perform sequential motor tasks with high

accuracy resulted in experience-dependent adaptive changes in the related regions of their brains. Results of another voxel-based morphometric study revealed increased gray matter density in the left inferior frontal gyrus (Broca area) of orchestra musicians [167]. The authors of the latter study hypothesized that long-term professional activity to increase visuospatial and audiospatial abilities led to increased gray matter density in the Broca area of orchestra musicians.

Doing mathematics is another unique feature of the brain. Mathematicians have to go through very intense and focused training. After their formal graduate education, mathematicians continue to spend hours, days, and even weeks to concentrate on solving mathematic problems or to create a mathematic model to explain the social and economic events throughout their professional life. In this study, we aimed to investigate whether the long-term intense training and practicing of mathematic thinking could induce structural plasticity in a mathematician's brain. We hypothesized that highly concentrated, focused, and professionally practiced mathematic thinking by mathematicians may create an enriched environment effect to develop experience-dependent structural plastic changes in their brains. To test our hypothesis, we investigated the possible gray and white matter density differences between a group of professional mathematicians (academicians at mathematics departments of universities) and the control subjects.

5.3.2 Materials and Methods

5.3.2.1 Subjects. We studied 26 mathematicians (19 men and 7 women; mean age, 35.50 ± 6.80 years) who were recruited from the volunteers who have been working as academicians at departments of mathematics. All of the mathematicians completed a 4-year undergraduate program of mathematics and had passed a 4-year-long PhD education program. Four of them were involved in algebra, 14 in applied mathematics, 3 in probabilistic analysis, and 2 in mathematic physics. The native language of all of the mathematicians and control subjects was Turkish. All of the mathematicians and control subjects could speak only English as a foreign language. The mathematicians

Table 5.7
Regions with increased grey matter density in the mathematicians

Data	Mathematicians	Control Subjects
Age, y	35.50 ± 6.95	35.43 ± 7.62
Sex (female/male)	9/17	7/16
Period of time spent as an academic, y	13.65 ± 6.95	14.13 ± 7.16

and control subjects were neither interested in music at a professional level nor could play a musical instrument. One mathematician who was more than 60 years of age and another who could play piano were not included in the study. Exclusion criteria for the mathematicians and control subjects also included any contraindication for MR imaging; alcohol or drug abuse; and any history of neurodegenerative disease, seizure, central nervous system infection, cerebrovascular disease, diabetes mellitus, and head trauma causing loss of consciousness that lasted more than 30 minutes or that required hospitalization. Cerebral lesions other than nonspecific cerebral white matter spots, present on T2-weighted images, were also accepted as exclusion criteria. The mean period of time spent as an academician after completing bachelor's degree was 13.65 ± 6.95 years. The demographic data of the participants are summarized in Table 5.7.

We recruited 23 sex- and age-matched control subjects (16 men and 7 women) among the volunteers of the academicians from the faculties of medicine and philosophy (mean age, 35.43 ± 7.62 years). All of the mathematicians and control subjects were right-handed (Edinburgh handedness inventory). Informed consent was taken from all of the participants, and the study was approved by the local human subject committee. Image

5.3.3   Image Acquisition

Cranial MR imaging studies were performed on a 1.5T superconducting whole-body MR imaging system (Symphony Maestro; Siemens Medical Systems, Erlangen, Germany) with a standard quadrature head coil. High-resolution anatomic images

of the whole brain were acquired from the mathematicians and control subjects with T1- weighted magnetization-prepared rapid acquisition gradient echo sequence (TR = 11.08 ms; TE = 4 ms; TI = 300 ms; relaxation delay time = 500 ms; flip angle = 15Â°; FOV = 256x192mm; matrix size = 256x192) yielding 128 sagittal sections with a defined voxel size of 1 x 1 x 1.3 mm. We also obtained the axial fast spin-echo T2-weighted images (TR = 9200 ms; TE = 110 ms; the number of acquisitions = 3) from all of the subjects to search for any pathologic findings defined in the study exclusion criteria.

5.3.4 Voxel-Based Morphometry Protocol and Data Preprocessing

The data preprocessing and analyses were performed with SPM2 (http://www.fil-.ion.ucl.ac.uk/spm/software/spm2; Wellcome Department of Cognitive Neurology, London, United Kingdom) running under Matlab (MathWorks, Natick, Mass). MR scanning produces images in Digital Imaging and Communications in Medicine (DICOM) format. All of the images in DICOM format were converted to ANALYSE format with the software MRIcro [168] (www.mricro. com). We applied an optimized method of voxel-based morphometry. Preprocessing of the data involved spatial normalization of all of the images into a standardized anatomic space, segmentation into gray and white matter, modulation, and spatial smoothing with a Gaussian kernel [14, 169, 170]. To reduce the scanner-specific bias,wecreated a customized gray matter by averaging the smoothened and normalized images of all of the participants. T1-weighted MR images were normalized to the standard T1 template of the Montreal Neurologic Institute (MNI). The normalized images were smoothed and averaged to obtain a study-specific T1 template. All of the original structural MRimages in native space were then normalized to this study-specific template. The normalized images were segmented into CSF, gray matter, and white matter compartments using the SPM2 priors. Afterward, CSF, gray matter, and white matter images were smoothened with an 8-mm full width at half maximum (FWHM) kernel and averaged to obtain study-specific CSF, gray matter, and white matter priors for later segmentation of native images. The original T1- weighted images were segmented with the study-specific T1 template and gray

matter, white matter, and CSF priors. This segmentation step involves an affine transformation of each scan to the template with a subsequent back projection into native space. We also performed a correction for volume changes (modulation) by modulating each voxel by the Jacobian determinants derived from the spatial normalization. An automated brain extraction procedure that incorporated a segmentation step was used to remove nonbrain tissue. The extracted gray matter images were then normalized to the group- specific gray matter template. The normalization parameters were then applied to the original structural images in native space to reduce any contribution from nonbrain voxels and afford optimal spatial normalization of gray matter. These normalized images were segmented into gray and white matter. Finally, the normalized and segmented images were smoothed with a 10-mm FWHM isotropic Gaussian kernel.

5.3.5   Statistical Analysis

We investigated the regionally specific gray and white matter density differences between the mathematician and control subjects using voxel-by-voxel analysis of variance test. Because the groups did not show a significant difference in age and sex distribution, we did not enter these variables as covariates. For the statistical analysis, we excluded all of the voxels with a gray or white matter value below 0.2 (of a maximum value of 1) to avoid possible edge effects around the border between gray and white matter and to include only voxels with sufficient gray and white matter, respectively. The findings were considered significant at a voxel level of $P<.0001$, uncorrected for multiple comparisons, with an extended threshold looking for clusters with at least 100 contiguous voxels. The relationship between the time duration of professional work and cortical gray matter density changes was investigated by regression analysis ($P<.05$, family-wise error [FWE] corrected). For localizing purposes, the MNI coordinates were converted to Talairach coordinates using a dedicated script (mni2tal.m; available at http://www.mrc-cbu.cam.ac.uk/Imaging/ Common/mnispace.shtml). Wherever a significant correlation was found between the mathematicians and control subjects, the gray matter density values were extracted for each of these voxel locations into SPSS for Microsoft Windows (SPSS, Chicago, Ill), and a linear regression analysis was per-

Table 5.8
Regions with increased grey matter density in the mathematicians

Anatomic Region (Brodmann Area)	Mathematicians vs Controls Talaraich Coordinates			Maximum *z* Values
	x	y	z	
Right inferior parietal lobule (BA 4)	54	−58	38	4.18
Right inferior parietal lobule (BA 7)	32	−46	60	4.08
Right inferior parietal lobule (BA 39)	57	−60	34	4.00
Left inferior parietal lobule (BA 40)	−38	−50	57	3.74
Left inferior frontal gyrus (BA 46)	−42	−34	12	3.51

formed to calculate the correlation coefficient. The statistical analyses in this study were carried out by a statistician.

5.3.6   Results

No significant difference was observed in education length and the parental education levels between mathematicians and control subjects (Table 5.7). In comparison with the age- and sex-matched control subjects, the mathematicians had significantly higher gray matter densities in the right inferior parietal lobule (Talaraich coordinates: x = 54, y = -58, z = 38 [Brodmann area, BA 4]; x = 32, y = -46, z = 60 [BA 7]; x = 57, y = -60, z = 34 [BA 39]); left inferior parietal lobule (x = -38, y = -50, z = 57 [BA 40]); and the left inferior frontal gyrus (x = -42, y = -34, z = 12 [BA 46]; Table 5.8; Fig 5.3.6). There was no region of decreased gray matter density in the mathematicians' brains compared with control subjects. The regression analyses revealed that the period of time spent as an academician was significantly associated with the gray matter density in the right parietal lobules of the mathematicians (Fig 5.3.6A). The gray matter density values extracted from the right inferior parietal lobule (x = 57, y = -60, z = 34 [BA 39]; z = 7.28; P < .05; FWE corrected) showed a strong correlation with the period of time spent as an academician (r =0.84; P< .01) on the SSPS correlation analysis (Fig 5.3.6B). The analysis of images revealed no difference in the white matter density of mathematicians and the control subjects.
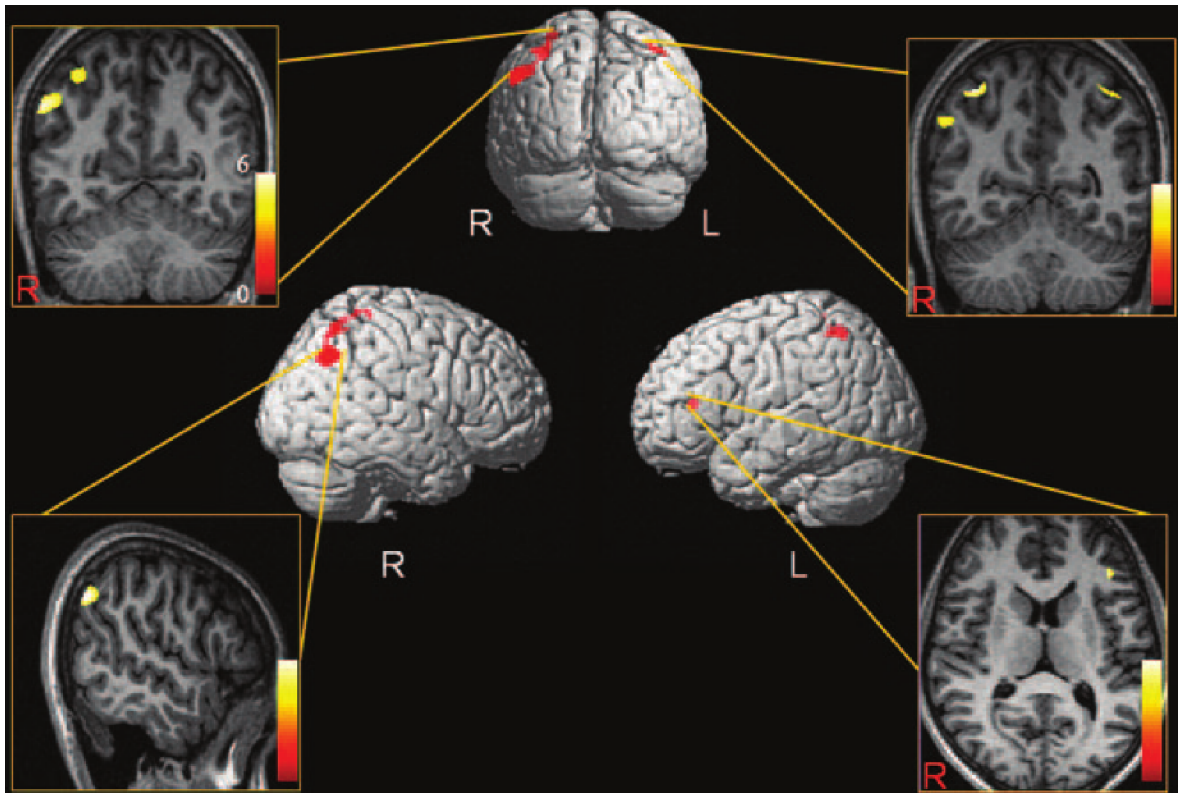
Figure 5.6 Distribution of significant voxels with increased gray matter density in the mathematicians relative to the control subjects (statistical significance is thresholded at P < .0001, uncorrected). Only clusters of voxels consisting of at least 100 voxels are displayed. The 3D overlay images demonstrate the regions with significantly increased gray matter density (red-labeled regions) in the mathematicians compared with the control subjects The anatomic sectional images show the overlay of the results on the normalized T1-weighted images of a mathematician. The color scale on the T1-weighted images shows the ranges of T values.

5.3.7 Discussion

The relationship between the morphology and functions of the human brain has attracted the interest of neuroscientists since the beginning of 20th century [171, 172]. Postmortem studies of some famous musicians, intellectual political leaders, and scientists were reported in search of the associations between the outstanding skills and the extraordinary cerebral morphology [173–175]. In some of these reports, the famous musicians had larger supramarginal gyrus than the normal population [174]. The postmortem study of Albert Einstein's brain showed that his inferior parietal lobule was larger than that of the control subjects and had a very exceptional parietal gyral morphology [175]. It has been speculated that there might be an association between the exceptionally enlarged inferior parietal lobules and his outstanding creativity in
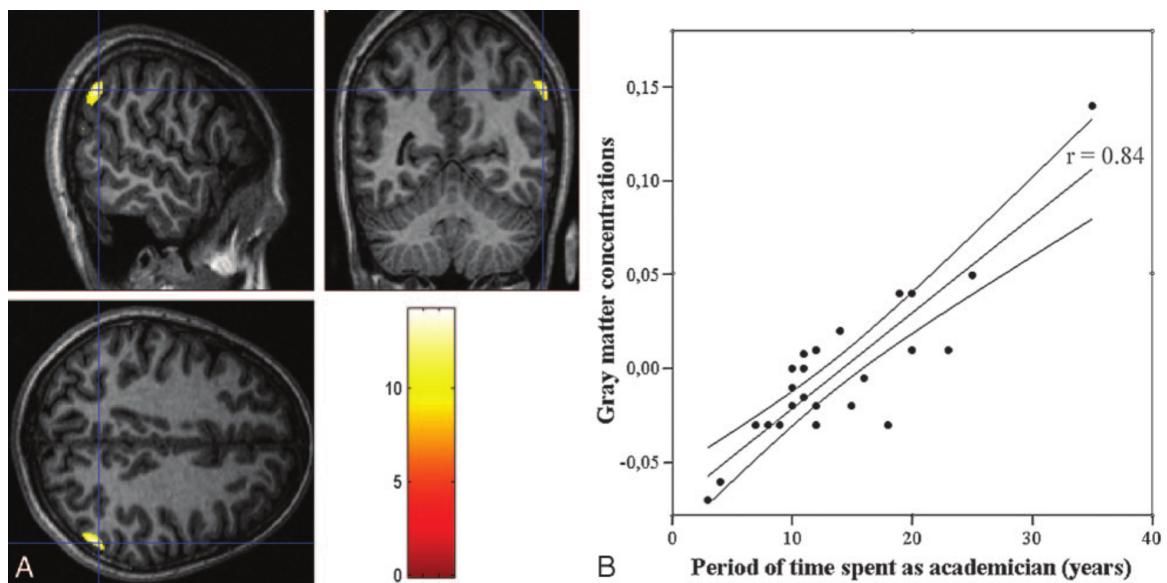
Figure 5.7 A, The result of the regression analysis testing the correlation between gray matter density of the mathematicians and period of time spent as an academician is overlayed on the normalized T1-weighted images. They show that gray matter density in the right inferior parietal region (Talaraich coordinates: x = 57, y = -60, z = 34) of the mathematicians is strongly correlated with the duration of time spent as an academician (z = 7.28; P < .05, FWE corrected). B, The gray matter density values from the voxels showing the maximum correlation on the SPM regression analysis are extracted into SPSS. The scatter-plot graph shows the linear regression between the gray matter density and the duration of time spent as an academician (r = 0.84; P < .01). The middle line represents the linear regression, and the curves around it represent the 95% confidence intervals.

mathematic thinking. Similarly, the postmortem study of the brain of another famous mathematician, Johann Karl Friedrich Gauss, revealed a remarkably convoluted appearance of the parietal lobes [171, 173]. Today, we know from the recent in vivo morphometric MR studies that the morphology of the human brain is determined by genetic factors but may also be modified by experiences.

Several cross-sectional morphometry studies have been conducted in musicians to investigate the morphologic differences of their brains from normal control subjects and to search the association between morphologic differences and the training and practicing of musical skills [159–164, 166]. Results of these studies revealed that musicians had anatomic differences in several regions of their brain that have been involved in motor and auditory processing. The morphologic differences observed in mathematicians' brains were significantly correlated with the musical skills and ages of commencement for musical training [163, 164]. Amunts et al [163] reported a strong

negative correlation between the commencement age of musical training and sizes of hand-motor cortical regions of pianists. In another study, musicians who began the musical training earlier than age 7 years had larger anterior corpus callosums than the musicians who started the training later [162]. Musicians with an absolute pitch skill (ability to discriminate musical tones without a need for a reference tone) had larger planum temporale than the musicians without an absolute pitch [164]. Because they are strongly associated with training periods and professional skills, it has been proposed that morphologic differences observed in the brains of musicians were experience-dependent structural changes developed as a result of intense, long-term training and practicing musical skills [159]. In the study conducted with the taxi drivers in London, Maguire et al [22] reported a significant association between the increased gray matter density in the right posterior hippocampus of the taxi drivers and the period of time spent as a taxi driver. They proposed that long-term training and practicing to memorize a hugeamount of spatial information might cause an experience-dependent structural change in the hippocampus of the taxi drivers in which the spatial information is processed. They also found that the control subjects had larger gray matter volumes in the anterior hippocampus. They hypothesized that extensive navigation experience led to redistribution of gray matter in the hippocampus. In our study, we did not observe any finding that might indicate the presence of gray matter redistribution in the mathematicians. Recent longitudinal morphometry studies demonstrated that repeated practicing of a visuomotor task and intense learning of abstract information could lead to gray matter density changes in task-related regions of brain [60, 157, 176]. In summary, the results of cross-sectional and longitudinal in vivo morphometric MR imaging studies point to the presence of experience-dependent structural plasticity in the human brain.

Voxel-based morphometry is a statistical imaging method that gives opportunities to investigate regionally specific subtle gray matter differences between various study groups [14]. To the best of our knowledge, this is the first in vivo study investigating morphologic differences of mathematicians' brains. We hypothesized that long-term and specific training of mathematics and practicing of mathematic thinking might cause an experience-dependent structural alteration in mathematicians' brains.

We conducted an optimized voxel-based morphometry study to test our hypothesis [169, 170]. Our results suggest that gray matter density of mathematicians shows diverse distribution in the inferior parietal lobules and left inferior frontal gyrus compared with age- and sex-matched control subjects. In addition, we found a strong correlation between the gray matter density in the right inferior parietal lobule of the mathematicians and the period of time spent as an academician. We know from previous functional MR imaging studies that processing of mental arithmetic calculations has language- and visuospatial-related components, which take place in different regions of the brain [177–179]. The exact arithmetic calculation skills, such as multiplying, have language- specific representations in the brain and are processed in the language-related left inferior frontal and left angular gyri. The arithmetic calculations requiring approximations and comparison of numbers, such as subtraction, have visuospatial representations in the brain and are processed in the bilateral parietal regions around the intraparietal sulci. In our study,we found significant gray matter density increase in the same regions where the mental arithmetic calculations are processed. The strong correlation between gray matter density change in the right inferior parietal lobule and the period of time spent as an academician indicates that structural difference observed in this region may result from an experience-dependent process. Long-term and intense mental practice with numeric data may lead to experience-dependent plastic changes in the related regions of brain. Mathematicians not only do arithmetic calculations, but they also deal with advanced mathematic problems that require mental imagery, mental creativity, and manipulation of 3D objects, which are all processed in parietal lobes. Mathematicians have a unique ways of scientific thinking, which they use in problem solving. It was stated in a self-description by Albert Einstein as, ". . . Words and language whether written or spoken, do not seem to play any part inmy thought process. The psychological entities that serve as building blocks from my thought are certain signs or images, more or less clear, that I can reproduce or recombine at will." In his statements, he emphasized the visuospatial rather than verbal type of scientific thinking. Another famous mathematician, Jacques Hadamard, declared that his scientific thinking mainly relied on visuospatial rather than verbal processes. Throughout their academic lives, mathematicians practice this visuospatial data processing, which may contribute to the increased gray matter density in the parietal lobules [175].

The gray matter changes observed in the left inferior parietal lobule and left inferior frontal gyrus did not correlate with the period of time spent as a mathematician. However, this does not rule out the possibility that gray matter density differences, which are observed in the left inferior frontal gyrus and left inferior parietal lobule, are experience-dependent structural changes. Results of recently reported longitudinal studies revealed that experience-dependent structural changes may develop within weeks or months after the stimuli [157, 176]. Structural changes observed in left inferior frontal gyrus and left inferior parietal lobule may develop in earlier times of the professional careers of mathematicians. Left inferior frontal gyrus is a language-related region of arithmetic processing. It would be good to test performances on verbal-related arithmetic calculations and to investigate the association between the gray matter density and test performances. Because most of the participants were not willing receive such a test, we were not able to investigate this association.

Histologic correlation of experience-dependent adaptive plasticity in the human brain has not been exactly defined yet. Neurogenesis, microglia proliferation, synaptogenesis, angiogenesis, axonal sprouting, modulation of synaptic transmission, and change in excitatory/inhibitory transmission balance have been postulated as the possible mechanisms of experience-dependent plasticity [180–192]. Adaptive neurogenesis in the adult brain was first reported in animal studies. Food hiding and seeking behavior in food-storing bird species, which requires the storage of spatial information, stimulates the neurogenesis in the hippocampal region known as the spatial navigation center [186, 191]. Male canaries sing during their breeding season and learn new songs every year. Just before their breeding season, the high vocal center (a region in the brains of birds that is related to singing) of male canaries enlarges with the addition of new neurons [186–192]. It has also been demonstrated that enriched environments in the experimental conditions may stimulate the neurogenesis in the hippocampus of adult mammalian brains [190]. Synaptogenesis is the other mechanism that has been postulated to explain the mechanism of experience-dependent plasticity [180, 189, 190, 193]. Long-term sensory stimuli increase the number of synapses that that modify the sensitivity of sensory system. Thus, newly generated synapses increase the complexity of the neuronal network that may enable the processing of complex data.

It is known from the previous studies that intelligence quotient (IQ) levels of individuals may influence the cortical gray matter distribution. It would be good to perform IQ measurements and consider IQ scores as a cofactor in the statistical analyses (analysis of covariance) of voxel-based morphometry. However, most of our subjects did not agree to get an IQ test. However, there was no significant difference in the education levels between the study groups, and all of the subjects in both groups were academicians. So, the individuals from both groups would be expected to have similar IQ levels. There is no objective evidence for a significant IQ level difference between the mathematicians and control subjects.

5.3.8   Conclusion

In conclusion,wefound that mathematicians had significantly increased cortical gray matter density in the bilateral inferior parietal lobules and left inferior frontal gyrus, which are known to be involved in arithmetic calculations and visuospatial processing. Significant association of gray matter density changes in the right inferior parietal lobule with the period of time spent as an academician proposed that the structural change in this location is an experience-dependent process, which might be caused by the long-term practices of visuospatial and arithmetic data processing.

6. General Summary and Conclusion

VBM has many stages in its processing pipeline. Changes in the methods and/or parameters along this pipeline (methods used for the segmentation and registration, using or omitting modulation, the width of the kernel for the smoothing, and methods and thresholds used in the statistical inferences) have ability to change the results [36, 40, 41, 43, 48, 63, 194]. Therefore, it's crucial to determine the rules and regulations in the VBM processing. In order to determine these rules and regulations, the effects of parameters at each stage should be explored.

Modulation was introduced into the VBM analysis for the aim of regaining the original volume which is shrinked or enlarged during the registration (normalization) step. Modulation was achieved by multiplying the voxels by the Jacobian determinants that are obtained during the registration. However, maybe because of its straightforward aim, proving its validity had been omitted for a long time. Radua et al (2014) [43] claimed that modulation decreases the sensitivity, we have also demonstrated it by simulation data in 2009 [44], although not in grey matter but in white matter, but technically there should not be any difference between the grey matter and white matter in this issue. Later in 2016 [49], we have demonstrated in grey matter too, by using both simulated and Parkinson's Disease patients that omitting the modulation step increases the sensitivity.

From the aspect of masking, in SPM, if a previously prepared mask was not used (which is rarely used), either a constant value (absolute) or a fraction to each image's global value (relative) is used. A larger mask can lower the detection power of VBM, however, a smaller mask might exclude the regions that might possibly show the atrophied regions in most of the neurodegenerative diseases. An alternative masking strategy is proposed by Ridgeway (2009) [36]: using a threshold which increases the maximum correlation between the average image and the binarized thresholded average image. By using our both simulated and PD data, we have found that this increases

the sensitivity of VBM analysis.

When using the abovementioned two points together, unmodulation and average-based masking, we have found that the sensitivity increases even better with respect to the cases where they were used alone. We have also found that, in this way, VBM reveals the regions in early non-demented PD patients that were not be able to revealed with modulation and absolute thresholding. Those regions were previously detected by other studies employing other methods besides VBM in similar cohorts, or by VBM in PD patients in whom the disease had progressed. Therefore, using this real PD data, we can claim that modulation and average-based thresholding increases the sensitivity as proved in simulation data.

VBM is a very widely used morphometry method. So far, it has been implemented by some dedicated tools with several changeable parameters or the combination of various image processing and statistical tools again with various parameters. The variations in these parameters can potentially change the VBM results. Therefore, it is crucial for the users to understand the stages of the VBM processing. This thesis gives detailed descriptions of its stages to make the users aware of what VBM actually does, gives brief summaries about the discussions in the literature to warn the users about the pitfalls and the limitations of VBM, and also gives information about the alternative morphometric tools to give a view about where VBM stands at. This thesis studies also the three clinical studies which are about the effects of learning (mathematicians [3]), disease (subacute sclerosing panencephalitis [1]), and exposure to substance (solvent [2]) in which we used VBM for the analysis. Finally, this thesis studies deeply on two parameters/options in the VBM processing pipeline: modulation and average based masking for the statistics. It has been concluded that not using modulation and using average based masking instead of absolute threshold increases the sensitivity of VBM.

APPENDIX A. List of Publications Originated from this Thesis

SCI or SCIE indexed Journals:

1. Effects of Unmodulation and Thresholding by Average-Based Masking on Voxel-based Morphometry: O. Ozmen Okur, C. Ozturk, *Journal of Medical Imaging and Health Informatics*, 2016.

2. Reduced Gray Matter Volume in the Frontotemporal Cortex of Patients with Early Subacute Sclerosing Panencephalitis: K. Aydin, O. Ozmen Okur, B. Tatli, SG. Sarwar, C. Ozturk, C. Dilber, *American Journal of Neuroradiology*, vol.30(2), pp.271-75, 2009.

3. Smaller Gray Matter Volumes in Frontal and Parietal Cortices of Solvent Abusers Correlate with Cognitive Deficits: K. Aydin, S. Kircan, S. Sarwarb, O. Ozmen Okur, E. Balaban, *American Journal of Neuroradiology*, vol.30(10), pp.1922-1928, 2009.

4. Increased Gray Matter Density Density in the Parietal Cortex of Mathematicians: K. Aydin, A. Ucar, K.K. Oguz, O. Ozmen Okur, A. Agayev, Z. Unal, S. Yilmaz, C. Ozturk, *American Journal of Neuroradiology*, vol.28, pp. 1859-1900, 2007.

Conferences:

1. Effects of the Modulation in the White Matter Voxel Based Morphometry: O. Ozmen Okur, C. Ozturk, K. Aydin, *Proceedings, International Society for Magnetic Resonance in Medicine*, 17, 4685, Honolulu, USA, 2009.

2. Evaluation of non-rigid registration of SPM5 in normal children: O. Ozmen Okur, K. Aydin, C. Ozturk, *Proceedings of 25th Annual Meeting of ESMRMB*, Valencia, Spain, 2008.

3. Morphological Differences in the Grey Matters of Mathematicians: A Voxel-Based Morphometry Study: O. Ozmen Okur, A. Agayev, C. Ozturk, K. Aydin *Proceedings, International Society for Magnetic Resonance in Medicine*, Berlin, Germany, May 2007.

4. Comparison of SPM and Freesurfer Brain Morphometry Analyses Results: Ozmen Okur, O., Ozturk, C., Aydin, K., *Proceedings of 14th National Biomedical Engineering Conference:BIYOMUT 2009*, Izmir, 2009.

REFERENCES

1. Aydin, K., O. Okur, B. Tatli, S. Sarwar, C. Ozturk, and C. Dilber, "Reduced gray matter volume in the frontotemporal cortex of patients with early subacute sclerosing panencephalitis," *American Journal of Neuroradiology*, Vol. 30, no. 2, pp. 271–275, 2009.

2. Aydin, K., S. Kircan, S. Sarwar, O. Okur, and E. Balaban, "Smaller gray matter volumes in frontal and parietal cortices of solvent abusers correlate with cognitive deficits," *American Journal of Neuroradiology*, Vol. 30, no. 10, pp. 1922–1928, 2009.

3. Aydin, K., A. Ucar, K. Oguz, O. Okur, A. Agayev, Z. Unal, S. Yilmaz, and C. Ozturk, "Increased gray matter density in the parietal cortex of mathematicians: a voxel-based morphometry study," *American Journal of Neuroradiology*, Vol. 28, no. 10, pp. 1859–1864, 2007.

4. Andreasen, N. C., S. Arndt, V. Swayze, T. Cizadlo, M. Flaum, D. O'Leary, J. C. Ehrhardt, and W. Yuh, "Thalamic abnormalities in schizophrenia visualized through magnetic resonance image averaging," *Science*, Vol. 266, no. 5183, pp. 294–298, 1994.

5. Wright, I., P. McGuire, J.-B. Poline, J. Travere, R. Murray, C. Frith, R. Frackowiak, and K. Friston, "A voxel-based method for the statistical analysis of gray and white matter density applied to schizophrenia," *Neuroimage*, Vol. 2, no. 4, pp. 244–252, 1995.

6. Wright, I., Z. Ellison, T. Sharma, K. Friston, R. Murray, and P. McGuire, "Mapping of grey matter changes in schizophrenia," *Schizophrenia research*, Vol. 35, no. 1, pp. 1–14, 1999.

7. Vargha-Khadem, F., K. E. Watkins, C. Price, J. Ashburner, K. J. Alcock, A. Connelly, R. S. Frackowiak, K. J. Friston, M. Pembrey, M. Mishkin, *et al.*, "Neural basis of an inherited speech and language disorder," *Proceedings of the National Academy of Sciences*, Vol. 95, no. 21, pp. 12695–12700, 1998.

8. Shah, P. J., K. P. Ebmeier, M. F. Glabus, and G. M. Goodwin, "Cortical grey matter reductions associated with treatment-resistant chronic unipolar depression. controlled magnetic resonance imaging study.," *The British journal of psychiatry*, Vol. 172, no. 6, pp. 527–532, 1998.

9. Krams, M., R. Quinton, J. Ashburner, K. Friston, R. Frackowiak, P. Bouloux, and R. Passingham, "Kallmann's syndrome mirror movements associated with bilateral corticospinal tract hypertrophy," *Neurology*, Vol. 52, no. 4, pp. 816–816, 1999.

10. Abell, F., M. Krams, J. Ashburner, R. Passingham, K. Friston, R. Frackowiak, F. Happé, C. Frith, and U. Frith, "The neuroanatomy of autism: a voxel-based whole brain analysis of structural scans," *Neuroreport*, Vol. 10, no. 8, pp. 1647–1651, 1999.

11. Woermann, F. G., S. L. Free, M. J. Koepp, J. Ashburner, and J. S. Duncan, "Voxel-by-voxel comparison of automatically segmented cerebral gray matter, a rater independent comparison of structural mri in patients with epilepsy," *Neuroimage*, Vol. 10, no. 4, pp. 373–384, 1999.

12. Sowell, E. R., P. M. Thompson, C. J. Holmes, R. Batth, T. L. Jernigan, and A. W. Toga, "Localizing age-related changes in brain structure between childhood and adolescence using statistical parametric mapping," *Neuroimage*, Vol. 9, no. 6, pp. 587–597, 1999.

13. May, A., J. Ashburner, C. Büchel, D. McGonigle, K. Friston, R. Frackowiak, and P. Goadsby, "Correlation between structural and functional changes in brain in an idiopathic headache syndrome," *Nature medicine*, Vol. 5, no. 7, pp. 836–838, 1999.

14. Ashburner, J., and K. J. Friston, "Voxel-based morphometry–the methods.," *NeuroImage*, Vol. 11, pp. 805–21, jun 2000.

15. Agosta, F., E. Canu, T. Stojković, M. Pievani, A. Tomić, L. Sarro, N. Dragašević, M. Copetti, G. Comi, V. S. Kostić, and M. Filippi, "The topography of brain damage at different stages of Parkinsons disease.," *Human brain mapping*, Vol. 34, pp. 2798–807, nov 2013.

16. Ferreira, L. K., B. S. Diniz, O. V. Forlenza, G. F. Busatto, and M. V. Zanetti, "Neurostructural predictors of Alzheimers disease: A meta-analysis of VBM studies," *Neurobiology of Aging*, Vol. 32, no. 10, pp. 1733–1741, 2011.

17. Whitwell, J. L., R. Avula, A. Master, P. Vemuri, M. L. Senjem, D. T. Jones, C. R. Jack, and K. A. Josephs, "Disrupted thalamocortical connectivity in PSP: A resting-state fMRI, DTI, and VBM study," *Parkinsonism and Related Disorders*, Vol. 17, no. 8, pp. 599–605, 2011.

18. Bodini, B., Z. Khaleeli, M. Cercignani, D. H. Miller, A. J. Thompson, and O. Ciccarelli, "Exploring the relationship between white matter and gray matter damage in early primary progressive multiple sclerosis: An in vivo study with TBSS and VBM," *Human Brain Mapping*, Vol. 30, no. 9, pp. 2852–2861, 2009.

19. Radua, J., O. A. van den Heuvel, S. Surguladze, and D. Mataix-Cols, "Meta-analytical comparison of voxel-based morphometry studies in obsessive-compulsive disorder vs other anxiety disorders," *Archives of general psychiatry*, Vol. 67, no. 7, pp. 701–711, 2010.

20. Rüsch, N., L. T. Van Elst, P. Ludaescher, M. Wilke, H.-J. Huppertz, T. Thiel, C. Schmahl, M. Bohus, K. Lieb, B. Hesslinger, *et al.*, "A voxel-based morphometric mri study in female patients with borderline personality disorder," *Neuroimage*, Vol. 20, no. 1, pp. 385–392, 2003.

21. Colloby, S. J., M. J. Firbank, A. Vasudev, S. W. Parry, A. J. Thomas, and J. T. O'Brien, "Cortical thickness and VBM-DARTEL in late-life depression," *Journal of Affective Disorders*, Vol. 133, no. 1-2, pp. 158–164, 2011.

22. Maguire, E. A., D. G. Gadian, I. S. Johnsrude, C. D. Good, J. Ashburner, R. S. Frackowiak, and C. D. Frith, "Navigation-related structural change in the hippocampi of taxi drivers," *Proceedings of the National Academy of Sciences*, Vol. 97, no. 8, pp. 4398–4403, 2000.

23. Mechelli, A., J. T. Crinion, U. Noppeney, J. O'Doherty, J. Ashburner, R. S. Frackowiak, and C. J. Price, "Neurolinguistics: structural plasticity in the bilingual brain," *Nature*, Vol. 431, no. 7010, pp. 757–757, 2004.

24. Kennedy, K. M., K. I. Erickson, K. M. Rodrigue, M. W. Voss, S. J. Colcombe, A. F. Kramer, J. D. Acker, and N. Raz, "Age-related differences in regional brain volumes: a comparison of optimized voxel-based morphometry to manual volumetry," *Neurobiology of aging*, Vol. 30, no. 10, pp. 1657–1676, 2009.

25. Papagni, S. A., S. Benetti, S. Arulanantham, E. McCrory, P. McGuire, and A. Mechelli, "Effects of stressful life events on human brain structure: a longitudinal voxel-based morphometry study," *Stress*, Vol. 14, no. 2, pp. 227–232, 2011.

26. Evans, A. C., D. L. Collins, S. Mills, E. Brown, R. Kelly, and T. M. Peters, "3d statistical neuroanatomical models from 305 mri volumes," in *Nuclear Science Symposium and Medical Imaging Conference, 1993., 1993 IEEE Conference Record.*, pp. 1813–1817, IEEE, 1993.

27. Good, C. D., I. S. Johnsrude, J. Ashburner, R. N. A. Henson, K. J. Friston, and R. S. J. Frackowiak, "A Voxel-Based Morphometric Study of Ageing in 465 Normal Adult Human Brains," Vol. 36, no. 1998, pp. 21–36, 2000.

28. Ashburner, J., and K. J. Friston, "Unified segmentation," *NeuroImage*, Vol. 26, no. 3, pp. 839–851, 2005.

29. Ashburner, J., "A fast diffeomorphic image registration algorithm.," *NeuroImage*, Vol. 38, pp. 95–113, oct 2007.

30. Ashburner, J., and K. J. Friston, "Diffeomorphic registration using geodesic shooting and gauss–newton optimisation," *NeuroImage*, Vol. 55, no. 3, pp. 954–967, 2011.

31. Jenkinson, M., C. F. Beckmann, T. E. J. Behrens, M. W. Woolrich, and S. M. Smith, "Fsl," *NeuroImage*, Vol. 62, no. 2, pp. 782–790, 2012.

32. Friston, K. J., K. J. Worsley, R. Frackowiak, J. C. Mazziotta, and A. C. Evans, "Assessing the significance of focal activations using their spatial extent," *Human brain mapping*, Vol. 1, no. 3, pp. 210–220, 1994.

33. Nichols, T. E., "Multiple testing corrections, nonparametric methods, and random field theory," *NeuroImage*, Vol. 62, no. 2, pp. 811–815, 2012.

34. Penny, W. D., K. J. Friston, J. T. Ashburner, S. J. Kiebel, and T. E. Nichols, *Statistical parametric mapping: the analysis of functional brain images*, Academic press, 2011.

35. Worsley, K. J., S. Marrett, P. Neelin, A. C. Vandal, K. J. Friston, A. C. Evans, *et al.*, "A unified statistical approach for determining significant signals in images of cerebral activation," *Human brain mapping*, Vol. 4, no. 1, pp. 58–73, 1996.

36. Ridgway, G. R., R. Omar, S. Ourselin, D. L. G. Hill, J. D. Warren, and N. C. Fox, "Issues with threshold masking in voxel-based morphometry of atrophied brains.," *NeuroImage*, Vol. 44, pp. 99–111, jan 2009.

37. Bookstein, F. L., ""Voxel-based morphometry" should not be used with imperfectly registered images.," *NeuroImage*, Vol. 14, pp. 1454–62, dec 2001.

38. Ashburner, J., and K. J. Friston, "Why voxel-based morphometry should be used," *Neuroimage*, Vol. 14, no. 6, pp. 1238–1243, 2001.

39. Bookstein, F. L., *Linear methods for nonlinear maps*, Academic Press, San Diego, 1999.

40. Pereira, J. M. S., L. Xiong, J. Acosta-Cabronero, G. Pengas, G. B. Williams, and P. J. Nestor, "Registration accuracy for VBM studies varies according to region and degenerative disease grouping.," *NeuroImage*, Vol. 49, pp. 2205–15, feb 2010.

41. Mak, H. K.-F., Z. Zhang, K. K.-W. Yau, L. Zhang, Q. Chan, and L.-W. Chu, "Efficacy of voxel-based morphometry with DARTEL and standard registration as imaging biomarkers in Alzheimers disease patients and cognitively normal older adults at 3.0 Tesla MR imaging.," *Journal of Alzheimers disease : JAD*, Vol. 23, pp. 655–64, jan 2011.

42. Nordenskjöld, R., F. Malmberg, E.-M. Larsson, A. Simmons, S. J. Brooks, L. Lind, H. Ahlström, L. Johansson, and J. Kullberg, "Intracranial volume estimated with commonly used methods could introduce bias in studies including brain volume measurements.," *NeuroImage*, Vol. 83, pp. 355–60, dec 2013.

43. Radua, J., E. J. Canales-Rodríguez, E. Pomarol-Clotet, and R. Salvador, "Validity of modulation and optimal settings for advanced voxel-based morphometry.," *NeuroImage*, Vol. 86, pp. 81–90, feb 2014.

44. Okur, O. O., C. Ozturk, and K. Aydin, "Effects of the modulation in the white matter voxel based morphometry,"

45. Salmond, C., J. Ashburner, F. Vargha-Khadem, A. Connelly, D. Gadian, and K. Friston, "Distributional assumptions in voxel-based morphometry," *Neuroimage*, Vol. 17, no. 2, pp. 1027–1030, 2002.

46. Shen, S., and A. Sterr, "Is DARTEL-based voxel-based morphometry affected by width of smoothing kernel and group size? A study using simulated atrophy.," *Journal of magnetic resonance imaging : JMRI*, Vol. 000, pp. 1–8, nov 2012.

47. Scarpazza, C., S. Tognin, S. Frisciata, G. Sartori, and A. Mechelli, "False positive rates in voxel-based morphometry studies of the human brain: Should we be worried?," *Neuroscience & Biobehavioral Reviews*, Vol. 52, pp. 49–55, 2015.

48. Bennett, C. M., G. L. Wolford, and M. B. Miller, "The principled control of false positives in neuroimaging.," *Social cognitive and affective neuroscience*, Vol. 4, pp. 417–22, dec 2009.

49. *NeuroImage*, Vol. 55, no. 3, pp. 954–967, 2016.

50. Scarpazza, C., G. Sartori, M. De Simone, and A. Mechelli, "When the single matters more than the group: very high false positive rates in single case voxel based morphometry," *Neuroimage*, Vol. 70, pp. 175–188, 2013.

51. Peelle, J. E., R. Cusack, and R. N. a. Henson, "Adjusting for global effects in voxel-based morphometry: gray matter decline in normal aging.," *NeuroImage*, Vol. 60, pp. 1503–16, apr 2012.

52. Takao, H., N. Hayashi, and K. Ohtomo, "Effects of study design in multi-scanner voxel-based morphometry studies.," *NeuroImage*, Vol. 84, pp. 133–40, jan 2014.

53. Focke, N. K., G. Helms, S. Kaspar, C. Diederich, V. Tóth, P. Dechent, A. Mohr, and W. Paulus, "NeuroImage Multi site voxel based morphometry, Not quite there yet," *NeuroImage*, Vol. 56, no. 3, pp. 1164–1170, 2011.

54. Jovicich, J., M. Marizzoni, R. Sala-Llonch, B. Bosch, D. Bartr??s-Faz, J. Arnold, J. Benninghoff, J. Wiltfang, L. Roccatagliata, F. Nobili, T. Hensch, A. Tr??nkner, P. Sch??nknecht, M. Leroy, R. Lopes, R. Bordet, V. Chanoine, J. P. Ranjeva, M. Didic, H. Gros-Dagnac, P. Payoux, G. Zoccatelli, F. Alessandrini, A. Beltramello, N. Bargall??,

O. Blin, and G. B. Frisoni, "Brain morphometry reproducibility in multi-center 3T MRI studies: A comparison of cross-sectional and longitudinal segmentations," *NeuroImage*, Vol. 83, pp. 472–484, 2013.

55. Pell, G. S., R. S. Briellmann, C. H. P. Chan, H. Pardoe, D. F. Abbott, and G. D. Jackson, "Selection of the control group for vbm analysis: influence of covariates, matching and sample size," *Neuroimage*, Vol. 41, no. 4, pp. 1324–1335, 2008.

56. Friston, K., "Ten ironic rules for non-statistical reviewers," *Neuroimage*, Vol. 61, no. 4, pp. 1300–1310, 2012.

57. Hupe, J.-M., "Statistical inferences under the null hypothesis: common mistakes and pitfalls in neuroimaging studies," *Frontiers in neuroscience*, Vol. 9, 2015.

58. Shen, S., A. J. Szameitat, and A. Sterr, "VBM lesion detection depends on the normalization template: a study using simulated atrophy.," *Magnetic resonance imaging*, Vol. 25, pp. 1385–96, dec 2007.

59. Tardif, C. L., D. L. Collins, and G. B. Pike, "Sensitivity of voxel-based morphometry analysis to choice of imaging protocol at 3 t," *Neuroimage*, Vol. 44, no. 3, pp. 827–838, 2009.

60. Draganski, B., C. Gaser, V. Busch, G. Schuierer, U. Bogdahn, and A. May, "Neuroplasticity: changes in grey matter induced by training," *Nature*, Vol. 427, no. 6972, pp. 311–312, 2004.

61. Thompson, W. K., D. Holland, A. D. N. Initiative, *et al.*, "Bias in tensor based morphometry stat-roi measures may result in unrealistic power estimates," *NeuroImage*, Vol. 57, no. 1, pp. 1–4, 2011.

62. Ashburner, J., and G. R. Ridgway, "Symmetric diffeomorphic modeling of longitudinal structural mri," *Front Neurosci*, Vol. 6, p. 197, 2012.

63. Rajagopalan, V., G. H. Yue, and E. P. Pioro, "Do preprocessing algorithms and statistical models influence voxel-based morphometry (VBM) results in amyotrophic lateral sclerosis patients? A systematic comparison of popular VBM analytical methods," *Journal of Magnetic Resonance Imaging*, Vol. 40, no. 3, pp. 662–667, 2014.

64. Popescu, V., M. M. Schoonheim, A. Versteeg, N. Chaturvedi, M. Jonker, R. X. De Menezes, F. G. Garre, B. M. J. Uitdehaag, F. Barkhof, and H. Vrenken, "Grey matter atrophy in multiple sclerosis: Clinical interpretation depends on choice of analysis method," *PLoS ONE*, Vol. 11, no. 1, pp. 1–17, 2016.

65. Diaz-de Grenu, L. Z., J. Acosta-Cabronero, Y. F. V. Chong, J. Pereira, S. A. Sajjadi, G. B. Williams, and P. J. Nestor, "A brief history of voxel-based grey matter analysis in alzheimer's disease," *Journal of Alzheimer's Disease*, Vol. 38, no. 3, pp. 647–659, 2014.

66. Toga, A. W., *Brain mapping: An encyclopedic reference*, Academic Press, 2015.

67. Hutton, C., E. De Vita, J. Ashburner, R. Deichmann, and R. Turner, "Voxel-based cortical thickness measurements in mri," *Neuroimage*, Vol. 40, no. 4, pp. 1701–1710, 2008.

68. Hutton, C., B. Draganski, J. Ashburner, and N. Weiskopf, "A comparison between voxel-based cortical thickness and voxel-based morphometry in normal aging," *Neuroimage*, Vol. 48, no. 2, pp. 371–380, 2009.

69. Greve, D. N., "An absolute beginners guide to surface-and voxel-based morphometric analysis," in *Proc Intl Soc Mag Reson Med*, Vol. 19, 2011.

70. Toews, M., W. Wells, D. L. Collins, and T. Arbel, "Feature-based morphometry: Discovering group-related anatomical patterns," *NeuroImage*, Vol. 49, no. 3, pp. 2318–2327, 2010.

71. Wang, H., Y. Ren, L. Bai, W. Zhang, and J. Tian, "Morphometry based on effective and accurate correspondences of localized patterns (meacolp)," *PLoS ONE*, Vol. 7, no. 4, 2012.

72. Chen, Y., J. Storrs, L. Tan, L. J. Mazlack, J. H. Lee, and L. J. Lu, "Detecting brain structural changes as biomarker from magnetic resonance images using a local feature based SVM approach," *Journal of Neuroscience Methods*, Vol. 221, pp. 22–31, 2014.

73. Gaonkar, B., K. Pohl, and C. Davatzikos, "Pattern based morphometry.," *Medical image computing and computer-assisted intervention : MICCAI ... International Conference on Medical Image Computing and Computer-Assisted Intervention*, Vol. 14, no. Pt 2, pp. 459–66, 2011.

74. Orr??, G., W. Pettersson-Yeo, A. F. Marquand, G. Sartori, and A. Mechelli, "Using Support Vector Machine to identify imaging biomarkers of neurological and psychiatric disease: A critical review," *Neuroscience and Biobehavioral Reviews*, Vol. 36, no. 4, pp. 1140–1152, 2012.

75. Ellfolk, U., J. Joutsa, and J. O. Rinne, "Striatal volume is related to phonemic verbal fluency but not to semantic or alternating verbal fluency in early Parkinson ' s disease," *J Neural Transm*, Vol. i, pp. 33–40, 2014.

76. Gerrits, N. J. H. M., Y. D. van der Werf, M. Hofman, E. M. J. Foncke, M. Klein, H. W. Berendse, and O. A. van den Heuvel, "Gray matter differences contribute to variation in cognitive performance in Parkinsons disease.," *European journal of neurology : the official journal of the European Federation of Neurological Societies*, Vol. 21, pp. 245–52, feb 2014.

77. Herman, T., K. Rosenberg-Katz, Y. Jacob, N. Giladi, and J. M. Hausdorff, "Gray matter atrophy and freezing of gait in Parkinsons disease: Is the evidence black-on-white?," *Movement disorders : official journal of the Movement Disorder Society*, Vol. 29, pp. 134–9, jan 2014.

78. Lee, H. M., K.-Y. Kwon, M.-J. Kim, J.-W. Jang, S.-I. Suh, S.-B. Koh, and J. H. Kim, "Subcortical grey matter changes in untreated, early stage Parkinsons disease without dementia.," *Parkinsonism & related disorders*, Vol. 20, pp. 622–6, jun 2014.

79. Menke, R. a. L., K. Szewczyk-Krolikowski, S. Jbabdi, M. Jenkinson, K. Talbot, C. E. Mackay, and M. Hu, "Comprehensive morphometry of subcortical grey matter structures in early-stage Parkinsons disease.," in *Human brain mapping*, Vol. 35, pp. 1681–90, apr 2014.

80. Lin, C.-H., C.-M. Chen, M.-K. Lu, C.-H. Tsai, J.-C. Chiou, J.-R. Liao, and J.-R. Duann, "VBM Reveals Brain Volume Differences between Parkinsons Disease and Essential Tremor Patients.," *Frontiers in human neuroscience*, Vol. 7, p. 247, jan 2013.

81. Rosenberg-Katz, K., T. Herman, Y. Jacob, N. Giladi, T. Hendler, and J. M. Hausdorff, "Gray matter atrophy distinguishes between Parkinson disease motor subtypes.," *Neurology*, Vol. 80, pp. 1476–84, apr 2013.

82. Pereira, J. B., N. Ibarretxe-Bilbao, M.-J. Marti, Y. Compta, C. Junqué, N. Bargallo, and E. Tolosa, "Assessment of cortical degeneration in patients with Parkinsons disease by voxel-based morphometry, cortical folding, and cortical thickness.," *Human brain mapping*, Vol. 33, pp. 2521–34, nov 2012.

83. Compta, Y., N. Ibarretxe-Bilbao, J. B. Pereira, C. Junqué, N. Bargalló, E. Tolosa, F. Valldeoriola, E. Muñoz, A. Camara, M. Buongiorno, and M. J. Martí, "Grey matter volume correlates of cerebrospinal markers of Alzheimer-pathology in Parkinsons disease and related dementia.," *Parkinsonism & related disorders*, Vol. 18, pp. 941–7, sep 2012.

84. Ibarretxe-Bilbao, N., C. Junque, M. J. Marti, and E. Tolosa, "Cerebral basis of visual hallucinations in Parkinsons disease: structural and functional MRI studies.," *Journal of the neurological sciences*, Vol. 310, pp. 79–81, nov 2011.

85. Kato, S., H. Watanabe, J. Senda, M. Hirayama, M. Ito, N. Atsuta, T. Kaga, M. Katsuno, S. Naganawa, and G. Sobue, "Widespread cortical and subcortical brain atrophy in Parkinsons disease with excessive daytime sleepiness.," *Journal of neurology*, Vol. 259, pp. 318–26, feb 2012.

86. Hong, J. Y., J. E. Lee, Y. H. Sohn, and P. H. Lee, "Neurocognitive and atrophic patterns in Parkinsons disease based on subjective memory complaints.," *Journal of neurology*, Vol. 259, pp. 1706–12, aug 2012.

87. Martin, W. R. W., M. Wieler, M. Gee, and R. Camicioli, "Temporal lobe changes in early, untreated Parkinsons disease.," *Movement disorders : official journal of the Movement Disorder Society*, Vol. 24, pp. 1949–54, oct 2009.

88. Pereira, J. B., C. Junqué, M.-J. Martí, B. Ramirez-Ruiz, N. Bargalló, and E. Tolosa, "Neuroanatomical substrate of visuospatial and visuoperceptual impairment in Parkinsons disease.," *Movement disorders : official journal of the Movement Disorder Society*, Vol. 24, pp. 1193–9, jun 2009.

89. Wattendorf, E., A. Welge-Lüssen, K. Fiedler, D. Bilecen, M. Wolfensberger, P. Fuhr, T. Hummel, and B. Westermann, "Olfactory impairment predicts brain atrophy in Parkinsons disease.," *The Journal of neuroscience : the official journal of the Society for Neuroscience*, Vol. 29, pp. 15410–3, dec 2009.

90. Feldmann, A., Z. Illes, P. Kosztolanyi, E. Illes, A. Mike, F. Kover, I. Balas, N. Kovacs, and F. Nagy, "Morphometric changes of gray matter in Parkinsons disease with depression: a voxel-based morphometry study.," *Movement disorders : official journal of the Movement Disorder Society*, Vol. 23, pp. 42–6, jan 2008.

91. Beyer, M. K., C. C. Janvin, J. P. Larsen, and D. Aarsland, "A magnetic resonance imaging study of patients with Parkinsons disease with mild cognitive impairment and dementia using voxel-based morphometry.," *Journal of neurology, neurosurgery, and psychiatry*, Vol. 78, pp. 254–9, mar 2007.

92. Nagano-Saito, a., Y. Washimi, Y. Arahata, T. Kachi, J. P. Lerch, a. C. Evans, A. Dagher, and K. Ito, "Cerebral atrophy and its relation to cognitive impairment in Parkinson disease.," *Neurology*, Vol. 64, pp. 224–9, jan 2005.

93. Burton, E. J., I. G. McKeith, D. J. Burn, E. D. Williams, and J. T. OBrien, "Cerebral atrophy in Parkinsons disease with and without dementia: a comparison with Alzheimers disease, dementia with Lewy bodies and controls.," *Brain : a journal of neurology*, Vol. 127, pp. 791–800, apr 2004.

94. Yousry, T. A., U. D. Schmid, H. Alkadhi, D. Schmidt, A. Peraud, A. Buettner, and P. Winkler, "Localization of the motor hand area to a knob on the precentral gyrus A new landmark," *Brain : a journal of neurology*, Vol. 120, pp. 141–157, 1997.

95. Acosta-Cabronero, J., G. B. Williams, J. M. S. Pereira, G. Pengas, and P. J. Nestor, "The impact of skull-stripping and radio-frequency bias correction on grey-matter segmentation for voxel-based morphometry.," *NeuroImage*, Vol. 39, pp. 1654–65, feb 2008.

96. Ashburner, J., "VBM Tutorial," pp. 1–14, 2010.

97. Ibarretxe-Bilbao, N., C. Junque, B. Segura, H. C. Baggio, M. J. Marti, F. Valldeoriola, N. Bargallo, and E. Tolosa, "Progression of cortical thinning in early Parkinsons disease.," *Movement disorders : official journal of the Movement Disorder Society*, Vol. 27, pp. 1746–53, dec 2012.

98. Pellicano, C., F. Assogna, F. Piras, C. Caltagirone, F. E. Pontieri, and G. Spalletta, "Regional cortical thickness and cognitive functions in non-demented Parkinsons disease patients: a pilot study.," *European journal of neurology : the official journal of the European Federation of Neurological Societies*, Vol. 19, pp. 172–5, jan 2012.

99. Garg, R., "Subacute sclerosing panencephalitis," *Postgraduate medical journal*, Vol. 78, no. 916, pp. 63–70, 2002.

100. Yalaz, K., B. Anlar, Y. Renda, S. Aysun, M. Topcu, and E. Özdirim, "Subacute sclerosing panencephalitis in turkey: epidemiological features," *Journal of tropical pediatrics*, Vol. 34, no. 6, pp. 301–305, 1988.

101. Brismar, J., G. G. Gascon, K. V. von Steyern, and S. Bohlega, "Subacute sclerosing panencephalitis: evaluation with ct and mr.," *American journal of neuroradiology*, Vol. 17, no. 4, pp. 761–772, 1996.

102. Anlar, B., I. Saatci, G. Kose, and K. Yalaz, "Mri findings in subacute sclerosing panencephalitis," *Neurology*, Vol. 47, no. 5, pp. 1278–1283, 1996.

103. Akdal, G., B. Baklan, H. Çakmakçi, and A. Kovanlikaya, "Mri follow-up of basal ganglia involvement in subacute sclerosing panencephalitis," *Pediatric neurology*, Vol. 24, no. 5, pp. 393–395, 2001.

104. Tuncay, R., G. Akman-Demir, A. Gökyigit, M. Eraksoy, M. Barlas, R. Tolun, and G. Gürsoy, "Mri in subacute sclerosing panencephalitis," *Neuroradiology*, Vol. 38, no. 7, pp. 636–640, 1996.

105. Öztürk, A., C. Gürses, B. Baykan, A. Gökyiğit, and M. Eraksoy, "Subacute sclerosing panencephalitis: clinical and magnetic resonance imaging evaluation of 36 patients," *Journal of child neurology*, Vol. 17, no. 1, pp. 25–29, 2002.

106. Aydin, K., B. Tatli, M. Ozkan, K. Ciftci, Z. Unal, S. Sani, M. Ozmen, M. Caliskan, N. Aydinli, and S. Guven, "Quantification of neurometabolites in subacute sclerosing panencephalitis by 1h-mrs," *Neurology*, Vol. 67, no. 5, pp. 911–913, 2006.

107. Alkan, A., K. Sarac, R. Kutlu, C. Yakinci, A. Sigirci, M. Aslan, and T. Baysal, "Early-and late-state subacute sclerosing panencephalitis: chemical shift imaging and single-voxel mr spectroscopy," *American journal of neuroradiology*, Vol. 24, no. 3, pp. 501–506, 2003.

108. Jabbour, J., J. H. Garcia, H. Lemmi, J. Ragland, D. A. Duenas, and J. L. Sever, "Subacute sclerosing panencephalitis: a multidisciplinary study of eight cases," *Jama*, Vol. 207, no. 12, pp. 2248–2254, 1969.

109. Dyken, P. R., A. Swift, and R. H. Durant, "Long-term follow-up of patients with subacute sclerosing panencephalitis treated with inosiplex," *Annals of neurology*, Vol. 11, no. 4, pp. 359–364, 1982.

110. Ohya, T., A. J. MARTINEZ, J. Jabbour, H. LEMMI, and D. A. DUENAS, "Subacute sclerosing panencephalitis correlation of clinical, neurophysiologic and neuropathologic findings," *Neurology*, Vol. 24, no. 3, pp. 211–211, 1974.

111. Kanemura, H., and M. Aihara, "Serial diffusion-weighted imaging in subacute sclerosing panencephalitis," *Pediatric neurology*, Vol. 38, no. 6, pp. 430–434, 2008.

112. Frisoni, G., C. Testa, A. Zorzan, F. Sabattoli, A. Beltramello, H. Soininen, and M. Laakso, "Detection of grey matter loss in mild alzheimers disease with voxel based morphometry," *Journal of Neurology, Neurosurgery & Psychiatry*, Vol. 73, no. 6, pp. 657–664, 2002.

113. Davidson, R. J., K. M. Putnam, and C. L. Larson, "Dysfunction in the neural circuitry of emotion regulation–a possible prelude to violence," *science*, Vol. 289, no. 5479, pp. 591–594, 2000.

114. Cahill, L., R. J. Haier, J. Fallon, M. T. Alkire, C. Tang, D. Keator, J. Wu, and J. L. Mcgaugh, "Amygdala activity at encoding correlated with long-term, free recall of emotional information," *Proceedings of the National Academy of Sciences*, Vol. 93, no. 15, pp. 8016–8021, 1996.

115. Cole, M. W., and W. Schneider, "The cognitive control network: integrated cortical regions with dissociable functions," *Neuroimage*, Vol. 37, no. 1, pp. 343–360, 2007.

116. Kanemura, H., M. Aihara, T. Okubo, and S. Nakazawa, "Sequential 3-d mri frontal volume changes in subacute sclerosing panencephalitis," *Brain and Development*, Vol. 27, no. 2, pp. 148–151, 2005.

117. Clinger, O. W., and N. A. Johnson, "Purposeful inhalation of gasoline vapors," *Psychiatric Quarterly*, Vol. 25, no. 1, pp. 557–567, 1951.

118. Lubman, D., M. Yücel, and A. Lawrence, "Inhalant abuse among adolescents: neurobiological considerations," *British journal of pharmacology*, Vol. 154, no. 2, pp. 316–326, 2008.

119. Medina-Mora, M. E., and T. Real, "Epidemiology of inhalant use," *Current Opinion in Psychiatry*, Vol. 21, no. 3, pp. 247–251, 2008.

120. Yücel, M., M. Takagi, M. Walterfang, and D. I. Lubman, "Toluene misuse and long-term harms: a systematic review of the neuropsychological and neuroimaging literature," *Neuroscience & Biobehavioral Reviews*, Vol. 32, no. 5, pp. 910–926, 2008.

121. Lubman, D. I., L. Hides, and M. Yucel, "Inhalant misuse in youth: time for a coordinated response," *Medical journal of Australia*, Vol. 185, no. 6, p. 327, 2006.

122. Filley, C. M., W. Halliday, and B. Kleinschmidt-DeMasters, "The effects of toluene on the central nervous system," *Journal of Neuropathology & Experimental Neurology*, Vol. 63, no. 1, pp. 1–12, 2004.

123. Hormes, J. T., C. M. Filley, and N. L. Rosenberg, "Neurologic sequelae of chronic solvent vapor abuse," *Neurology*, Vol. 36, no. 5, pp. 698–698, 1986.

124. Knox, J. W., and J. R. Nelson, "Permanent encephalopathy from toluene inhalation," *New England Journal of Medicine*, Vol. 275, no. 26, pp. 1494–1496, 1966.

125. Rosenberg, N. L., B. Kleinschmidt-DeMasters, K. A. Davis, J. N. Dreisbach, J. T. Hormes, and C. M. Filley, "Toluene abuse causes diffuse central nervous system white matter changes," *Annals of neurology*, Vol. 23, no. 6, pp. 611–614, 1988.

126. Greenberg, M. M., "The central nervous system and exposure to toluene: a risk characterization," *Environmental research*, Vol. 72, no. 1, pp. 1–7, 1997.

127. Filley, C. M., R. K. Heaton, and N. L. Rosenberg, "White matter dementia in chronic toluene abuse," *Neurology*, Vol. 40, no. 3 Part 1, pp. 532–532, 1990.

128. Yamanouchi, N., S. Okada, K. Kodama, T. Sakamoto, H. Sekine, S. Hirai, A. Murakami, N. Komatsu, and T. Sato, "Effects of mri abnormalities on wais-r performance in solvent abusers," *Acta neurologica scandinavica*, Vol. 96, no. 1, pp. 34–39, 1997.

129. Rosenberg, N. L., J. Grigsby, J. Dreisbach, D. Busenbark, and P. Grigsby, "Neuropsychologic impairment and mri abnormalities associated with chronic solvent abuse," *Journal of Toxicology: Clinical Toxicology*, Vol. 40, no. 1, pp. 21–34, 2002.

130. Aydin, K., S. Sencer, T. Demir, K. Ogel, A. Tunaci, and O. Minareci, "Cranial mr findings in chronic toluene abuse by inhalation," *American Journal of Neuroradiology*, Vol. 23, no. 7, pp. 1173–1179, 2002.

131. Aydin, K., S. Sencer, K. Ogel, H. Genchellac, T. Demir, and O. Minareci, "Single-voxel proton mr spectroscopy in toluene abuse," *Magnetic resonance imaging*, Vol. 21, no. 7, pp. 777–785, 2003.

132. Caldemeyer, K., R. Pascuzzi, C. Moran, and R. Smith, "Toluene abuse causing reduced mr signal intensity in the brain.," *AJR. American journal of roentgenology*, Vol. 161, no. 6, pp. 1259–1261, 1993.

133. Xiong, L., J. Matthes, J. Li, and J. Jinkins, "Mr imaging of" spray heads": toluene abuse via aerosol paint inhalation.," *American journal of neuroradiology*, Vol. 14, no. 5, pp. 1195–1199, 1993.

134. Yamanouchi, N., S.-i. Okada, K. Kodama, S. Hirai, H. Sekine, A. Murakami, N. Komatsu, T. Sakamoto, and T. Sato, "White matter changes caused by chronic solvent abuse.," *American Journal of Neuroradiology*, Vol. 16, no. 8, pp. 1643–1649, 1995.

135. Kamran, S., and R. Bakshi, "Mri in chronic toluene abuse: low signal in the cerebral cortex on t2-weighted images," *Neuroradiology*, Vol. 40, no. 8, pp. 519–521, 1998.

136. Unger, E., A. Alexander, T. Fritz, N. Rosenberg, and J. Dreisbach, "Toluene abuse: physical basis for hypointensity of the basal ganglia on t2-weighted mr images.," *Radiology*, Vol. 193, no. 2, pp. 473–476, 1994.

137. Escobar, A., and C. Aruffo, "Chronic thinner intoxication: clinico-pathologic report of a human case.," *Journal of Neurology, Neurosurgery & Psychiatry*, Vol. 43, no. 11, pp. 986–994, 1980.

138. von Euler, M., T. M. Pham, M. Hillefors, B. Bjelke, B. Henriksson, and G. von Euler, "Inhalation of low concentrations of toluene induces persistent effects on a learning retention task, beam-walk performance, and cerebrocortical size in the rat," *Experimental neurology*, Vol. 163, no. 1, pp. 1–8, 2000.

139. Korbo, L., O. Ladefoged, H. R. Lam, G. Ostergaard, M. J. West, and P. Arlien-Soborg, "Neuronal loss in hippocampus in rats exposed to toluene.," *Neurotoxicology*, Vol. 17, no. 2, pp. 359–366, 1995.

140. Meisenzahl, E., N. Koutsouleris, C. Gaser, R. Bottlender, G. Schmitt, P. McGuire, P. Decker, B. Burgermeister, C. Born, M. Reiser, *et al.*, "Structural brain alterations in subjects at high-risk of psychosis: a voxel-based morphometric study," *Schizophrenia research*, Vol. 102, no. 1, pp. 150–162, 2008.

141. kucuk, N., E. Kilic, E. Ibis, A. Aysev, E. Gencoglu, G. Aras, A. Soylu, and G. Erbay, "Brain spect findings in long-term inhalant abuse," *Nuclear medicine communications*, Vol. 21, no. 8, pp. 769–773, 2000.

142. Okada, S.-I., N. Yamanouchi, K. Kodama, Y. Uchida, S. Hirai, T. Sakamoto, S. Noda, N. Komatsu, and T. Sato, "Regional cerebral blood flow abnormalities in chronic solvent abusers," *Psychiatry and clinical neurosciences*, Vol. 53, no. 3, pp. 351–356, 1999.

143. Hirata, Y., H. Matsuda, K. Nemoto, T. Ohnishi, K. Hirao, F. Yamashita, T. Asada, S. Iwabuchi, and H. Samejima, "Voxel-based morphometry to discriminate early alzheimers disease from controls," *Neuroscience letters*, Vol. 382, no. 3, pp. 269–274, 2005.

144. Karas, G., E. Burton, S. Rombouts, R. Van Schijndel, J. OBrien, P. Scheltens, I. McKeith, D. Williams, C. Ballard, and F. Barkhof, "A comprehensive study of gray matter loss in patients with alzheimers disease using optimized voxel-based morphometry," *Neuroimage*, Vol. 18, no. 4, pp. 895–907, 2003.

145. Colom, R., F. J. Abad, M. A. Quiroga, P. C. Shih, and C. Flores-Mendoza, "Working memory and intelligence are highly related constructs, but why?," *Intelligence*, Vol. 36, no. 6, pp. 584–606, 2008.

146. Jung, R. E., and R. J. Haier, "The parieto-frontal integration theory (p-fit) of intelligence: converging neuroimaging evidence," *Behavioral and Brain Sciences*, Vol. 30, no. 02, pp. 135–154, 2007.

147. Gauthier, I., W. G. Hayward, M. J. Tarr, A. W. Anderson, P. Skudlarski, and J. C. Gore, "Bold activity during mental rotation and viewpoint-dependent object recognition," *Neuron*, Vol. 34, no. 1, pp. 161–171, 2002.

148. Jackson, P. L., A. N. Meltzoff, and J. Decety, "Neural circuits involved in imitation and perspective-taking," *Neuroimage*, Vol. 31, no. 1, pp. 429–439, 2006.

149. Zago, L., and N. Tzourio-Mazoyer, "Distinguishing visuospatial working memory and complex mental calculation areas within the parietal lobes," *Neuroscience letters*, Vol. 331, no. 1, pp. 45–49, 2002.

150. Buhner, M., S. Kroner, and M. Ziegler, "Working memory, visual–spatial-intelligence and their relationship to problem-solving," *Intelligence*, Vol. 36, no. 6, pp. 672–680, 2008.

151. Olesen, P. J., H. Westerberg, and T. Klingberg, "Increased prefrontal and parietal activity after training of working memory," *Nature neuroscience*, Vol. 7, no. 1, pp. 75–79, 2004.

152. Smith, E. E., and J. Jonides, "Storage and executive processes in the frontal lobes," *Science*, Vol. 283, no. 5408, pp. 1657–1661, 1999.

153. Conway, A. R., M. J. Kane, and R. W. Engle, "Working memory capacity and its relation to general intelligence," *Trends in cognitive sciences*, Vol. 7, no. 12, pp. 547–552, 2003.

154. Thompson, P. M., T. D. Cannon, K. L. Narr, T. Van Erp, V.-P. Poutanen, M. Huttunen, J. Lönnqvist, C.-G. Standertskjöld-Nordenstam, J. Kaprio, M. Khaledy, *et al.*, "Genetic influences on brain structure," *Nature neuroscience*, Vol. 4, no. 12, pp. 1253–1258, 2001.

155. Pol, H. E. H., H. G. Schnack, D. Posthuma, R. C. Mandl, W. F. Baaré, C. van Oel, N. E. van Haren, D. L. Collins, A. C. Evans, K. Amunts, *et al.*, "Genetic contributions to human brain morphology and intelligence," *The Journal of Neuroscience*, Vol. 26, no. 40, pp. 10235–10242, 2006.

156. Terrazas, A., and B. L. McNaughton, "Brain growth and the cognitive map," *Proceedings of the National Academy of Sciences*, Vol. 97, no. 9, pp. 4414–4416, 2000.

157. Draganski, B., C. Gaser, G. Kempermann, H. G. Kuhn, J. Winkler, C. Büchel, and A. May, "Temporal and spatial dynamics of brain structure changes during extensive learning," *The Journal of Neuroscience*, Vol. 26, no. 23, pp. 6314–6317, 2006.

158. May, A., and C. Gaser, "Magnetic resonance-based morphometry: a window into structural plasticity of the brain," *Current opinion in neurology*, Vol. 19, no. 4, pp. 407–411, 2006.

159. Münte, T. F., E. Altenmüller, and L. Jäncke, "The musicians brain as a model of neuroplasticity," *Nature Reviews Neuroscience*, Vol. 3, no. 6, pp. 473–478, 2002.

160. Schlaug, G., "The brain of musicians," *Annals of the New York Academy of Sciences*, Vol. 930, no. 1, pp. 281–299, 2001.

161. Schlaug, G., L. Jäncke, Y. Huang, J. F. Staiger, and H. Steinmetz, "Increased corpus callosum size in musicians," *Neuropsychologia*, Vol. 33, no. 8, pp. 1047–1055, 1995.

162. Schlaug, G., L. Jancke, Y. Huang, and H. Steinmetz, "In vivo evidence of structural brain asymmetry in musicians," *Science*, Vol. 267, no. 5198, p. 699, 1995.

163. Amunts, K., G. Schlaug, L. Jäncke, H. Steinmetz, A. Schleicher, A. Dabringhaus, and K. Zilles, "Motor cortex and hand motor skills: structural compliance in the human brain," *Human brain mapping*, Vol. 5, no. 3, pp. 206–215, 1997.

164. Keenan, J. P., V. Thangaraj, A. R. Halpern, and G. Schlaug, "Absolute pitch and planum temporale," *Neuroimage*, Vol. 14, no. 6, pp. 1402–1408, 2001.

165. Gaser, C., and G. Schlaug, "Brain structures differ between musicians and non-musicians," *The Journal of Neuroscience*, Vol. 23, no. 27, pp. 9240–9245, 2003.

166. Hutchinson, S., L. H.-L. Lee, N. Gaab, and G. Schlaug, "Cerebellar volume of musicians," *Cerebral cortex*, Vol. 13, no. 9, pp. 943–949, 2003.

167. Sluming, V., T. Barrick, M. Howard, E. Cezayirli, A. Mayes, and N. Roberts, "Voxel-based morphometry reveals increased gray matter density in brocas area in male symphony orchestra musicians," *Neuroimage*, Vol. 17, no. 3, pp. 1613–1622, 2002.

168. Rorden, C., and M. Brett, "Stereotaxic display of brain lesions," *Behavioural neurology*, Vol. 12, no. 4, pp. 191–200, 2000.

169. Good, C. D., I. S. Johnsrude, J. Ashburner, R. N. Henson, K. Fristen, and R. S. Frackowiak, "A voxel-based morphometric study of ageing in 465 normal adult human brains," in *Biomedical Imaging, 2002. 5th IEEE EMBS International Summer School on*, pp. 16–pp, IEEE, 2002.

170. Good, C. D., I. Johnsrude, J. Ashburner, R. N. Henson, K. J. Friston, and R. S. Frackowiak, "Cerebral asymmetry and the effects of sex and handedness on brain structure: a voxel-based morphometric analysis of 465 normal adult human brains," *Neuroimage*, Vol. 14, no. 3, pp. 685–700, 2001.

171. Finger, S., *Origins of neuroscience: a history of explorations into brain function*, Oxford University Press, USA, 2001.

172. Bentivoglio, M., "Cortical structure and mental skills: Oskar vogt and the legacy of lenins brain," *Brain research bulletin*, Vol. 47, no. 4, pp. 291–296, 1998.

173. Spitzka, E. A., "A study of the brains of six eminent scientists and scholars belonging to the american anthropometric society, together with a description of the skull of professor ed cope," *Transactions of the American Philosophical Society*, pp. 175–308, 1907.

174. Meyer, A., *The search for a morphological substrate in the brains of eminent persons including musicians: A historical review*, na, 1977.

175. Witelson, S. F., D. L. Kigar, and T. Harvey, "The exceptional brain of albert einstein," *The Lancet*, Vol. 353, no. 9170, pp. 2149–2153, 1999.

176. May, A., G. Hajak, S. Gänssbauer, T. Steffens, B. Langguth, T. Kleinjung, and P. Eichhammer, "Structural brain alterations following 5 days of intervention: dynamic aspects of neuroplasticity," *Cerebral Cortex*, Vol. 17, no. 1, pp. 205–210, 2007.

177. Dehaene, S., E. Spelke, P. Pinel, R. Stanescu, and S. Tsivkin, "Sources of mathematical thinking: Behavioral and brain-imaging evidence," *Science*, Vol. 284, no. 5416, pp. 970–974, 1999.

178. Cohen, L., S. Dehaene, F. Chochon, S. Lehericy, and L. Naccache, "Language and calculation within the parietal lobe: a combined cognitive, anatomical and fmri study," *Neuropsychologia*, Vol. 38, no. 10, pp. 1426–1440, 2000.

179. Stanescu-Cosson, R., P. Pinel, P.-F. van de Moortele, D. Le Bihan, L. Cohen, and S. Dehaene, "Understanding dissociations in dyscalculia," *Brain*, Vol. 123, no. 11, pp. 2240–2255, 2000.

180. Black, J. E., K. R. Isaacs, B. J. Anderson, A. A. Alcantara, and W. T. Greenough, "Learning causes synaptogenesis, whereas motor activity causes angiogenesis, in cerebellar cortex of adult rats.," *Proceedings of the National Academy of Sciences*, Vol. 87, no. 14, pp. 5568–5572, 1990.

181. Isaacs, K. R., B. J. Anderson, A. A. Alcantara, J. E. Black, and W. T. Greenough, "Exercise and the brain: angiogenesis in the adult rat cerebellum after vigorous physical activity and motor skill learning," *Journal of Cerebral Blood Flow & Metabolism*, Vol. 12, no. 1, pp. 110–119, 1992.

182. Anderson, B. J., X. Li, A. A. Alcantara, K. R. Isaacs, J. E. Black, and W. T. Greenough, "Glial hypertrophy is associated with synaptogenesis following motor-skill learning, but not with angiogenesis following exercise," *Glia*, Vol. 11, no. 1, pp. 73–80, 1994.

183. Kempermann, G., L. Wiskott, and F. H. Gage, "Functional significance of adult neurogenesis," *Current opinion in neurobiology*, Vol. 14, no. 2, pp. 186–191, 2004.

184. Kempermann, G., H. G. Kuhn, and F. H. Gage, "Experience-induced neurogenesis in the senescent dentate gyrus," *The Journal of Neuroscience*, Vol. 18, no. 9, pp. 3206–3212, 1998.

185. Bütefisch, C. M., B. C. Davis, S. P. Wise, L. Sawaki, L. Kopylev, J. Classen, and L. G. Cohen, "Mechanisms of use-dependent plasticity in the human motor cortex," *Proceedings of the national academy of sciences*, Vol. 97, no. 7, pp. 3661–3665, 2000.

186. Barinaga, M., "Newborn neurons search for meaning," *Science*, Vol. 299, no. 5603, pp. 32–34, 2003.

187. Ehninger, D., and G. Kempermann, "Regional effects of wheel running and environmental enrichment on cell genesis and microglia proliferation in the adult murine neocortex," *Cerebral Cortex*, Vol. 13, no. 8, pp. 845–851, 2003.

188. Van Turennout, M., L. Bielamowicz, and A. Martin, "Modulation of neural activity during object naming: effects of time and practice," *Cerebral Cortex*, Vol. 13, no. 4, pp. 381–391, 2003.

189. Kleim, J. A., T. M. Hogg, P. M. VandenBerg, N. R. Cooper, R. Bruneau, and M. Remple, "Cortical synaptogenesis and motor map reorganization occur during late, but not early, phase of motor skill learning," *The Journal of neuroscience*, Vol. 24, no. 3, pp. 628–633, 2004.

190. Song, H., G. Kempermann, L. O. Wadiche, C. Zhao, A. F. Schinder, and J. Bischofberger, "New neurons in the adult mammalian brain: synaptogenesis and functional integration," *The Journal of neuroscience*, Vol. 25, no. 45, pp. 10366–10368, 2005.

191. Barnea, A., and F. Nottebohm, "Seasonal recruitment of hippocampal neurons in adult free-ranging black-capped chickadees," *Proceedings of the National Academy of Sciences*, Vol. 91, no. 23, pp. 11217–11221, 1994.

192. Kirn, J., B. OLoughlin, S. Kasparian, and F. Nottebohm, "Cell death and neuronal recruitment in the high vocal center of adult male canaries are temporally related to changes in song," *Proceedings of the National Academy of Sciences*, Vol. 91, no. 17, pp. 7844–7848, 1994.

193. Aydin, K., K. Ciftci, E. Terzibasioglu, M. Ozkan, A. Demirtas, S. Sencer, and O. Minareci, "Quantitative proton mr spectroscopic findings of cortical reorganization in the auditory cortex of musicians," *American journal of neuroradiology*, Vol. 26, no. 1, pp. 128–136, 2005.

194. Henley, S., G. Ridgway, R. Scahill, S. Klöppel, S. Tabrizi, N. Fox, J. Kassubek, E. I. W. Group, *et al.*, "Pitfalls in the use of voxel-based morphometry as a biomarker: examples from huntington disease," *American Journal of Neuroradiology*, Vol. 31, no. 4, pp. 711–719, 2010.